The role of electron-electron scattering in spin transport for a GaAs semiconductor in the nondegenerate regime

Gionni Marchetti

Submitted for the Degree of
Doctor of Philosophy

Department of Physics
University of York

September 2013

Abstract

The long spin lifetimes observed in n-type semiconductors, in particular in n-GaAs, make them highly suitable for novel spintronic devices. Therefore it is of great importance to understand the spin dynamics in these semiconductors

We study the spin transport in a bulk GaAs using the ensemble Monte Carlo method, recently equipped for dealing with spin transport. This is a difficult many-body problem which involves the interactions of the electrons with acoustic phonons, polar optical phonons and single-charge impurities. The spin dephasing source which we include is the Dyakonov-Perel mechanism. This is the main decoherence mechanism in the regime we consider. We estimate the spin relaxation times at high temperatures ($280 \leq T \leq 400\ K$) and in doping concentrations ($n = 10^{16}$ to $2.5 \cdot 10^{17}\ cm^{-3}$), i.e., in the nondegenerate regime.

Our calculations are in very good agreement with experimental results with no adjustable parameters. Morevoer we include the electron-electron interaction which is still a big issue in ensemble Monte Carlo. Our results show that the electron-electron interaction plays an important role in spin transport in the same regime. This seems to extend the theoretical predictions made for a two-dimensional electron gas in GaAs to the three-dimensional case.

We introduce a method which reduces the probability of a three-body scattering event in the case of electron-electron collisions. This method works well in the high electronic concentration regime ($n_e \gtrsim 10^{17}\ cm^{-3}$) .

We also study the effect of varying temperature and applied bias on spin relaxation times without electron-electron interaction. Our results show that the spin relaxation times are longer at low temperatures and that increasing the applied bias yields enhancement of the spin polarization in the system.

Contents

List of Tables

List of Figures

Acknowledgements

I would like to thank Irene D'Amico for giving me an opportunity to study condensed matter theory in spite of my background in high-energy physics and mathematical physics, Matthew Hodgson for his collaboration, and professor Michael Oestreich for providing with experimental data. Many thanks to Phil for proofreading and Professor Gerard 't Hooft for the explanation of the electron spin in his unique style which I admire very much. I would like to thank Robert Greenall for making me curious to read *The Dancing Wu Li Masters*, a book which was on his office bookshelf. The title is so suggestive and in particular of the time in which it was written: the 70s. This recalls one thing I have to do with my friend James: a trip from Los Angeles to Las vegas with a very fast car with no top wearing Hawaian shirts because we need to celebrate our friendship in the spirit of Raoul Duke and Dr. Gionzo.

My human experience in York was really amazing. Like Umberto Eco I like to read J. L. Borges and make the lists. Below there is a list of names of friends with whom I shared unforgettable moments of my life, sometimes dancing probably like the electrons do in the matter or like the Wu Li masters of that infamous book, but surely with more passionate Latin rhythm. So there you go! Rebecca, Petya, Martha, Outi, Lourdes, Leonardo, Markus, James R., Leonardo Horacio, Rafael, Harold, Aya, Oyn, Carla, Joy, Angela, Daniela e Henning, Anette, Stefano e Gaetana, Vlado and Maria, Carlo, Luca and Valentina, Luca B., Henna, Martina, James W., Pankhaj, Spiros, Anna O., Antonio, Daniel, Tuyuan, Karisha, Pamela, Ingrid, Gabriela, Marija, Juan, Melissa, Simon, Jolyon and Jingdi, Joe, Tom, Ramon, Unai, Teresa, Noi and Jess, Julieta, Erica, Herve, Ondrej, Andy, Maria y Alfredo, Lorena, Francesca, Xinhua, Danielle, Mehmet, Marianna F., Annemarieke, Natalie, Adolfo, Javier, Giulia, Manolo, Rudraksh, Eli, Yuanyuan, Anna V., Farina, Maria Ana, Mariana L., Paloma, Nobuyuki, Ignacio, my housemates Jenefried and Paul and many others. As a last consideration, I am always surprised when mathematics can explain Nature so well. Probably Maimonides was right when in his *The guide for the perplexed* (1190) he wrote: "In the realm of Nature there is nothing purposeless, trivial, or unnecessary".

Declarations

I declare that the work presented in this thesis, except where otherwise stated, is based on my own research and has not been submitted previously for a degree in this or any other university. Parts of the work reported in this thesis have been published in:

S. Kapoor and G. Marchetti and F. Rossi and I. D'Amico , "Monte Carlo Study of Temperature and Bias dependence of Spin Transport in GaAs ", *J. Phys: Conf. Ser .* **303**, 012095, 2011

Gionni Marchetti , Matthew Hodgson , James Mchugh , Roy Chantrell and Irene D'Amico, "Spin Relaxation in GaAs: the importance of Electron-Electron interactions", *Materials*, submitted

Signed

Gionni Marchetti

Chapter 1

Thesis Overview

1.1 Motivation

Spintronics is an active field that encompasses both fundamental research in physics and practical applications. Its goal is to study and exploit spin-related properties in condensed matter, i.e., metals, semiconductors and semiconductor heterostructures [1, 2, 3, 4, 5, 6], and more exotic structures such as topological insulators probably in the far future [4]. Despite the fact that electrons have charge and spin, the latter being an internal degree of freedom with no classical counterpart, only recently have physicists started to look at them separately [7].

The discovery of the Giant Magneto Resistance (GMR) effect in 1988 by A. Fert and P. Grünberg for which they were awarded the Nobel Prize in Physics in 2007, is considered the beginning of this promising field. From the GMR effect, a new device, the spin-valve sensor was created allowing IBM to replace the traditional sensors in magnetoresistive hard disk drive read heads and increase rapidly up to 100% the data storage areal density.

As Fert stated in his Nobel lecture [7], the idea of the effect of spin on the electronic mobility in ferromagnets, which is related to the GMR effect, was already proposed by N. Mott in 1964. This is not a such a surprising fact in spintonics. For instance in 1971 M. I. Dyakonov and V. I. Perel predicted the Spin Hall Effect (SHE) which has been observed only after nearly thirty years. The reason is that only the recent considerable progress in material fabrication and engineering can test some previous and new, maybe wild, theoretical ideas about spin physics. It should also be noted that spintronics could not be so successful without the contribution of sophisticated experimental techniques, commonly known as optical orientation [8], which allow us to observe the spin dynamics in semiconductors.

The observation of spin dynamics on a sub-picosecond time scale and of the degree of spin polarization is made via photoluminescence, improved with the Hanle effect, or via more recent and innovative time-resolved techniques, based on time-resolved Faraday and time-resolved Kerr effects [8]. The latter techniques are pump and probe methods which produce a pulsed excitation through picosecond or femtosecond lasers followed by measurement. In general the interpretation of the signals from these experimental techniques is subtle according to R. T. Harley [8]. Therefore the experimental physicists who use these state-of-the-art techniques, need extremely good skills to give us reliable results for comparison with the theory.

Thus quantum mechanics machinery, optical orientation and material technologies together make this recent field very active, innovative and also challenging addressing new theoretical and engineering problems.

Roughly spintronics can be split in two sub-fields: metallic spintronics and semiconductor spintronics. The metallic spintronic field has already produced marvellous novel devices, especially for the data storage industry: spin-valve sensors, magnetic tunnel junctions and a heap of other important applications [2, 4]. The semiconductor spintronic field seems more rich for fundamental research but so far has not yet shown its potential practical applications for industrial and information technologies. An example is given by the spin-transistor idea proposed by S. Datta and B. Das in 1989 that has not yet found a suitable viable realization.

The spin-transistor exploits one of the most important features of semiconductors, the spin-orbit interaction [9]. This is also the origin of the SHE which consists in the separation of spin-up and spin-down currents along the opposite edges of the semiconductor slab, somewhat analogous to the Hall effect for electron (charge) current [10]. In materials the spin-orbit coupling may often increase the energy scale at which quantum effects become important [11] giving rise to interesting phenomena.

Besides potential novel faster, more energy efficient and smaller devices there is another aspect that makes the electron spin so appealing. Like the spin states of photon, or polarization states [12], the electron spin is a two-state quantum system and therefore an ideal candidate for Quantum Computation (QC) [13]. The quantum states are often called spin-qubits, or simply qubits, in strict analogy to the binary bits of classical computers. In order to manipulate the qubits efficiently QC processes require that they exhibit quantum coherence [12, 14] for a long enough time to perform quantum operations. Recently experimental physicists observed relatively long spin lifetimes in n-type semiconductors [15, 16, 17], making them suitable hardware for quantum computers. Unfor-

tunately the interaction of qubits with the environment affects their dynamics, i.e., their spin orientation is no longer conserved in time and space, and leads to spin dephasing or decoherence [18]. The sources of spin dephasing can be various. For instance in the case of a GaAs semiconductor there may be the Bir-Aronov-Pikus mechanism, the hyperfine interaction, the Elliott-Yafet mechanism and the Dyakonov-Perel mechanism [19].

In order to work properly, a semiconductor spintronic device should allow us to perform efficiently the following operations: spin injection, manipulation, storage, transfer of the spin information and its detection [20]. It is also important that we are able to convert electrical signals into spin signal and vice versa in a way that spintronics can be integrated into the conventional electronics [21].

We conclude this section mentioning the brilliant idea proposed by H. Ohno in 1998 [22] which is an typical example of how spintronics can be an exciting field which combines fundamental physics and technology. The traditional semiconductor devices use the electron charge meanwhile electron spin is used in recording information in magnetic materials. Ohno then suggested to combine both functionalities in the same material; he created new materials introducing a concentration of magnetic elements in nonmagnetic III-V semiconductors. Nowadays the study of dilute magnetic semiconductors is an active and promising field.

1.2 Thesis Aim and Objectives

This thesis focuses on many-body effects in spin-polarized transport, and especially on the role of electron-electron interaction. An example of a many-body effect is the Spin Coulomb Drag in which a spin current will decay due to the Coulomb interaction between the spin up and spin down populations [23]. In the present work we study the spin dephasing of an initially fully polarized electron ensemble via the Dyakonov-Perel mechanism. This is the dominant spin decoherence source for a n-GaAs semiconductor at the electron densities and temperatures of interest. We assume that it is possible to achieve an initial fully spin polarized configuration, despite the fact that for the electrical injection of spin-polarized electrons from a ferromagnetic metal into a semiconductor there is a well known obstacle denoted as the conductivity mismatch [20, 24].

The spin dephasing due to the Dyakonov-Perel mechanism can be thought of as a result of the action of varying effective magnetic fields, which depend

on the electrons' velocities and cause spin precession [8]. This mechanism is due to a type of spin-orbit interaction, the so called Dresselhaus term, which arises from the lack on inversion symmetry in bulk GaAs [25].

In order to understand the effects of the interacting electrons, phonons and impurities on the spin dynamics we resort to the Ensemble Monte Carlo method that very recently has been equipped for dealing with spin transport [26]. The Ensemble Monte Carlo method is a stochastic method devised to solve numerically the Boltzmann equation for charge transport in semiconductors [27]. This method allows us to calculate the spin relaxation times which we compare with the experimental results obtained by optical orientation techniques [28]. In this way we are able to understand if the many-body interactions, i.e., the strengths of the interactions, calculated through the scattering rates, and our way of modelling them are reasonable. In particular we are interested in the electron-electron interaction which is notoriously difficult to treat by the Ensemble Monte Carlo approach. As far as we know there are no previous results for the three-dimensional case when the electron-electron interaction is included.

1.3 What is the Electron Spin?

Before outlining the thesis, we want to say a few words about the main ingredient of this work, i.e., the electron spin. In general many physicists feel confortable to work with concepts that can be represented or understood through familiar objects in everyday life. A particle of spin 1 like a photon for example, can be understood through its polarization vector and the way this transforms for rotations in three-dimensional space [29]. What about a particle of spin $1/2$? From Stern-Gerlach experiment type or from the theoretical formalism one can easily infer that a rotation of an angle θ in the configuration space is related to a rotation $\theta/2$ in the internal spin state space [30]. This happens because the electron wavefunction is a spinor, a mathematical object which gives another representation of the group of rotations. Despite the fact that we can apply successfully the quantum mechanics formalism of spin $1/2$, this still remains a puzzling object. This happens because in our world there is no other object or a macroscopic physical system with the same rotational symmetry.

More importantly spin being a quantum angular momentum, we can argue if an electron really rotates around its axis. We asked this question and also if the spin may affect the electron's motion to G. 't Hooft who won the Nobel Prize in Physics in 1999 for his work which showed that the electro-weak theory is

renormalizable.

"Although we usually talk of "spin" of a particle, atom or molecule, what we really mean is "angular momentum", which usually equals the quantity ρxv integrated over space, where ρ is the mass density, x the coordinate and v the local velocity. Now in case of a particle such as an electron, angular momentum is just an abstract property that, when added to the orbital angular momentum, is conserved in the interactions. The electron is also pointlike, and in the early days, first half of the 20th century, this indeed caused concern. The electron spin, discovered by the Dutch physicists Uhlenbeck and Goudsmit, was thought to be something impossible, because, precisely as you said, how can a pointlike object rotate so fast? One can assign a finite size to the electron by observing that it cannot be smaller than a ball where all its electric charge, if distributed on the surface, would generate an electric field with more energy than represented by the mass of the electron, multiplied with c^2. But this ball is so small that the surface would have to spin faster than the speed of light, so this is not the right answer. The right answer is that one should not ask the question how fast the electron's surface rotates, because the electron has no surface in the classical sense. It's the way the electron behaves in its equations that counts, and as long as that is free from contradictions we have no problem with its description.

Spin does not affect the motion of a free particle, but does affect the way it interacts with other things. A tennis ball interacts with the floor and the racket; it also interacts with the air, but electrons are usually studied when moving in vacuum - there, also spinning electrons move straight. "

(G. 't Hooft, Universiteit Utrecht, Private Communication, September 2, 2013)

1.4 Thesis Structure

Chapter 2 provides the basic concepts and useful results of nonrelativistic scattering theory. Our calculations are based on the Ensemble Monte Carlo algorithm which strongly relies on scattering rates calculated from first order perturbation theory (Fermi's Golden Rule). Fermi's Golden rule entails the so-called Born approximation. The Born approximation can be defined in different ways, but its exact definition arises from the Born series which iteratively solves the Schwinger-Lippmann equation. The concept of the differential cross-section is also used to analyse our numerical calculations which include the electron-electron scattering in **Chapter 5**. We did not include the results of nonrelativistic scattering theory derived by the method of partial

waves which is commonly used for low energy collisions. The last section contains a brief discussion of the overlap integrals involved in the calculation of scattering rates for electrons in solids due to the periodic structure of the solid lattice (Bloch states).

In **Chapter 3** we discuss the many-body problem of the screened Coulomb interaction in the ensemble of conduction band electrons in the random phase approximation. The physical system in this study can be simply thought of as a jellium model. We calculated the finite temperature dielectric function for a three-dimensional interacting electron gas in the random phase approximation. How we implemented the finite temperature Lindhard function, is shown in the Appendix B. Then we briefly discuss the validity of the random phase approximation which neglects exchange and correlation effects for the physical system we consider. As for small perturbations the Thomas-Fermi theory is a good approximation of the dielectric function, we resorted to use it. As the latter relies on the Fermi-Dirac integrals then we had to find a way to implement some relatively recent algorithms [31] for their calculations. In the last section we explain in detail how we obtained the final result for the calculation of the screening length.

Chapter 4 is dedicated to the spinor formalism for the ensembles of spin $1/2$. The spin-orbit interaction is also considered together with its derivation from the Dirac's equation. We introduce the standard concepts of spin dephasing and recall the more important mechanisms of decoherence in GaAs semiconductors. Among them the dominant one for the regime in this study, is the Dyakonov-Perel mechanism. The so-called Dresselhaus term which causes it, is then introduced without using the group theory formalism, the latter being beyond the scope of this thesis. We explain how the ensemble Monte Carlo method works. Finally we show our results of spin relaxation times versus temperature and applied bias through the ensemble Monte Carlo method. We found that the spin relaxation times are longer at low temperatures and that increasing the applied bias yields enhancement of the spin polarization in the system. These calculations do not include electron-electron interaction.

In **Chapter 5** we discuss how we tackle the electron-electron scattering in ensemble Monte Carlo method. We accomplish this in a rather different way from previous literature [27], by using some simple physical assumptions. The electron-electron scattering as far as we know, is still a big issue in the ensemble Monte Carlo method. Importantly we also improved over the Born approximation using a scattering method which prevents multiple collisional events from happening (third-body rejection). This is done in strict analogy to the method proposed for the electron-impurity scattering [32]. The spin

time-evolution is also developed in a different way with respect to the previous results we obtained by a density matrix approach in Chapter 4, see Appendix E. Then we compare our theoretical results with the ones obtained by Oertel et al. via optical orientation techniques [28] . Our calculations for the spin relaxation times against electron density and temperature, are in very good agreement with the experimental data without using any free adjustable parameter. In particular we take the spin-orbit coupling value for the system under investigation from [28]. Moreover our calculations show that the electron-electron scattering in the nondegenerate regime, slows down the spin relaxation time. This result suggests that a theoretical prediction [33], derived solving the kinetic equation for a nondegenerate two-dimensional electron gas, can be extended to the three-dimensional case. On the basis of a discussion of the Born approximation, the random phase approximation, and the bare Coulomb electron-electron differential cross-section we give a plausible explanation of these results. This involves a calculation of a quantity, that we shall call "statistical integral "as it is related to the Boltzmann distribution.

Chapter 6 contains an interesting idea which may improve the previous results in higher electronic concentrations, retaining the same physical model. This is based on the Friedel sum rule and is work in progress. We also show how third-body rejection can be better understood from the point of view of an inverse problem in scattering theory. We also discuss briefly how it may be possible to improve further the ensemble Monte Carlo for the present model.

Finally notice that the International System of Units (SI units) will be used throughout this thesis.

Chapter 2

Scattering Theory

Since the discovery of the positive nuclei in the atoms by E. Rutherford in 1911 the scattering experiments have become one of the most effective and successful method used by physicists to investigate the structure of condensed matter. Indeed many phenomena in Nature can be explained in terms of collisions, for example, the blue color of the sky is due to the Rayleigh scattering of photons from the sun off the molecules of the atmosphere and in general the interaction of light with matter is high accurately described in terms of scattering between photon and electron fields in Quantum Electrodynamics (QED) [34] . Furthermore the breakthroughs of scattering experiments and theory (S-matrix theory) in hadronic physics in 1960s convinced some physicists, notably G. Chew among them, that it was possible to explain completely the strong interaction by a form of S-matrix theory only, called bootstrap model [35]. The failure of this too much optimistic expectation caused the physicists to leave it and pursue new roads. Curiously G. Veneziano studying the so-called Regge trajectories in S-matrix theory discovered in 1968 that a string may describe the strong interacting particles. It was the birth ot the first string theory [36]. In this chapter we recall the definitions and the main results of the potential scattering theory. As the speed of the electrons in semiconductors is small compared to speed of light only non-relativistic scattering is considered here.

2.1 The Total Cross-Section

The scattering total cross-section σ_{tot} which has the dimensions of an area, is the characteristic quantity in the collision experiments. Its definition arises naturally from the typical way the experimental physicists perform scattering experiments in their laboratories. Basically a collimated beam of particles A of well-defined energy E scatters off a macroscopic sample (the target) made

by the particles B and then the particles deflected into different directions are counted by means of suitable detectors. We shall consider only elastic collisions where the particles A and B are scattered without any change in their internal structure. In order to assume that only binary collisions between the particles A and the scattering centres B of the target are likely to happen, two assumptions are needed. Firstly the beam should have low particle density making the interactions between them negligible, secondly we wish to avoid multiple scattering events between the incoming particles and the target, therefore the latter must be thin enough to satisfy this assumption. If in a collision experiment these conditions are satisfied, then it is possible to define the cross-section σ_{tot} in the following way: *"The total cross-section σ_{tot} of a certain type of event in a given collision is the ratio of the number of events of this type per unit time and per unit scatterer, to the relative flux of the incident particles with respect to the target "*[37]. Here the relative flux of the incident particles relative to the target is the number of the particles A crossing per unit time a unit area perpendicular to the direction of the incident beam and at rest with respect to the target. Therefore the quantity σ_{tot} gives roughly the probability of the interaction between the particles A and B and must depend only on the energy of the collision and the microscopic properties of the physical system at study. Pictorially σ_{tot} can be interpreted as an effective area which the incoming particle may pass through to be scattered. Clearly we should not give too much importance to this simple geometrical picture as σ_{tot} may vary greatly even in a small energy range.

In a typical collision experiment the detectors count the number of the scattered particles in each direction, denoted by polar angles (θ, ϕ), at large distance from the scattering centre. Studying this angular distribution we get more information about the nature of the interaction and moreover we can use the useful concept of differential cross-section $\sigma(\theta, \phi)$ [1] a quantity which gives approximately the probability of a particle of energy E to be scattered in the differential solid angle $d\Omega$ along the direction (θ, ϕ). Its relation with the total cross-section σ_{tot} is obtained integrating it over all directions

$$\sigma_{tot} = \int \sigma(\theta, \phi) d\Omega = \int_0^{2\pi} d\phi \int_0^{\pi} \sigma(\theta, \phi) \sin\theta d\theta \,. \tag{2.1}$$

Finally we have to mention how the collisions are usually described using two different convenient systems. The laboratory system (LS) is defined as the frame of reference where the target particles B are at rest before the collision

[1] A very common notation for the differential cross-section used in many Quantum Mechanics books is the following $\sigma(\theta, \phi) = \frac{d\sigma}{d\Omega}(\theta, \phi)$

meanwhile the center of mass (CoM) is the frame of reference where the center of mass of the system is always at rest. The latter is more useful for theoretical calculations as the two-body problem is reduced to the problem of one particle in a scattering potential, see next section 2.2. Clearly the two descriptions should be equivalent as the physics must be coordinate-independent or in other words the total cross-section σ_{tot} is invariant under a Galileian transformation. Then as the same number of particles are scattered in the solid angle $d\Omega_L$ about (θ_L, ϕ_L) in laboratory as in the solid angle $d\Omega_{CoM}$ about $(\theta_{CoM}, \phi_{CoM})$ in the center of mass, it is straightforward to relate the differential differential-cross sections calculated in LS and CoM respectively. In fact let us consider the elastic collision of two particles A and B, the latter being at rest. If v_A is the speed of the particle A in the laboratory system, then the speed of the center of mass v_{CoM} is [38]

$$v_{CoM} = \frac{m_A v_A}{m_A + m_B}\,, \tag{2.2}$$

where m_A and m_B the masses of particles A and B respectively. The speed v_A^r of the particle A in the CoM system is [38]

$$v_A^r = v_A - v_{CoM} = \frac{m_B v_A}{m_A + m_B}\,. \tag{2.3}$$

The geometric configuration of the velocities v_A, v_A^r and v_{CoM} is shown in Figure 2.1. From Figure 2.1 the relation between the polar angles in the laboratory system and the CoM system, assuming that there is no dependence on the azimuthal angles (ϕ_L=ϕ_{CoM}), can be found from the two following equations

$$v_A^r \cos\theta_{CoM} + v_{CoM} = v_A \cos\theta_L\,, \tag{2.4}$$

$$v_A^r \sin\theta_{CoM} = v_A \sin\theta_L\,. \tag{2.5}$$

Eliminating v_A from equations (2.4) and (2.5), one gets [38]

$$\tan\theta_L = \frac{\sin\theta_{CoM}}{\zeta + \cos\theta_{CoM}}\,, \tag{2.6}$$

where $\zeta = v_{CoM}/v_A^r = m_A/m_B$. Because the same number of particles should be scattered into the differential solid angles $d\Omega_L$ and $d\Omega_{CoM}$, the following relation must hold

$$\sigma\ (\theta_L, \phi_L\ ) \sin\theta_L d\,\theta_L d\,\phi_L = \sigma\ (\theta_{CoM}, \phi_{CoM}\ ) \sin\theta_{CoM} d\,\theta_{CoM} d\,\phi_{CoM}\,, \tag{2.7}$$

and finally using (2.6) one obtains the following relationship [38]

$$\sigma\ (\theta_L, \phi_L\ ) = \frac{[\zeta^2 + 2\zeta\cos\theta_{CoM} + 1]^{\frac{3}{2}}}{|1 + \zeta\cos\theta_{CoM}|} \sigma\ (\theta_{CoM}, \phi_{CoM}\ )\,. \tag{2.8}$$

In the limiting case $m_B \gg m_A$, as $\theta_L = \theta_{CoM}$, the differential cross-sections in the two frames of reference give the same result.

2.2 Potential Scattering Theory

In the potential scattering theory the aim is to relate the scattering amplitude, a theoretical concept, to the differential cross-section which is determined by the scattering experiment. The non-relativistic scattering problem of two particles which interact through a real potential $V(r)$ depending only on their relative coordinate r, becomes simpler as the Hamiltonian of the whole system is split in two parts by a suitable change of coordinates. We recall here the main theoretical results assuming the whole system reaches a stationary state after a long-time action of a steady colliding beam. Let's define H the classical Hamiltonian of the whole system $A + B$ as the sum of the kinetic energies of particles A and B and their interaction potential

$$H = \frac{\mathbf{P_A}^2}{2m_A} + \frac{\mathbf{P_B}^2}{2m_B} + V(\mathbf{r_A} - \mathbf{r_B})\,, \tag{2.9}$$

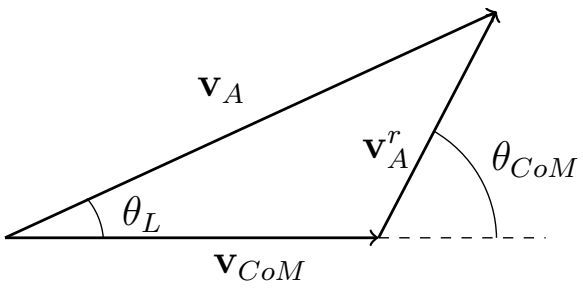

Figure 2.1: This geometrical construction shows the relations between the polar angles θ_L and θ_{CoM} in the *LS* and *CoM* reference systems respectively. The vectors $\mathbf{v}_A$ and $\mathbf{v}_A^r$ are the colliding particle velocities in the *LS* and *CoM* respectively. The center of mass velocity is the vector $\mathbf{v}_{CoM}$. Notice that there is no dependence on the azimuthal angle.

where $\mathbf{r_A}, \mathbf{r_B}, \mathbf{P_A}, \mathbf{P_B}$ are respectively the coordinates and momenta of the particles A, B. Given the usual quantum mechanics prescription for momentum operators in coordinate representation $\mathbf{p_A} \to -i\hbar\nabla_{\mathbf{r_A}}$, $\mathbf{p_B} \to -i\hbar\nabla_{\mathbf{r_B}}$ and solving the time-dependent Schrödinger equation, one gets the following relation for the two-body wave function $\phi(\mathbf{r_A}, \mathbf{r_B})$ [37]

$$\Big[-\frac{\hbar^2}{2m_A}\nabla^2_{\mathbf{r_A}} - \frac{\hbar^2}{2m_B}\nabla^2_{\mathbf{r_B}} + V(\mathbf{r_A} - \mathbf{r_B})\Big]\phi(\mathbf{r_A}, \mathbf{r_b}) = E_{tot}\phi(\mathbf{r_A}, \mathbf{r_B}), \tag{2.10}$$

where E_{tot} is the total energy. As the potential V depends only on the difference of the coordinates, one introduces new suitable coordinates $\mathbf{r}$, $\mathbf{R}$ in the following way

$$\begin{cases} \mathbf{R} = \frac{m_A\mathbf{r_A} + m_B\mathbf{r_B}}{m_A + m_B} \\ \mathbf{r} = \mathbf{r_A} - \mathbf{r_B}\,. \end{cases}$$

Clearly $\mathbf{R}$ is the center of mass coordinate vector, while $\mathbf{r}$ denotes the relative coordinate vector. By means of this change of variables $(\mathbf{r_A}, \mathbf{r_B}) \to (\mathbf{R}, \mathbf{r})$ the Hamiltonian operator $\hat{H}$, see (2.10), becomes

$$\hat{H} = -\frac{\hbar^2}{2M}\nabla^2_{\mathbf{R}} - \frac{\hbar^2}{2\mu_r}\nabla^2_{\mathbf{r}} + \hat{V}(\mathbf{r}), \tag{2.11}$$

where $M = m_A + m_B$ is the total mass of the system and μ_r is the reduced mass of the particles A and B

$$\mu_r = \frac{m_A m_B}{m_A + m_B}\,. \tag{2.12}$$

It is now straightforward to separate the motion of the center of mass and the relative motion of a particle with a reduced mass μ_r in a scattering potential $V(\mathbf{r})$. We search for a complete set of solutions of the following type

$$\phi(\mathbf{R}, \mathbf{r}) = \Phi(\mathbf{R})\psi(\mathbf{r}), \tag{2.13}$$

and we get the following time-independent Schrödinger equations

$$-\frac{\hbar^2}{2M}\nabla^2_{\mathbf{R}}\Phi(\mathbf{R}) = E_{CoM}\Phi(\mathbf{R}), \tag{2.14}$$

and

$$\left(-\frac{\hbar^2}{2\mu_r}\nabla^2_{\mathbf{r}} + V(\mathbf{r})\right)\psi(\mathbf{r}) = E_r\psi(\mathbf{r}), \tag{2.15}$$

with

$$E_{tot} = E_{CoM} + E_r\,. \tag{2.16}$$

Equation (2.14) shows that the center of mass behaves like a free particle of mass M and energy E_{CoM} and (2.15) describes the relative motion of a particle

of reduced mass μ_r and energy E_r in a potential $V(\mathbf{r})$. In a scattering problem the known energy E_r associated with the relative motion, belongs to the continuous spectrum of the Hamiltonian operator $\hat{H}$ and can be related to the energy E of the incoming particles A in the (LS) from the following relation [38]

$$E_r = \frac{m_B}{m_A + m_B} E \,. \tag{2.17}$$

This shows that only a part of the colliding energy E in the (LS) is available for the collision of the so-called "relative "particle. Finally in order to solve the equation (2.15) we need the physical boundary conditions for the scattering problem. Far away from the scattering centre before the collision the motion is that of a free particle of definite initial momentum $\mathbf{p_i}$ that we assume along the z-axis whose origin is the same of the vector $\mathbf{r}$ and where there is the scattering centre. Then the energy dispersion is parabolic

$$E_r = \frac{p_i^2}{2\mu_r} = \frac{\hbar^2 k_i^2}{2\mu_r} \,, \tag{2.18}$$

where the relation between the initial momentum $\mathbf{p_i}$ and the initial wavevector $\mathbf{k_i}$ is

$$\mathbf{p_i} = \hbar \mathbf{k_i} \,. \tag{2.19}$$

We denote the magnitudes of the vectors $\mathbf{p_i}$ and $\mathbf{k_i}$ with p_i and k_i respectively. On the physical basis a particular solution of (2.15), called stationary scattering wavefunction $\psi^{(+)}_{\mathbf{k_i}}$ is assumed to have the following asymptotic boundary condition, valid for $r \to \infty$ where $V(\mathbf{r})$ can be neglected [37]

$$\psi^{(+)}_{\mathbf{k_i}} \simeq \exp(i\mathbf{k_i} \cdot \mathbf{r}) + f(\theta, \phi) \frac{\exp(ik_i r)}{r} \,. \tag{2.20}$$

the angular function $f(\theta, \phi)$ is called the scattering amplitude and the θ, ϕ are the polar and azimuthal angles respectively in a polar coordinate system set up according to the geometric configuration for the scattering events described above. The scattering amplitude is also an energy-dependent function, so it may be written as $f(\theta, \phi\,; E)$ as well. From the relation (2.20) we see that well far away from the localized scattering centre (the target) the scattered wavefunction $\psi^{(+)}_{\mathbf{k_i}}$ is a superposition of the incident plane-wave of the wavevector $\mathbf{k_i}$ and an outgoing spherical wave with an amplitude depending on the direction (θ, ϕ) and decreases with the distance as r^{-1}.

The boundary condition (2.20) holds provided that the scattering potential $V(\mathbf{r})$ goes to zero faster than r^{-1} for $r \to \infty$. Therefore the potential scattering theory cannot be applied to a pure coulombic potential but only for short-

range ones such as the so-called Yukawa potential. Moreover we will consider here only local potentials, i.e., potentials which are diagonal in the coordinate representation

$$\left\langle \mathbf{r}' \right| V \left| \mathbf{r} \right\rangle = V(\mathbf{r})\delta(\mathbf{r}-\mathbf{r}'), \tag{2.21}$$

where δ is the delta function of Dirac. It is worthwhile to observe that in many situations there is no dependence of the scattering upon the azimuthal angle ϕ as the system is axially symmetric about the direction of $\mathbf{k_i}$. This always happen for spherically symmetric potentials, i.e., coulombic-type potentials.

Some considerations are now necessary to explain the use of the plane-wave description for particle states in the formalism above. It is evident from what we said about the boundary conditions of the scattering problem, that the colliding relative particle is not localized in space having a definite momentum during all the scattering process. This is in agreement with the Heisenberg's uncertainty principle. As the incident and scattered waves are spread out over all the space, this picture seems in contrast with our physical idea of a particle traveling towards a scattering centre and then scattered by it along any direction. It is possible to recover this physical picture, building up a normalized wave-packet, i.e. gaussian wave-packet, with an approximate momentum $\mathbf{k_i}$ and finite spatial extent. The calculations using the wave-packet are shown to give the same results of the formalism we have just discussed insofar the spread of the wave-packet due to its time-evolution is small and the momentum is sufficiently well determined [37], [39]. One assumes that the transverse size of the wave-packet is small compared to the size of the region of detection, its longitudinal size is greater than the linear dimension of the the scatterer and eventually the time of the scattering event is not too long. The constrains given by the wave-packet scattering analysis are usually met by most of the experiments [37]. In addition the use of wave-packets has the advantage to avoid the complicated matter of the scattering wavefunctions normalization, as clearly plane-waves and $\psi^{(+)}_{\mathbf{k_i}}$ they are not square integrable [37]. Eventually K. Huang explains the equivalence of the two approaches on a physical basis. When two particles collide, their wavefunctions overlap and both the particles see each other like a plane-wave of definite momentum instead of a well localized wavepacket [40]. We shall discuss the case of time-dependent potential scattering theory in the case of one of the most important and useful result of physics, the so-called the Fermi Golden Rule (FGR), in section 2.6.

2.3 The Scattering Amplitude

The scattering amplitude $f(\theta,\phi)$ contains all our theoretical knowledge and is the brigde between theory and experiments as it can be related to the differential cross-section $\sigma(\theta,\phi)$ via the probability current density $\mathbf{j}(\mathbf{r},t)$. Let us first recall the definition of $\mathbf{j}$ for a general wavefunction $\psi(\mathbf{r},t)$ of a particle of mass m [41]

$$\mathbf{j}(\mathbf{r},t) = -\left(\frac{i\hbar}{2m}\right)\left[\psi^*\nabla\psi - (\nabla\psi^*)\,\psi\right], \tag{2.22}$$

or, equivalently

$$\mathbf{j}(\mathbf{r},t) = \left(\frac{\hbar}{m}\right)\mathrm{Im}\left(\psi^*\nabla\psi\right), \tag{2.23}$$

where ψ^* is the complex conjugate of wavefunction ψ. It should be noted that (2.22) holds only if the potential operator $\hat{V}$ is hermitian operator or equivalently the function V is real [41]. According to the probabilistic interpretation given by Max Born the squared wavefunction gives the probability density ρ which satisfies the following continuity equation

$$\frac{\partial\rho}{\partial t} = -\nabla\cdot\mathbf{j}, \tag{2.24}$$

which assures the conservation of probability. Applying these general results to the stationary scattering wavefunction $\psi^{(+)}_{\mathbf{k_i}}$ and writing the gradient operator ∇ in spherical polar coordinates we find that the current probability density $\mathbf{j}$ along any direction, denoted by the unit vector $\hat{\mathbf{r}}$ can be written as sum of three terms

$$\mathbf{j}\cdot\hat{\mathbf{r}} = (\mathbf{j_{inc}} + \mathbf{j_{out}} + \mathbf{j_{int}})\cdot\hat{\mathbf{r}}, \tag{2.25}$$

where $\mathbf{j_{inc}}$, $\mathbf{j_{out}}$ are the contributions from the incident wave and outgoing spherical wave in $\psi^{(+)}_{\mathbf{k_i}}$ respectively, while $\mathbf{j_{int}}$ is the result of their interference. It can be shown still using a wave-packet description that in any direction, except in the forward direction scattering ($\theta = 0$), the latter gives no contribution to the current probability density due to their destructive intereference [37]. In other words there is no intereference between the incident plane-wave and the outgoing spherical wave for $\theta \neq 0$. Then calculating the flux of the scattered particles through in the differential solid angles $d\Omega$ far away from the scattering centre and dividing it by the incident flux one eventually finds the desired fundamental relations between the scattering amplitude and the cross-sections

$$\sigma(\theta,\phi) = |f(\theta,\phi)|^2, \tag{2.26}$$

and

$$\sigma_{tot} = \int \sigma(\theta,\phi) d\Omega = \int_0^{2\pi} d\phi \int_0^{\pi} |f(\theta,\phi)|^2 \sin\theta d\theta \,. \tag{2.27}$$

For the sake of completeness we conclude this section talking about the reason for which there should be interference in the forward direction ($\theta = 0$) and its important consequence, i.e., the so-called optical theorem or Bohr- Peierls-Placzek relation. Looking at the stationary scattering wavefunction (2.20) it seems there is no depletion of the incident wave after the scattering. Clearly if some scattering events happen the number of the particles in the incident flux shoud be diminished in the forward direction and then in order to conserve the probability there should be an expected intereference between the two wave terms in (2.20) for $\theta = 0$.

We shall recall an important and useful relation in the scattering theory, the optical theorem [37, 39]. Let us write the left-hand side of the equation (2.25) corresponding to the wavefunction $\psi^{(+)}_{\mathbf{k_i}}$ explicitly [37]

$$\mathbf{j}\cdot\hat{\mathbf{r}} = Re\left[A^*A\frac{\hbar}{mi}\left(e^{-ik_i r\cos\theta} + f^*(\Omega)\frac{e^{-ik_i r}}{r}\right)\frac{\partial}{\partial r}\left(e^{ik_i r\cos\theta} + f(\Omega)\frac{e^{ik_i r}}{r}\right)\right], \tag{2.28}$$

where A is the normalization coefficient of the incoming plane wave, i.e.,

$$\psi_{\mathbf{k_i}} = A\exp(i\mathbf{k}_i\cdot\mathbf{r}) \,. \tag{2.29}$$

Then the flux through a unit area normal to the incident unit vector $\hat{\mathbf{k}}_\mathbf{i}$ is given by [37]

$$\mathbf{j}_{inc}\cdot\hat{\mathbf{k}}_i = Re\left[A^*A\frac{\hbar}{mi}\exp(-ik_i z)\frac{d}{dz}\exp(ik_i z)\right] = A^*A\frac{\hbar k_i}{m} \,. \tag{2.30}$$

The outgoing spherical wave alone gives the following probability flux

$$\mathbf{j}_{out}\cdot\hat{\mathbf{r}} = Re\left[A^*A\frac{\hbar}{mi}f^*(\Omega)\frac{\exp(-ik_i r)}{r}\partial_r\left(f(\Omega)\frac{\exp(ik_i r)}{r}\right)\right] . \tag{2.31}$$

If now we neglect terms of higher order in $1/r$, (2.31) can be written [37] as

$$\mathbf{j}_{out}\cdot\hat{\mathbf{r}} = A^*A\frac{\hbar k_i}{m}|f(\Omega)|^2 + \cdots \tag{2.32}$$

Then the interference probability flux defined by the equation (2.25) is

$$\mathbf{j}_{int}\cdot\hat{\mathbf{r}} = Re\left[A^*A\frac{\hbar}{mi}\left(e^{-ik_ir\cos\theta}\partial_r\left(f(\Omega)\frac{e^{ik_ir}}{r}\right)\right)+f^*(\Omega)\frac{e^{-ik_ir}}{r}\partial_r e^{ik_ir\cos\theta}\right], \quad (2.33)$$

which neglecting terms of higher order in $1/r$ again, becomes [37]

$$\mathbf{j}_{int}\cdot\hat{\mathbf{r}} = Re\left[A^*A\frac{\hbar}{mi}\left(ik_if(\Omega)\frac{e^{ik_ir(1-\cos\theta)}}{r}+ik_i\cos\theta f^*(\Omega)\frac{e^{-ik_ir(1-\cos\theta)}}{r}\right)\right]+\cdots \quad (2.34)$$

We wish to study the radial flux in the forward direction ($\theta = 0$). Let us consider an area $r^2\delta\Omega$ centered about the z axis, see Figure 2.2. Now we integrate the intereference term given by (2.34) over the small angular interval sketched in Figure putting all the smoothly varying factors equals to their value at $\theta = 0$, then we obtain [37]

$$\int_{\cos\delta\theta}^{1} d(\cos\theta)\exp[ik_ir(1-\cos\theta)] = i/k_ir + \text{oscillating terms}, \quad (2.35)$$

and recalling that the scattering amplitude is independent of ϕ in the forward direction, we have [37]

$$r^2\int_{\delta\Omega} d\Omega\,\mathbf{j}_{int}\cdot\hat{\mathbf{r}} = -4\pi A^*A\frac{\hbar}{m}\operatorname{Im}f(\theta=0). \quad (2.36)$$

Then the continuity equation $\nabla\cdot\mathbf{j} = 0$ provides

$$r^2\int_{\delta\Omega} d\Omega\,\mathbf{j}\cdot\hat{\mathbf{r}} = 0. \quad (2.37)$$

Now using the equation (2.25), noting that the flux by $\mathbf{j}_{inc}$ is zero, and letting $r\to\infty$ one obtains [37]

$$A^*A\frac{\hbar}{m}\left(k_i\int|f(\Omega)|^2d\Omega - 4\pi\operatorname{Im}f(\theta=0)\right) = 0. \quad (2.38)$$

Finally with the help of (2.27) one finds the following important and useful relation (the optical theorem) [37, 39].

$$\sigma_{tot} = \frac{4\pi}{k_i}\operatorname{Im}f(\theta=0). \quad (2.39)$$

The optical theorem says that the amount of the removed particles in the incident flux by the scattering events in the forward direction which is pro-

portional to $f(\theta = 0)$ is in turn proportional to the total cross-section σ_{tot} as required by the conservation of the probability according to the continuity equation (2.24) that in the stationary case reduces to $\nabla \cdot \mathbf{j} = 0$.

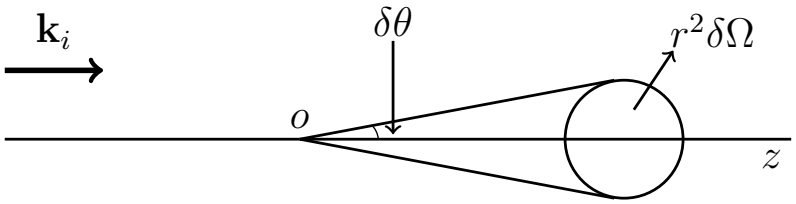

Figure 2.2: Geometrical configuration of the optical theorem.

2.4 The Lippmann-Schwinger Equation

The Lippmann-Schwinger (L-S) equation replaces the original time-independent Schrödinger equation (2.15) with an integral equation for the stationary scattering wavefunction $\psi^{(+)}_{\mathbf{k_i}}$ which also incorporates the boudary condition (2.20) [37][41]. The L-S gives a formal solution to the potential scattering problem; using some approximate methods like the Born series is possible to work out its solutions at any desired perturbation order. Let us define the reduced potential $U(\mathbf{r})$

$$U(\mathbf{r}) = \frac{2\mu_r}{\hbar^2} V(\mathbf{r}) \,. \tag{2.40}$$

This gives the following time-independent Schrödinger equation for the wavefunction $\psi(k, \mathbf{r})$, which is a function of magnitude of the momentum k or equivalently energy

$$\left[\nabla^2 + k_i^2\right] \psi(k, \mathbf{r}) = U(\mathbf{r}) \psi(k, \mathbf{r}) \,. \tag{2.41}$$

Using the standard Green function theory for the differential equation is then possible to find the following integral equation [37] for the solution $\psi^{(+)}_{\mathbf{k_i}}$ of (2.41)

$$\psi^{(+)}_{\mathbf{k_i}}(\mathbf{r}) = \frac{\exp(i\mathbf{k_i} \cdot \mathbf{r})}{(2\pi)^{3/2}} + \int G_0^+(\mathbf{r}, \mathbf{r}') U(\mathbf{r}') \psi^{(+)}_{\mathbf{k_i}}(\mathbf{r}') d\mathbf{r}' \,, \tag{2.42}$$

The previous notation is consistent with the choice of $G_0^+(\mathbf{r}, \mathbf{r}')$, the Green's function, solution of the Helmholtz equation

$$\left[\nabla^2 + k_i^2\right] G_0^+(\mathbf{r}, \mathbf{r}') = \delta(\mathbf{r} - \mathbf{r}') \,. \tag{2.43}$$

$G_0^+(\mathbf{r}, \mathbf{r}')$ can be written explicitly using the boundary condition (2.20) which requires that the stationary scattering wavefunction is an outgoing wavefunction far away from the scattering centre. This is the way that the integral equation

(2.42) contains the boundary condition together with the Schrödinger equation. The Green function then becomes [37]

$$G_0^+(\mathbf{r},\mathbf{r}') = -\frac{1}{4\pi}\frac{\exp\left(ik_i\left|\mathbf{r}-\mathbf{r}'\right|\right)}{\left|\mathbf{r}-\mathbf{r}'\right|}\,. \tag{2.44}$$

Clearly G_0^+ is translationally invariant as it derived from the Hamiltonian of a free particle, moreover is invariant for rotations as well. There is still a technical issue about the normalization of the plane-waves in the derivation of L-S equation. The choice of the normalization for a general plane-wave $\Phi_{\mathbf{k}}$ of wavevector $\mathbf{k}$ is the following

$$\Phi_{\mathbf{k}} = \frac{\exp(i\mathbf{k}\cdot\mathbf{r})}{(2\pi)^{3/2}}\,, \tag{2.45}$$

and introducing the Dirac's bra and ket formalism

$$\Phi_{\mathbf{k}}(\mathbf{r}) \equiv \langle \mathbf{r} \mid \mathbf{k}\rangle = \frac{\exp(i\mathbf{k}\cdot\mathbf{r})}{(2\pi)^{3/2}}\,. \tag{2.46}$$

Then the orthogonality relation between two plane-waves $\Phi_{\mathbf{k}}$ and $\Phi_{\mathbf{k}'}$ of wavevectors $\mathbf{k}$, $\mathbf{k}'$ respectively is

$$\langle \Phi_{\mathbf{k}} \mid \Phi_{\mathbf{k}'}\rangle \equiv \left\langle \mathbf{k} \mid \mathbf{k}'\right\rangle = \delta\left(\mathbf{k}-\mathbf{k}'\right)\,, \tag{2.47}$$

and the closure relation in Dirac's notation becomes

$$\int d\mathbf{k}\,|\mathbf{k}\rangle\,\langle\mathbf{k}| = 1\,. \tag{2.48}$$

The L-S gives only a formal solution of the potential scattering problem as the stationary scattering wavefuntion appears in both sides of (2.42), therefore we need some approximate methods to solve it, for example the Born series. We conclude this section giving an integral expression of the scattering amplitude suitable for the Born series method. Firstly, let us choose the normalization constant $(2\pi)^{-3/2}$ for the expression of $\psi_{\mathbf{k_i}}^{(+)}$ in (2.20) for $r\to\infty$

$$\psi_{\mathbf{k_i}}^{(+)} \simeq \frac{1}{(2\pi)^{-\frac{3}{2}}}\left[\exp(i\mathbf{k_i}\cdot\mathbf{r}) + f(\theta,\phi)\frac{\exp(ik_i r)}{r}\right]. \tag{2.49}$$

Secondly, let us write the final wavevector $\mathbf{k_f}$

$$\mathbf{k_f} = k_f\hat{\mathbf{r}}\,, \tag{2.50}$$

where $\hat{\mathbf{r}}$ is the unit vector which points in the direction of the detector and then

the final wavevector has spherical polar coordinates (k_f, θ, ϕ). The integral representation of the scattering amplitude is [37]

$$f = -\frac{(2\pi)^{3/2}}{4\pi} \int \exp(-i\mathbf{k_f}\cdot\mathbf{r}')U(\mathbf{r}')\psi^{(+)}_{\mathbf{k_i}}(\mathbf{r}')\,d\mathbf{r}'\,, \tag{2.51}$$

or equivalently if we introduce the plane-wave $\Phi_{\mathbf{k_f}}$ corresponding to the final wavevector $\mathbf{k_f}$

$$\Phi_{\mathbf{k_f}}(\mathbf{r}) = \frac{1}{(2\pi)^{-3/2}} \exp(i\mathbf{k_f}\cdot\mathbf{r})\,, \tag{2.52}$$

it can be written as

$$f = -2\pi^2 \left\langle \Phi_{\mathbf{k_f}} \middle| U \middle| \psi^{(+)}_{\mathbf{k_i}} \right\rangle . \tag{2.53}$$

2.5 The Born Approximation

The Born series is a perturbative expansion of the wavefunction $\psi^{(+)}_{\mathbf{k_i}}$, or equivalently of the scattering amplitude f, in powers of the scattering potential. It arises from the attempt to solve L-S equation (2.42) by iteration. Let us consider the free plane-wave $\Phi_{\mathbf{k_i}}$ as the zero order approximation, then the iterative solution is given by the following ansatz

$$\psi^{(+)}_{\mathbf{k_i}}(\mathbf{r}) = \sum_{m=0}^{\infty} \phi_m(\mathbf{r})\,. \tag{2.54}$$

This is the Born series for the scattering wavefunction and its convergence is discussed later. Its terms are given by

$$\phi_0(\mathbf{r}) = \Phi_{\mathbf{k_i}}(\mathbf{r})\,, \tag{2.55}$$

$$\phi_1(\mathbf{r}) = \int G_0^+(\mathbf{r},\mathbf{r}')U(\mathbf{r}')\phi_0(\mathbf{r}')\,d\mathbf{r}'\,, \tag{2.56}$$

$$\vdots$$

$$\phi_n(\mathbf{r}) = \int G_0^+(\mathbf{r},\mathbf{r}')U(\mathbf{r}')\phi_{n-1}(\mathbf{r}')\,d\mathbf{r}'\,, \tag{2.57}$$

$$\vdots$$

The integral representation of the scattering amplitude (2.51) yields the Born series for the scattering amplitude, whose terms are given by

$$f_{B1} = -2\pi^2 \left\langle \Phi_{\mathbf{k_f}} \right| U \left| \phi_0 \right\rangle , \tag{2.58}$$

$$f_{B2} = -2\pi^2 \left\langle \Phi_{\mathbf{k_f}} \right| U \left| \phi_0 + \phi_1 \right\rangle , \tag{2.59}$$

$$\vdots$$

$$f_{Bn} = -2\pi^2 \left\langle \Phi_{\mathbf{k_f}} \right| U \left| \phi_0 + \phi_1 + \cdots + \phi_{n-1} \right\rangle . \tag{2.60}$$

The series terms $f_{B1}, f_{B2}, \cdots, f_{bn}$ are called respectively the first Born approximation, the second Born approximation and so on to the scattering amplitude. The quantity f_{B1} is usually referred to the scattering amplitude in the Born Approximation (BA) . We shall now give the most important results about the BA as it is greatly exploited in the present work. Firstly let us write f_{B1} explicitly

$$f_{B1} = -2\pi^2 \left\langle \Phi_{\mathbf{k_f}} \right| U \left| \Phi_{\mathbf{k_i}} \right\rangle = -\frac{1}{4\pi} \int U(\mathbf{r}) e^{i(\mathbf{k_i} - \mathbf{k_f})\cdot \mathbf{r}} \, d\mathbf{r} , \tag{2.61}$$

then let us define the wavevector transfer $\mathbf{q}$

$$\mathbf{q} = \mathbf{k_i} - \mathbf{k_f} , \tag{2.62}$$

in a way that the momentum transfer in the scattering process is

$$\hbar \mathbf{q} = \hbar \left(\mathbf{k_i} - \mathbf{k_f} \right) = \mathbf{p_i} - \mathbf{p_f} . \tag{2.63}$$

As we consider real potentials here, the scattering is an elastic process and then $|\mathbf{k_i}| = |\mathbf{k_f}| = k$. Therefore the magnitude of the vector $\mathbf{q}$ is

$$q = 2k \sin \frac{1}{2}\theta , \tag{2.64}$$

where θ is the scattering angle, see the Figure 2.3.

Finally using the equation (2.61) we can write the scattering amplitude in Born approximation as

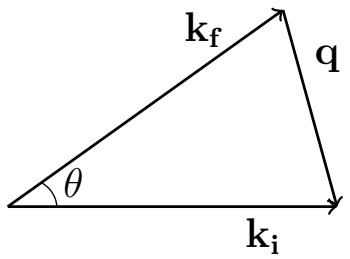

Figure 2.3: The vector $\mathbf{q}$ is the momentum transfer in Born approximation

$$f_{B1}(k,\theta,\phi) = -\frac{1}{4\pi}\int U(\mathbf{r})e^{i\mathbf{q}\cdot\mathbf{r}}\,d\mathbf{r}\,. \tag{2.65}$$

which is evidently proportional to the Fourier transform of the potential corresponding to the momentum transfer $\mathbf{q}$ during the collision.

Then the differential cross-section $\sigma^1(\theta,\phi)$ in BA follows from (2.26)

$$\sigma^1(\theta,\phi) = |f_{B1}|^2\,, \tag{2.66}$$

which shows that in BA there is no difference between an attractive and repulsive potential of the same strength, as $U(\mathbf{r})$ or $-U(\mathbf{r})$ do not make any difference in (2.66). Moreover if we consider a central potential $U(\mathbf{r})$ which is spherically symmetric, choosing the vector $\mathbf{q}$ along the polar axis and performing the angular integrals [2], (2.65) becomes

$$f_{B1}(q) = -\frac{1}{q}\int_0^\infty r\sin(qr)\,U(r)\,dr\,. \tag{2.67}$$

Therefore we conclude that the scattering amplitude for a central potential is real and depends on the scattering angle θ and the wavevector k only via the magnitude of the wavevector transfer q .

Because for a central potential $f_{B1} = f_{B1}^*$, we see that $\mathrm{Im}\, f_{B1}(0) = 0$. Evidently the first Born scattering amplitude does not satisfy the optical theorem. However for the scattering amplitude f_{B2} in second Born approximation there is an important result. In fact the optical theorem in BA gives the total first Born cross-section σ_{tot}^1 via f_{B2} [37]

$$\sigma_{tot}^1 = \frac{4\pi}{k}\,\mathrm{Im}\, f_{B2}(\theta = 0)\,, \tag{2.68}$$

which shows the non-linear character of the optical theorem. This equation is very useful to check the calculations in second Born approximation.

We shall conclude this section giving some important criteria for the convergence of the Born series. A sufficient condition for the convergence at all energies is given by [37]

$$\frac{1}{4\pi}\,max_{(\mathbf{r})}\int\frac{|U(\mathbf{r})|}{|\mathbf{r}-\mathbf{r}'|}\,d\mathbf{r}' < 1\,, \tag{2.69}$$

where $max_{(\mathbf{r})}$ denotes the maximum obtained by varying $\mathbf{r}$. In the case of a

[2] The Jacobian of the spherical coordinates is given by $r^2\sin\theta$.

central potential which satisfies the two following conditions

$$\int_0^\infty r\,|U(r)|\,dr < \infty, \tag{2.70}$$

$$r^2\,|U(r)| \leq M < \infty, \tag{2.71}$$

where M is a positive constant, the inequality (2.69) becomes

$$\int_0^\infty r\,|U(r)|\,dr < 1\,. \tag{2.72}$$

According to Bargmann "*for a central potential U(r) satisfying the conditions* (2.70)-(2.71), *the Born series converges for all energies if the potential* $-|U(r)|$ *does not support any bound state* "[37].

Another sufficient condition for the validity of BA is obtained assuming that the incident plane-wave is slightly distorted by the scattering potential, yielding the following inequality to be satisfied [37]

$$\frac{1}{4\pi}\left|\frac{\exp(ikr')}{r'}U(\mathbf{r}')\exp(i\mathbf{k_i}\cdot\mathbf{r}')\,d\mathbf{r}'\right| \ll 1\,. \tag{2.73}$$

Applying the above inequality to a central potential of strength $|U_0(r)|$ that can be thought as the depth or height of square well or square barrier respectively and range a, which roughly is defined as the distance from the origin such that the effect of the scattering potential can be neglected for values of r larger than a, (2.73) becomes [37]

$$\frac{|U_0(r)|}{4k^2}\left|e^{2ika} - 2ika - 1\right| \ll 1\,. \tag{2.74}$$

In the low energy limit $ka \to 0$ it gives

$$\frac{1}{2}\,|U_0|\,a^2 \ll 1\,, \tag{2.75}$$

and at high energies,

$$\frac{|U_0|\,a}{2k} \ll 1\,, \tag{2.76}$$

The low energy condition (2.75) says the potential $-|U_0(r)|$ is not sufficiently attractive to form bound states.

The previous analysis of the validiy of BA can be applied to short-range po-

tential, i.e., a Yukawa-type potential $V(r)$ [3]

$$V(r) = -\frac{Ze^2}{r}e^{-r/a}, \tag{2.77}$$

where e is the elementary charge and Z is a multiple of e that denotes the product of the charges involve in the interaction. Unfortunately it can be shown that in low energy limit BA is not a good approximation for the potential in (2.77) [37]. This means that more terms in Born series are needed for an accurate evaluation of the scattering amplitude and then the differential cross-section. Instead the good news comes from the calculation of the differential cross-section in BA of (2.77) as it gives the correct differential cross-section for the pure Coulomb potential (Rutherford formula) once we let the range a in (2.77) go to infinity (no screening case). The derivation of Rutherford was classical but he got the same result from the quantum mechanical calculation. The explanation of this fact is that the scattering amplitude may not have negiglible corrections arising from higher order terms in the Born series, but in the case of the pure Coulomb potential these corrections only change the phase of the scattering amplitude [39]. Therefore we conclude that the BA gives the correct differential cross-section $\sigma^c(\theta)$ for the Coulomb potential, that is [37]

$$\sigma^c(\theta) = \frac{Z^2e^4}{16E_r^2}\frac{1}{\sin^4\left(\frac{1}{2}\theta\right)}. \tag{2.78}$$

As expected from BA the formula (2.78) does not depend on the sign of the potential. Moreover the $\sigma^c(\theta)$ is infinite in forward direction $(\theta = 0)$ and also the total cross-section is infinite. The reason is that the pure Coulomb potential is an infinite range potential which goes to zero slowly, like $1/r$ and hence the particles still experience scattering even at great distance from the scattering centre. We should not be concerned about this divergence as in actual physical situations the Coulomb field is always shielded by other charges and becomes a screened Coulomb potential.

2.6 Fermi's Golden Rule

Actually in every real collision process there is a time-dependence, therefore the scattering potential should be considered a time-dependent function $V(\mathbf{r},t)$. Generally we may think that during a scattering event the interaction potential V is switched on at $t = t_0$ and then switched off at a later time $t = t_0 + \Delta t$ remaining constant during the time-interval Δt. Another important case is that

[3] Notice that here the finite range of the potential is roughly a, the screening length.

of an adiabatic interaction. Then the potential can be written as [37]

$$V(\mathbf{r},t) = V(\mathbf{r})\exp(-\varepsilon|t|)\,, \tag{2.79}$$

where we assume that $t_0 = 0$ and ε is a small positive real number. The time-dependent potential scattering theory is formulated through the causal or time-retarded Green's function, also called propagator [37]. Here we are interested in one of most important results of the time-dependent potential theory, the Fermi Golden Rule formula as E. Fermi called it for its uselfulness in solving time-dependent problems. FGR can be simply derived by the standard quantum mechanics time-dependent perturbation theory. Let us assume that the Hamiltonian $\hat{H}$ of a system can be written the following way

$$\hat{H} = \hat{H}_0 + \hat{V}(t)\,, \tag{2.80}$$

where $\hat{H}_0$ is the time-independent Hamiltonian and $\hat{V}$ is small enough to be considered a perturbation. Moreover we assume we know the eigenstates $|n\rangle$ and their eigenvalues E_n of the eigenvalue equation

$$\hat{H}_0|n\rangle = E_n|n\rangle\,, \tag{2.81}$$

then an arbitrary state represented by the ket $|\alpha\rangle$ at time $t_0 = 0$ can be expanded in eigenstates of $\hat{H}_0$

$$|\alpha\rangle = \sum_n c_n(0)|n\rangle\,. \tag{2.82}$$

Due to the time-evolution, the state $|\alpha, t_0 = 0, t\rangle$ at time $t > 0$ can be written as [41]

$$|\alpha, t_0 = 0, t\rangle = \sum_n c_n(t) e^{-iE_n t/\hbar}|n\rangle\,, \tag{2.83}$$

(2.83) says that time-dependence of the expansion coefficients $c_n(t)$ is merely due to the potential $\hat{V}$ time-dependence. This is more evident in the Interaction Picture (I.P) representation of the time evolution of the system [42] . Eventually a coupled system of differential equations is obtained for the $c_n(t)$

$$i\hbar\frac{d}{dt}c_n(t) = \sum_n V_{nm}(t)e^{i\omega_{nm}t}c_m(t)\,, \tag{2.84}$$

where V_{nm} denotes the matrix elements

$$V_{nm} = \langle n|V|m\rangle\,, \tag{2.85}$$

and we define the frequencies ω_{nm} as

$$\omega_{nm} = \frac{E_n - E_m}{\hbar}\,. \tag{2.86}$$

The coupled system of the differential equations (2.84) can be solved exactly for only a few cases. In general one has to resort to approximate solutions using perturbation expansions

$$c_n(t) = c_n^{(0)} + c_n^{(1)} + c_n^{(2)} + \cdots \tag{2.87}$$

where the $c_n^{(k)}$ represent the contribution to the amplitude c_n at the order k in the Dyson's perturbation expansion for the evolution operator in I.P [41]. If at $t_0 = 0$ the system is in one of the eigenstates of $\hat{H}_0$, let us say $|i\rangle$, then it is straightforward to write down explicitly the terms in the series (2.87) as in [41]

$$c_n^{(0)} = \delta_{ni}\,, \tag{2.88}$$

$$c_n^{(1)}(t) = \frac{1}{i\hbar}\int_0^t e^{i\omega_{ni}t'} V_{ni}(t')dt'\,. \tag{2.89}$$

Therefore according to the quantum probabilistic meaning of the squared amplitude, we can say that $\left|c_n^{(1)}(t)\right|^2$ is the probability in first order perturbation theory that at time t the system is in the state $|n\rangle$ or, in other words, that the transition $|i\rangle \to |n\rangle$ has happened. The validity of first order perturbation relies on the fact that these transitions are very small, that is that the initial state $|i\rangle$ is only slightly depleted, $\left|c_i^{(1)}(t)\right|^2 \approx 1$ [43]. Now let us consider a constant perturbation turned on at $t = 0$, i.e.,

$$V(t) = \begin{cases} 0 & \text{for} \quad t < 0\,, \\ V & \text{for} \quad t \gg 0\,, \end{cases} \tag{2.90}$$

assuming that the system is initially in the state $|i\rangle$, then (2.89) gives

$$c_n^{(1)}(t) = \frac{V_{ni}}{E_n - E_i}\left(1 - e^{i\omega_{ni}t}\right)\,, \tag{2.91}$$

and

$$\left|c_n^{(1)}(t)\right|^2 = \frac{4\left|V_{ni}\right|^2}{\left|E_n - E_i\right|^2}\sin^2\left[\frac{(E_n - E_i)\,t}{2\hbar}\right]\,. \tag{2.92}$$

In most of cases of physics of scattering, the final states have energy $E \sim E_n$ and thus they form a continuum of states with nearly the same energy. Let us define the function f from the equation (2.92)

$$f(\omega) = 4\frac{\sin^2(\omega t/2)}{\omega^2}, \tag{2.93}$$

where $\omega = (E_n - E_i)/\hbar$. If for fixed t, the time interval during which the perturbation acts on the system, we plot the function f, see Figure 2.4, we can see that the height of central peak is t^2 and its width is proportional to $1/t$. Thus it becomes evident that $\left|c_i^{(1)}(t)\right|^2 \approx 1$ is appreciable only for the final states that satisfy

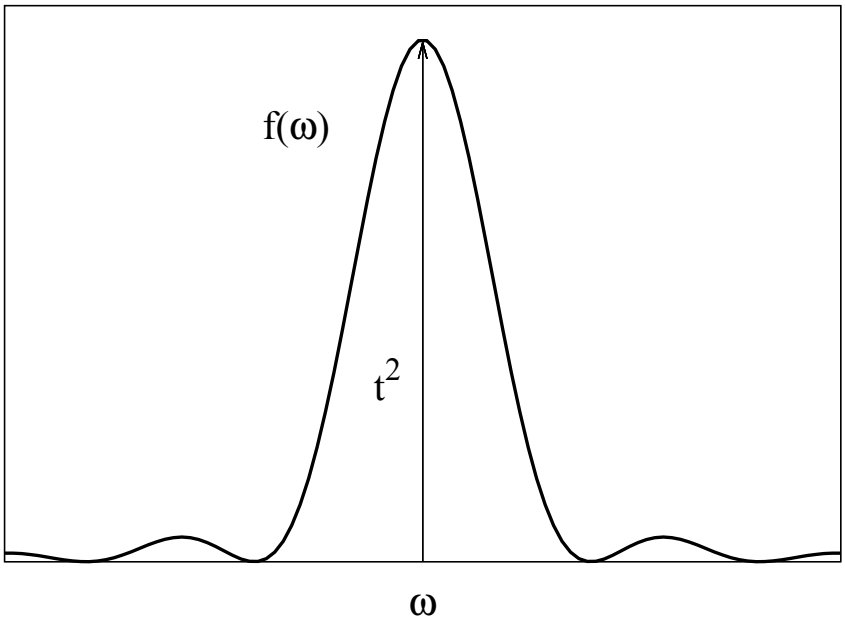

Figure 2.4: The height of the middle peak at $\omega = 0$ is t^2, meanwhile its width is proportional to $1/t$. The zeros of $f(\omega)$ shown in Figure are $\pm 2\pi/t$, $\pm 4\pi/t$.

$$t \sim \frac{2\pi}{|\omega|}. \tag{2.94}$$

If ΔE denotes the energy involved in the transition, then the time-energy uncertainty relation [43] gives

$$t\Delta E \sim \hbar, \tag{2.95}$$

which says that only long time interval perturbations can guarantee energy conservation. In the case of energy conservation processes, i.e., $E_n = E_i$, from (2.92) one obtains

$$\left|c_n^{(1)}(t)\right|^2 = \frac{1}{\hbar^2}|V_{ni}|^2 t^2, \tag{2.96}$$

which is a probability quadratic in time and not linear as we would expect. Apparently this seems an odd result because the transition rate, i.e., the transition probability for unit time becomes proportional to the time interval t during which the perturbation has been turned on. Actually this quadratic dependence is removed if we recall that in most of the realistic situations the final states form a continuous energy spectrum in the neighbourhood of E_i [41]. In fact we need to calculate the transition probabilities summed over the final states with $E_n \simeq E_i$ [41]

$$\sum_{n,\, E_n \simeq E_i} \left| c_n^{(1)} \right|^2 . \tag{2.97}$$

In order to calculate the probability (2.97), we need to introduce the concept of the density of final states (DOS) per unit energy with energy E in the neighbourhood of the initial state energy E_i, denoted by $\rho_f(E)$. The quantity $\rho_f(E)dE$ gives the number of the states with energy in the interval E to $E+dE$, see formula (A.2) in Appendix A for the case of a three-dimensional electron gas. Then we can write [41]

$$\sum_{n,\, E_n \simeq E_i} \left| c_n^{(1)} \right|^2 = \int dE_n \, \rho_f(E_n) \left| c_n^{(1)} \right|^2 , \tag{2.98}$$

which gives

$$\sum_{n,\, E_n \simeq E_i} \left| c_n^{(1)} \right|^2 = 4 \int dE_n \, \rho_f(E_n) \frac{|V_{ni}|^2}{|E_n - E_i|^2} \sin^2 \left[\frac{(E_n - E_i)\, t}{2\hbar} \right] . \tag{2.99}$$

Now letting $t \to \infty$ and recalling the following mathematical relation [41]

$$\lim_{\alpha \to \infty} \frac{1}{\pi} \frac{\sin^2 \alpha x}{\alpha^2 x} = \delta(x) , \tag{2.100}$$

one finds

$$\lim_{t \to \infty} \frac{1}{|E_n - E_i|^2} \sin^2 \left[\frac{(E_n - E_i)\, t}{2\hbar} \right] = \frac{\pi t}{2\hbar} \delta \left(E_n - E_i \right) . \tag{2.101}$$

Within this narrow energy range of the final states, the quantities $\rho_f(E_n)$ and $|V_{ni}|^2$ can be taken constant making the integral in the equation (2.99) easy to solve. Finally one finds

$$\lim_{t \to \infty} \int dE_n \, \rho_f(E_n) \left| c_n^{(1)} \right|^2 = \left(\frac{2\pi}{\hbar} \right) |V_{ni}|^2 \, \rho_f(E_n)\, t , \tag{2.102}$$

where $E_n \simeq E_i$. Then we get the probability per unit time $w_{fi}^{(1)}$ of the transition

from the initial state $|i\rangle$ to the final $|f\rangle$ [37]

$$w_{fi}^{(1)} = \frac{2\pi}{\hbar} \left|V_{fi}\right|^2 \rho_f(E_f)\,. \tag{2.103}$$

The equation (2.103) is the useful Fermi Golden Rule. $w_{fi}^{(1)}$ is also called transition rate. FGR is often written in the following equivalent way [43]

$$w_{fi}^{(1)} = \frac{2\pi}{\hbar} \left|V_{fi}\right|^2 \delta(E_f - E_i)\,, \tag{2.104}$$

where the Dirac delta function implies an integration over a continuum of states $\rho_f(E_f)dE_f$. The transition rates give by FGR are clearly time independent. Moreover from the form (2.104) of the FGR it is evident that in the transitions the final states must have the same energy of the initial state as the Dirac delta function automatically enforces the energy conservation. In order to achieve it in the derivation of the formula (2.104) one assumes that the transition occurs in an infinite time interval t, or formally for $t \to \infty$. At finite times it is found that the spread in energy of final states (the so-called collisional broadening of states) ΔE is given by the following relation [37]

$$\Delta E \simeq \frac{2\pi\hbar}{t}\,, \tag{2.105}$$

that says that the energy is not conserved exactly at short times. In systems where the collision events are very frequent, the limit $t \to \infty$ can no longer be legitimate as the final states may have short lifetime due to the successive scattering event. In this case the Dirac delta function must be replaced by a proper finite energy width function. This effect is called Collisional Broadening and it may be relevant to some semiconductor devices [44]. We conclude this section recalling the important relation between the FGR and the differential cross-section. In a scattering event, there are many final states $\left|\mathbf{k}_f\right\rangle$ with energy $E = \hbar^2 k^2/2m$ corresponding to different directions of the wavevector $\mathbf{k}_f$. If we denote with $\rho_f(E)d\Omega dE$ the number of the states whose $\mathbf{k}_f$ lies within the solid angle $d\Omega$ and whose energy belongs to the interval $(E, E+dE)$, then [4][37]

$$\rho_f(E)d\Omega dE = d\mathbf{k}_f = k^2 dk d\Omega\,, \tag{2.106}$$

or equivalently

$$\rho_f(E) = k^2 dk/dE\,. \tag{2.107}$$

Therefore the transition rate corresponding to the particles scattered within

[4]The formula (2.106) depends on the choice of the normalization , see formula (2.45).

a solid angle $d\Omega$ is given by [37]

$$dw_{fi}^{(1)} = \frac{2\pi}{\hbar} \left|V_{fi}\right|^2 \rho_f(E_f) d\Omega\,, \tag{2.108}$$

and dividing (2.108) by the incident flux with speed v, $\Phi = (2\pi)^{-3} v$, one obtains the differential cross-section σ^1 in the Born approximation corresponding the transition $\mathbf{k}_i \to \mathbf{k}_f$ [37]

$$\sigma^1(\theta,\phi) = \frac{(2\pi)^4}{\hbar v} \left|V_{fi}\right|^2 \rho_f(E_f) d\Omega\,. \tag{2.109}$$

We find finally (using natural units)

$$\sigma^1(\theta,\phi) = \frac{1}{16\pi^2} \left| \int \exp\left(i\Delta\cdot\mathbf{r}\right) U\left(\mathbf{r}\right) d\,\mathbf{r} \right|^2 \tag{2.110}$$

where $\Delta = \mathbf{k_f} - \mathbf{k_i}$.

2.7 Overlap Integrals

In the present work we deal with electrons in a n-type bulk GaAs semiconductor, therefore due to the translational invariance of the crystalline structure, we expect that the electronic states should be Bloch states. We are considering the electrons within a single independent particle approximation consistent with a mean field theory and with the Born-Oppenheimer approximation. Then according to the Bloch theorem the wavefunction $\psi_{n\mathbf{k}}$ of an electron with wavevector $\mathbf{k}$ in an energy band of index n is [45]

$$\psi_{n\mathbf{k}}(\mathbf{r}) = e^{i\mathbf{k}\cdot\mathbf{r}} u_{n\mathbf{k}}(\mathbf{r})\,. \tag{2.111}$$

The Bloch function $u_{n\mathbf{k}}$ has the the same periodicity of the crystal lattice

$$u_{n\mathbf{k}}(\mathbf{r}+\mathbf{l}) = u_{n\mathbf{k}}(\mathbf{r})\,, \tag{2.112}$$

where $\mathbf{l}$ denotes a Bravais Lattice vector [5]. From the previous discussion it is clear that the subject of the scattering rate calculations in semiconductors becomes more complicated than in the free case. Now in general the plane waves are slightly modified by the periodic Bloch functions (2.112), the scattering rates need to include a new factor, the so-called overlap integral $\mathscr{G}$ over the unit cell V_c . Let us consider the scattering of electrons by the lattice. Then

[5]The Bloch theorem is a direct consequence of the abelian structure of the group of the translations [46].

a quantum state $|\alpha\rangle$ of the the electron-lattice system can be written in the following way [27]

$$|\alpha\rangle = |\mathbf{k};n\rangle\,|\mathbf{c}\rangle \tag{2.113}$$

where $|\mathbf{c}\rangle$ denotes a Fock state of the lattice in occupation number formalism of Second Quantization (S.Q) . Phonons are sound waves quantized into bosonic collective excitations. In the spirit of the S.Q the electron-phonon interacting potential which enters in the matrix element of FGR is written as a linear combination of annihilation and creation operators of phonons $\hat{a}_{\mathbf{k}}, \hat{a}^{\dagger}_{\mathbf{k}}$. In the present work we consider two possible interactions of the electrons with the lattice, the electron-acoustic phonon and the electron-polar optical phonon interactions, the latter due to the polar nature of GaAs. In the first case the acoustic deformation potential $\hat{V}_{e-ap}$ [27, 47] is given by

$$\hat{V}_{e-ap} = i\sum_{\mathbf{q}}\sum_{l,j=1}^{3}\left[\frac{\hbar}{2\rho_m V\omega_q}\right]^{1/2}\left(\hat{a}_{\mathbf{q}} + \hat{a}^{\dagger}_{-\mathbf{q}}\right)e^{i\mathbf{q}\cdot\mathbf{r}}\mathscr{E}_{lj}q_l\xi_j\,, \tag{2.114}$$

where V is the crystal volume, ρ_m the mass density of the GaAs, ω_q the phonon angular frequency relative to mode q, ξ its polarization vector and $\mathscr{E}_{lj}$ is a stress tensor which gives the shift of the electronic band per unit deformation due to the propagation of the acoustic waves in the semiconductor. The interaction with polar optical phonons (POP) is determined by the potential $\hat{V}_{e-pop}$ from the so-called Fröhlich Hamiltonian [47], i.e.,

$$\hat{V}_{e-pop} = i\left(\frac{\hbar e^2\omega_{LO}}{2V}\right)^{1/2}\left[\frac{1}{\varepsilon_0\left(\varepsilon_\infty - \varepsilon_b\right)}\right]^{1/2}\sum_{\mathbf{q}}\frac{1}{q}\left(\hat{a}_{\mathbf{q}}e^{i\mathbf{q}\cdot\mathbf{r}} + \hat{a}^{\dagger}_{-\mathbf{q}}e^{-i\mathbf{q}\cdot\mathbf{r}}\right), \tag{2.115}$$

where ω_{LO} is the longitudinal POP mode frequency, ε_0 is the vacuum permittivity, ε_∞ is the high-frequency dielectric constant, ε_b is the static dielectric constant and the dielectric constants are related via the so-called Lyddane-Sachs-Teller relation [32]

$$\frac{\varepsilon_b}{\varepsilon_\infty} = \frac{\omega_{LO}^2}{\omega_{TO}^2}\,. \tag{2.116}$$

where ω_{TO} is the transverse POP mode frequency. The numerical values of these constants together with other important GaAs parameters are given in the table in Appendix A.

Fermi's Golden Rule applied to electronic systems in crystalline lattice gives for a general potential $\hat{V}$ provides the following scattering rate [27]

$$w\left(\mathbf{k},c;\mathbf{k}',c'\right) = \frac{(2\pi)^4}{\hbar V^2}\left|\mathscr{G}\sum_{q}\left\langle c'\right|\hat{V}\left|c\right\rangle\right|^2\delta\left[E\left(\mathbf{k}',c'\right) - E\left(\mathbf{k},c\right)\right], \tag{2.117}$$

where $\mathscr{G}$ denotes the so-called overlap integrals [6]

$$\mathscr{G}(\mathbf{k_f}, \mathbf{k_i}) = \int_{V_c} u^*_{n'\mathbf{k_f}}(\mathbf{r}) u_{n\mathbf{k_i}}(\mathbf{r}) e^{i\mathbf{G}\cdot\mathbf{r}}\, d\,r\,. \tag{2.118}$$

$\mathbf{G}$ is a reciprocal lattice vector. Here $n' = n$ as we consider only intravalley scattering events. The collisions in which $\mathbf{G} = 0$ are called normal processes (or "N "processes) meanwhile in the other case they are called Umklapp processes (or "U "processes). In general the latter are negiglible in semiconductors and especially in GaAs [32]. Therefore in principle in our simulations of carriers in n-GaAs we should deal with the following overlap integrals of Bloch functions

$$\mathscr{G}(\mathbf{k_f}, \mathbf{k_i}) = \int_{V_c} u^*_{n\mathbf{k_f}}(\mathbf{r}) u_{n\mathbf{k_i}}(\mathbf{r})\, d\,\mathbf{r}\,. \tag{2.119}$$

The calculations of these integrals is very important in the electron collisions in solids and the band-to-band Auger recombination in semiconductors [48]. In some cases the calculations can be performed using only the information from the energy gap and the effective mass provided by the semiconductor band-structure avoiding the use of some approximation for the modulating parts of the Bloch functions [48].

In general the calculations of these integrals depend upon the magnitude and direction of $\mathbf{k_f}$ and $\mathbf{k_i}$ in reciprocal space. As in this study we shall consider only the electronic dynamics in a neighbourhood of the centre of the Brillouin Zone (BZ) , it results that [32]

$$\mathscr{G}(\mathbf{k_f}, \mathbf{k_i}) = 1\,. \tag{2.120}$$

This happens because the periodic Bloch functions do not vary rapidly with $\mathbf{k}$ in that region, i.e., $u_{\mathbf{k}} \approx u_{\mathbf{k}+\mathbf{q}}$ with $|\mathbf{q}|$ small. In general it can be shown that the integrals (2.119) have values smaller than unity [27, 48].

[6] Notice that the functions $u_{n\mathbf{k}}(\mathbf{r})$ are normalized over the unit cell.

Chapter 3

Screened Coulomb Interaction in RPA

When physicists study condensed matter systems, they have to tackle a huge number of interacting particles. This is referred to as "the many-body problem ". At first sight it seems an almost impossible task to solve, even considering just a classical system of three interacting particles. For the latter the mathematical-physicist Henry Poincaré showed that in general there is no analytical solution. Instead in solids it is found that many systems of interacting particles can be mapped into systems of weakly interacting (or non-interacting) fictitious bodies called elementary excitations of the system and then the methods of nonrelativistic quantum field theory QFT and density functional theory (DFT) can often be applied successfully to solve the many-body problem [49]. The elementary excitations can be quasiparticles, i.e. quasi-electrons, Majorana fermions [50], etc or collective excitations like plasmons, phonons, etc that involve collective motions of all particles in the system. Quasi-particles can be thought like the real individual particles ("bare "particles) of the system in study surrounded by a cloud that screens them [49]. Then quasi-particles are in general characterized by an effective mass, different from the bare mass, and a lifetime. According to this physical picture of a many-body system one realizes that also the interparticle interaction potential becomes different from the bare potential, usually screened or, defined in a more appealing term, "renormalized ". In the present chapter we shall give the main theoretical results of Linear Response Theory (LRT) [51] that help us to determine the renormalized interaction potential in the Random Phase Approximation (RPA) [51]. LRT can be applied to any physical system insofar its premises hold. One of its most important results for an electron gas in RPA is the dielectric function. In the last part of the chapter we will present the Thomas-Fermi approximation which gives a very good approximation of the dielectric func-

tion in the case of the long-wavelength limit [52, 53]. Finally the theoretical results will be applied to a n-type GaAs semiconductor.

3.1 Linear Response Theory in a Nutshell

If we observe a physical system on which a small perturbation, for example an external electrostatic potential, is acting we can gain some useful information about the system itself. Linear Response Theory allows us to get this information via "linear response functions "which depend on the properties of the unperturbed system. Let us consider a system described by a time-independent Hamiltonian $\hat{H}$ on which acts an external time-dependent field $F(t)$. Moreover $F(t)$ couples linearly to an observable $\hat{B}$, so that we can define the following total Hamiltonian $\hat{H}_F$

$$\hat{H}_F(t) = \hat{H} + F(t)\hat{B}\,. \tag{3.1}$$

Let $\hat{A}$ be another observable of the system. Its equilibrium thermal average value $\langle\hat{A}\rangle_0$ up to the time t_0 is

$$\langle\hat{A}\rangle_0 = \sum_n P_n \left\langle \psi_n \middle| \hat{A} \middle| \psi_n \right\rangle , \qquad t \leq t_0\,, \tag{3.2}$$

where $|\psi_n\rangle$ are the eigenstates of the total Hamiltonian $\hat{H}$ relative to the eigenvalues E_n, and P_n are their occupation probabilities given by

$$P_n = \frac{e^{-\beta E_n}}{Z}\,, \tag{3.3}$$

where $\beta = 1/k_B T$, k_B is the Boltzmann constant, T is the temperature of the system and Z is the usual partition function

$$Z = \sum_n e^{-\beta E_n}\,. \tag{3.4}$$

Now if we apply the external perturbation we may ask how much the expectation value $\langle\hat{A}\rangle_F(t)$ of the observable $\hat{A}$ at time t later than t_0 differs from the above equilibrium average (3.2). At first order in the perturbative expansion of the time-evolution operator in powers of $F(t)$ it is found [51]

$$\langle\hat{A}\rangle_F(t) - \langle\hat{A}\rangle_0 = -\frac{i}{\hbar}\int_{t_0}^{t} \left\langle \left[\hat{A}(t), \hat{B}(t')\right] \right\rangle_0 F(t')\,dt'\,, \tag{3.5}$$

where the time-dependent operators $\hat{A}$, $\hat{B}$ are in the Heisenberg picture and $\left[\hat{A}, \hat{B}\right]$ is the usual commutator of two operators. Then the retarded or causal

linear response function χ_{AB} is defined by [51]

$$\chi_{AB}(\tau) = -\frac{i}{\hbar}\Theta(\tau)\left\langle\left[\hat{A}(\tau),\hat{B}\right]\right\rangle_0, \tag{3.6}$$

where $\tau = t - t' > 0$ and $\Theta(\tau)$ is the Heaviside step-function. Then the linear response at first order $\hat{A}_1(t)$ for the observable $\hat{A}$ due to the the system invariance for time-tranlation can be written as [51]

$$\begin{aligned}\hat{A}_1(t) &= \langle\hat{A}\rangle_F(t) - \langle\hat{A}\rangle_0 \\ &= \int_0^{t-t_0}\chi_{AB}(\tau)F(t-\tau)\,d\tau,\end{aligned} \tag{3.7}$$

As there is no dependence on the initial time t_0 in (3.7), provided that the perturbation goes to zero for $t \to -\infty$, then it is possible to write the linear response in the following way [51]

$$\hat{A}_1(t) = \int_0^{\infty}\chi_{AB}(\tau)F(t-\tau)\,d\tau. \tag{3.8}$$

In the case of a periodic perturbing potential $F(t)$ with an adiabatic switching-on $e^{\eta_0 t}$ where η_0 is positive quantity then we can write

$$F(t) = F_\omega e^{-i(\omega+i\eta_0)t} + c.c, \tag{3.9}$$

where F_ω is a complex number amplitude and $c.c$ stands for complex conjugate. Therefore in this case $\hat{A}_1(t)$ becomes

$$\hat{A}_1(t) = \chi_{AB}(\omega)F_\omega e^{-i\omega t} + c.c, \tag{3.10}$$

where $\chi_{AB}(\omega)$ the Fourier transform of the response function, i.e.

$$\chi_{AB}(\omega) = -\frac{i}{\hbar}\lim_{\eta_0\to 0}\int_0^{\infty}\left\langle\left[\hat{A}(\tau),\hat{B}\right]\right\rangle_0 e^{i(\omega+i\eta_0)\tau}\,d\tau, \tag{3.11}$$

Extending the frequency ω to the complex plane, due to the fact that χ_{AB} is analytic in the upper half complex ω-plane, the following important relation is found [51]

$$\chi_{AB}(\omega) = -\frac{i}{\pi}\mathscr{P}\int_{-\infty}^{\infty}\frac{\chi_{AB}(\nu)}{\omega-\nu}\,d\nu, \tag{3.12}$$

where $\mathscr{P}$ is the principal part of the integral in the Cauchy sense. The equation (3.12) is called Kramers-Krönig (K-K) dispersion relation and it is generally written using the real part $\Re e\chi_{AB}(\omega)$, also called polarizability, and the immaginary $\Im m\chi_{AB}(\omega)$, also called absorption, of the causal response function

respectively

$$\Re e\chi_{AB}(\omega) = \frac{2}{\pi}\mathscr{P}\int_0^\infty \frac{\nu\Im m\chi_{AB}(\nu)}{\nu^2-\omega^2}\,d\nu\,, \tag{3.13}$$

and

$$\Im m\chi_{AB}(\omega) = -\frac{2\omega}{\pi}\mathscr{P}\int_0^\infty \frac{\Re e\chi_{AB}(\nu)}{\nu^2-\omega^2}\,d\nu\,, \tag{3.14}$$

The analytic properties of χ_{AB} ensure the causality which means no response before there is a perturbation. This is clearly evident in the definition of χ_{AB} itself, see (3.6), as it contains the temporal step-function $\Theta(t)$.

3.2 The Jellium Model for the Electron Gas

In the present work we study the dynamics of the electrons in the conduction band (CB) of a n-type bulk III-V semiconductor. Therefore the electrons move in a positive background provided by the host semiconductor which in turn due to its bandstructure renormalizes their bare mass m_e and their Coulomb interaction. In the case of GaAs which is a direct band gap semiconductor, see Figure 3.1, the effective electron mass m^* is determined by the curvature of the bandstructure, that is by the inverse effective-mass tensor [27]

$$\left(\frac{1}{m^*}\right)_{ij} = \frac{1}{\hbar^2}\left(\frac{\partial^2 E(\mathbf{k})}{\partial k_i \partial k_j}\right), \tag{3.15}$$

where $E(\mathbf{k})$ is the energy-wavevector relationship given by the semiconductor bandstructure $E-k$ diagram as in Figure 3.1. Here we consider the electron dynamics in the Γ-valley only, that is around the symmetry point Γ in BZ. Around the minimum Γ we can assume a parabolic dispersion relation for E versus $\mathbf{k}$

$$E(\mathbf{k}) = \frac{\hbar^2 k^2}{2m^*}\,, \tag{3.16}$$

that gives a scalar effective mass, $m^* = 0.067m_e$ in the case of GaAs.

It is also possible to include the nonparabolicity of the valley trough the Kane relation [27]

$$\frac{\hbar^2 k^2}{2m^*} = E\,(1+\alpha E)\,, \tag{3.17}$$

In the case of the Γ valley, the nonparabolicity parameter α is given by [27]

$$\alpha = \frac{1}{E_g}\left(1-\frac{m^*}{m_e}\right). \tag{3.18}$$

The numerical values of the energy gap E_g and α can be found in Appendix A.

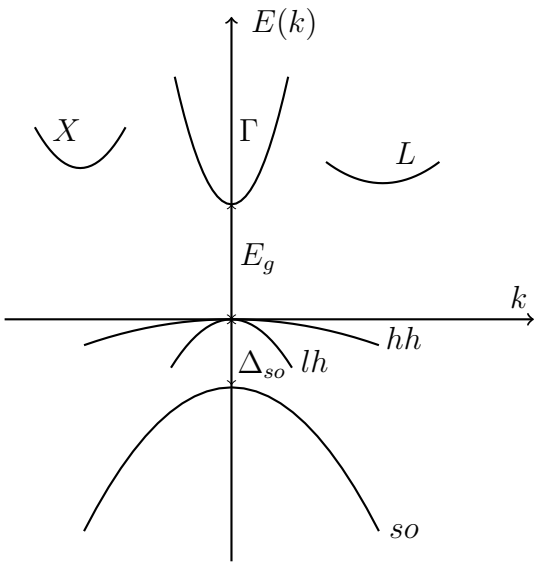

Figure 3.1: Schematic Bandstructure of bulk GaAs. The figure shows the energy valleys Γ, *L*,*X* in CB. The Γ valley in the centre of the BZ, the *L* valley is along the direction $< 111 >$ and the *X* valley is along the direction $< 100 >$. The bands for holes are also shown: heavy hole (*hh*) valence band, light hole (*lh*) valence band and split-off (*so*) band . The values of the energy gap E_g , the spin-orbit splitting Δ_{so} and other relevant parameters are given in the table A.1 in Appendix A

The bare Coulomb interaction is reduced from its value in the free space by the static dielectric constant or relative permittivity ε_b. These modifications of the bare mass and the interelectronic potential due to the semiconductor lattice, in the first approximation allow us to ignore the structure of the host semiconductor and imagine an electron gas moving in a smeared-out homogeneous positive charge background. This is the so-called jellium model. It is translationally invariant. This model, suitable for an ideal metal, together with the random phase approximation is widely used for Ensemble Monte Carlo (EMC) simulations, see [27]. Even though it is a very simple model, it is used successfully for semiconductor systems [51].

The Hamiltonian for a jellium model of *N* electrons which interact via Coulomb potential is [51]

$$\hat{H} = \sum_i \frac{\hat{P}_i}{2m^*} + \frac{1}{4\pi\varepsilon} \sum_{i \neq j} \frac{e^2}{\left|\hat{\vec{r}}_i - \hat{\vec{r}}_j\right|} + \hat{H}_{e-b} + \hat{H}_{b-b}\,, \tag{3.19}$$

where $\varepsilon = \varepsilon_b \varepsilon_0$ is the permittivity. The first term gives the kinetic energy of the electronic system, the second term gives the interaction between the electrons through a bare Coulomb potential, finally $\hat{H}_{e-b}$ and $\hat{H}_{b-b}$ give the electron-background and background-background interactions respectively. We do not

need here to write them explicitly, meanwhile it is worthwhile to note that due to the long range Coulomb interaction, H_{e-b} and H_{b-b} diverge. The procedure to remove this unpleasant problem is named Coulomb interaction regularization [51]. In this procedure at the beginning one assumes that a Coulomb interaction of Yukawa form with a finite range, namely δ^{-1}, then the Hamiltonian (3.19) is rewritten according to this assumption. Then it can be shown that in the thermodynamic limit $V \to \infty$ and after taking the limit $\mu \to 0$, the $q = 0$ component of the electronic electron-electron interaction Hamiltonian H_{e-e}, see the second term in the equation (3.20) below, cancels the last two divergent terms out exactly. The Coulomb interaction regularization gives the following Hamiltonian for jellium model in S.Q [51]

$$\hat{H} = \sum_{\mathbf{k}\sigma} \frac{\hbar^2 k^2}{2m^*} \hat{c}^\dagger_{\mathbf{k}\sigma} \hat{c}_{\mathbf{k}\sigma} + \frac{e^2}{2\varepsilon V} \sum_{\mathbf{q}\neq 0} v_q \sum_{\mathbf{k}_1\sigma_1, \mathbf{k}_2\sigma_2} \hat{c}^\dagger_{\mathbf{k}_1+\mathbf{q}\sigma_1} \hat{c}^\dagger_{\mathbf{k}_2-\mathbf{q}\sigma 2} \hat{c}_{\mathbf{k}_2\sigma_2} \hat{c}_{\mathbf{k}_1\sigma_1} \,, \tag{3.20}$$

where $v_q \propto 1/q^2$ is the Fourier component of wavevector $\mathbf{q}$ of the bare Coulomb potential (see Appendix B) and $\hat{c}^\dagger_{\mathbf{k}\sigma}$, $\hat{c}_{\mathbf{k}\sigma}$ are the fermionic creation and annihilation operators respectively, of a particle with momentum $\hbar\mathbf{k}$ and σ the z-component of the spin in units of $\hbar/2$ [1].

For the jellium model, there are two important quantities which can give us a lot of information about the behaviour of the system itself, one is the average distance between two electrons and the second one, defined in the case of weakly interacting electrons, is the Fermi wavevector. The effective Bohr radius a^*_b is defined by [51]

$$a^*_0 = \frac{4\pi\varepsilon_b\varepsilon_0\hbar^2}{m^* e^2} = \frac{\varepsilon_b}{(m^*/m_e)} a_0 \,. \tag{3.21}$$

where a_0 is the Bohr radius [2]. From Table A.1 $a^*_0 = 192.5 a_0 = 101.9\mathring{A}$.

Then the average distance between two electrons can be express by the dimensionless parameter r_s in effective Bohr radius units from the following relation [51]

$$\frac{1}{n_e} = \frac{4\pi}{3} (r_s a^*_0)^3 \,, \tag{3.22}$$

being n_e the electron density. The parameter r_s against electronic densities of interest at $T = 300K$ for GaAs is plotted in Figure 3.2. The importance of this parameter is due to the fact that it can be shown, that it is roughly the ratio of the average potential energy to the average kinetic energy of the system

[1] The single-particle normalized wave function corresponding to the state $|\mathbf{k}\sigma\rangle$ can be written as $\phi_\sigma(r,s) = \frac{1}{\sqrt{V}} e^{i\mathbf{k}\cdot r} \delta_{s\sigma}$.

[2] The Bohr radius is given by $a_0 = \frac{4\pi\varepsilon_b\varepsilon_0\hbar^2}{m^* e^2} = 0.529\mathring{A}$ [43].

[51]. Therefore r_s estimates the coupling strength and in particular we can distinguish two limiting regimes. When r_s is small the kinetic energy rules the physics and therefore the system behaves like a non-interacting Fermi gas; in the opposite case the potential energy dominates the kinetic energy and the system behaves like a classical ensemble of charged particles. In this case the system becomes highly non-uniform and for some critical values of r_s, which depend on the physical system under study, can give rise to a crystalline state, named Wigner crystal [54].

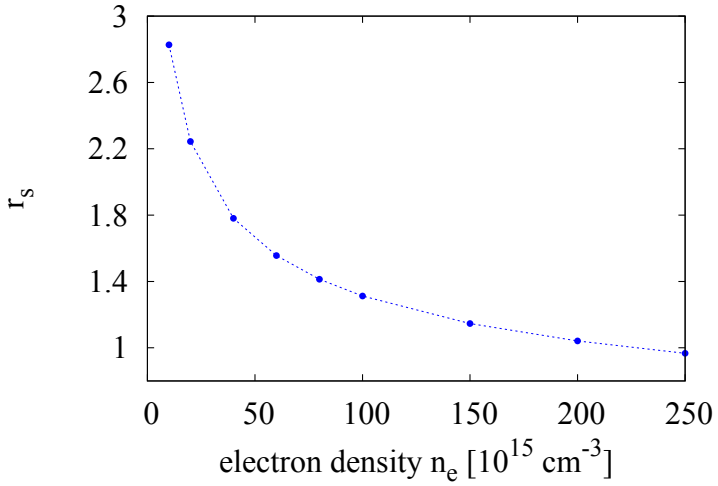

Figure 3.2: The parameter r_s against electronic densities of interest at $T = 300K$ for GaAs.

We conclude this section recalling the important concepts of Fermi sphere and Fermi wavevector k_F of an ideal Fermi gas whose Hamiltonian is given by the first term of equation (3.20). Its ground state is built from a Slater determinant of lowest energy single particle states labelled by their wavevector $\mathbf{k}$ and spin σ. Due to the Pauli exclusion principle, they form a sphere in wavevector space, named Fermi sphere, of radius k_F , whose relation with the electron density in the paramagnetic state, i.e., equal number of up and down spins, is given by [51]

$$k_F = \left(3\pi^2 n\right)^{\frac{1}{3}} . \tag{3.23}$$

k_F is called Fermi wavevector. This spatially homogeneous state is often referred to as the paramagnetic Fermi sea.

Another important useful concept for an ideal electron gas is the Fermi temperature T_F , given by

$$E_F = k_B T_F , \tag{3.24}$$

where the Fermi energy E_F is given by an $E = \hbar^2 k_F^2 / 2m^*$ and k_B is the Boltz-

mann constant. For an electron gas at equilibrium at a certain temperature T, a comparison of T with T_F can give information about which statistics better describes the system. Then we can state that an electronic system behaves like a classical (nondegenerate regime) or quantum gas (degenerate regime) when $T \gg T_F$ and $T \ll T_F$ respectively.

3.3 The Lindhard Function

Now we consider an (noninteracting) electron gas in the GaAs conduction band. We wish to apply the previous results of Linear Response Theory to this physical system. Let $\hat{A}$ and $\hat{B}$ be two operators, then we can calculate the expectation value of $\hat{A}$ when there is a time-dependent perturbation $F(t)$ which couples linearly to $\hat{B}$. The total Hamiltonian is then

$$\hat{H}(t) = \hat{H}_0 + F(t)\hat{B}, \tag{3.25}$$

where $\hat{H}_0$ is the first term in equation (3.20). Then in this case the Fourier transform of the linear response function $\chi^0_{AB}(t)$ is given by [51]

$$\chi^0_{AB}(\omega) = \sum_{\alpha\beta} \frac{n_\alpha - n_\beta}{\hbar\omega + E_\alpha - E_\beta + i\hbar\eta} A_{\alpha\beta} B_{\beta\alpha}\,. \tag{3.26}$$

Here n_α, n_β denote the average occupation probabilities of single particle state labelled by α and β respectively [3], given by Fermi-Dirac statistics. $A_{\alpha\beta}$, $B_{\beta\alpha}$ are the matrix elements of the operators $\hat{A}$ and $\hat{B}$ and finally E_α and E_β are the energies of the states labelled by α, β respectively.

We are interested in the calculation of the density-density response function for a homogeneous non-interacting paramagnetic electron gas which describes the response of the expectation value of the number density operator at position $\vec{r}$

$$\hat{n}(\vec{r}) = \sum_i \delta(\vec{r} - \vec{r}_i)\,, \tag{3.27}$$

when a scalar potential $V_{ext}(\vec{r'},t)$ couples linearly to the density operator $\hat{n}(\vec{r'})$ at a point $\vec{r'}$. In order to do this we can use the equation (3.26) once we identify$\hat{A}$, $\hat{B}$ with $\hat{n}_{\vec{q}}$ and $\hat{n}_{-\vec{q}}$ respectively being the latters the Fourier transforms of the density operator written in S.Q. Then one finds the so-called Lindhard function

[3] The Fermi-Dirac distribution gives the average occupation probability $n_\alpha = \frac{1}{e^{\beta(E_\alpha - \mu)}+1}$ where E_α is the energy of the state $|\alpha\rangle$, μ the chemical potential and $\beta = k_B T$ where T is the temperature.

$\chi^{(0)}_{nn}$ [51]

$$\chi^{(0)}_{nn}(q,\omega) = \frac{1}{V}\sum_{\vec{k}\sigma}\frac{n_{\vec{k}\sigma} - n_{\vec{k}+\vec{q}\sigma}}{\hbar\omega + E_{\vec{k}\sigma} - E_{\vec{k}+\vec{q}\sigma} + i\hbar\eta}\,. \tag{3.28}$$

which depends upon the wavevector $\vec{q}$ only through its magnitude q. We shall denote it simply as $\chi_0(q,\omega)$. The analytical expression for $T = 0$ was derived by Lindhard in 1954, see [49]. We shall give the expression for the Lindhard function at finite temperature $\chi_0(q,\omega,T)$, firstly derived by Maldague for the case of a two-dimensional gas [55]. The real part $\Re e\chi_0$ and immaginary part $\Im m\chi_0$ can be found for example in [51] and for the three-dimensional gas are

$$\frac{\Re e\chi_0(q,\omega,T)}{N(0)} = -\int_0^\infty dx \frac{F(x,T)}{2\bar{q}}\left(\ln\left|\frac{x-v_-}{x+v_+}\right| - \ln\left|\frac{x-v_+}{x+v_+}\right|\right), \tag{3.29}$$

$$\frac{\Im m\chi_0(q,\omega,T)}{N(0)} = -\frac{\pi}{2}\left(\frac{\omega}{qv_F} + \frac{k_BT}{\hbar qv_F}\ln\frac{1+e^{\beta\left[v_-^2E_F-\mu\right]}}{1+e^{\beta\left[v_+^2E_F-\mu\right]}}\right), \tag{3.30}$$

where we have introduced the following function $F(x,T)$

$$F(x,T) = \frac{x}{e^{\beta\left[x^2E_F-\mu\right]}+1}\,, \tag{3.31}$$

and the total density of states per unit volume at the Fermi energy for a non-interacting electron gas $N(0)$

$$N(0) = \frac{mk_F}{\pi^2\hbar^2}\,, \tag{3.32}$$

and finally the useful dimensionless quantities $\bar{q}$ and $v_\pm$ are given respectively by

$$\bar{q} = \frac{q}{k_F}\,, \tag{3.33}$$

$$v_\pm = \frac{\omega}{qv_F} \pm \frac{q}{2k_F}\,, \tag{3.34}$$

$v_F = \frac{\hbar k_F}{m^*}$ being the Fermi velocity . The implementation of $\chi_0(q,\omega,T)$ is described in Appendix B. The plots of $-\frac{\chi_0(q,\omega,T)}{N(0)}$ for temperatures $T = 5, 77, 300\,K$ and $q = 0.5k_F$ are shown in Figures 3.3, 3.4, 3.5 respectively. We notice that the functions $\Re e\chi_0$ and $\Im m\chi_0$ flatten increasing the temperature T. This happens because at finite temperature the Fermi-Dirac distribution is smeared out over an interval of width kB/T around the Fermi energy [64].

The immaginary part of $\chi_0(q,\omega,T)$ differs from zero only in the shaded region in the plane (q,ω), see Figure 3.6, whose boundaries are defined in Appendix B. This region is called the electron-hole continuum and it relates to the

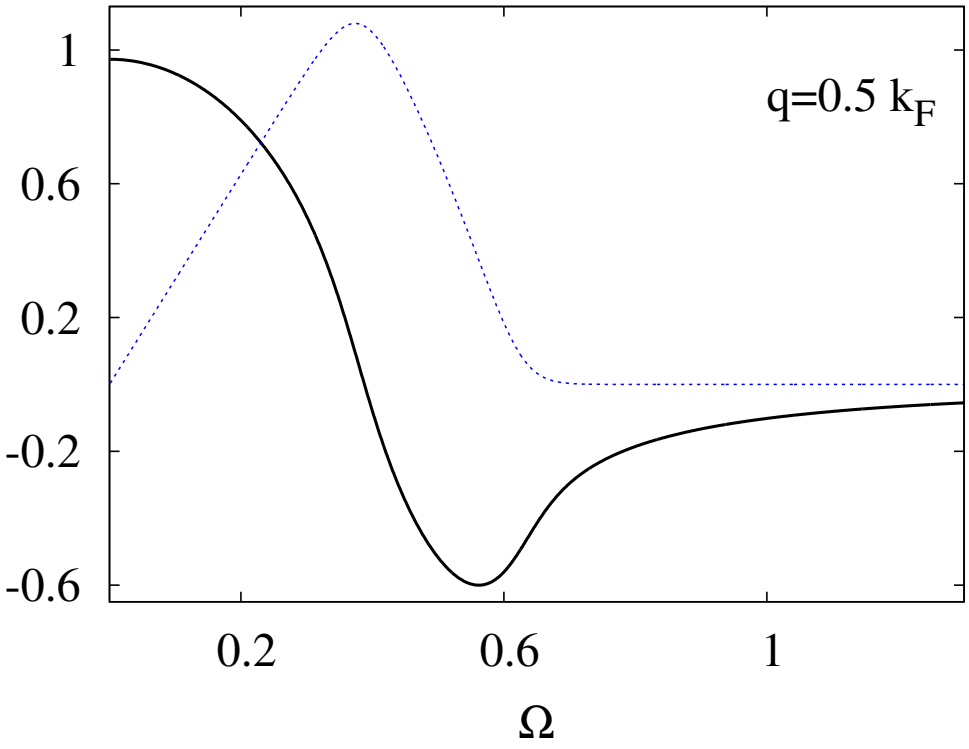

Figure 3.3: The real part (black line) and immaginary part (blue line) of $-\frac{\chi_0(q,\omega,T)}{N(0)}$ against the dimensionless variable $\Omega = \frac{\hbar\omega}{2E_F}$ for n-GaAs at electron density $n_e = 2.8 \times 10^{16}\ cm^{-3}$ and $T = 5K$ ($T_F = 58.2K$).

electron-hole excitation energies.

3.4 The Dielectric Function for the Interacting Electron Gas in RPA

Let us now consider an interacting electron gas. An external electron which moves fast or an external pointlike single charge impurity gives rise to a perturbing potential $V_{ext}(\vec{r},t)$. As a consequence the density deviates from its equilibrium value. The resulting screened potential $V_{sc}(\vec{r},t)$ that affects a test charge for a homogeneous interacting electron liquid within the random phase approximation, is given by [51]

$$V_{sc}(q,\omega) = \frac{V_{ext}(q,\omega)}{\varepsilon(q,\omega)}. \tag{3.35}$$

Here $\varepsilon(q,\omega)$ [4] denotes the dielectric function in RPA defined by the following equation

$$\varepsilon(q,\omega) = 1 - v_q \chi_0(q,\omega), \tag{3.36}$$

[4] We may also write $\varepsilon(q,\omega,T)$ if temperature dependence is included.

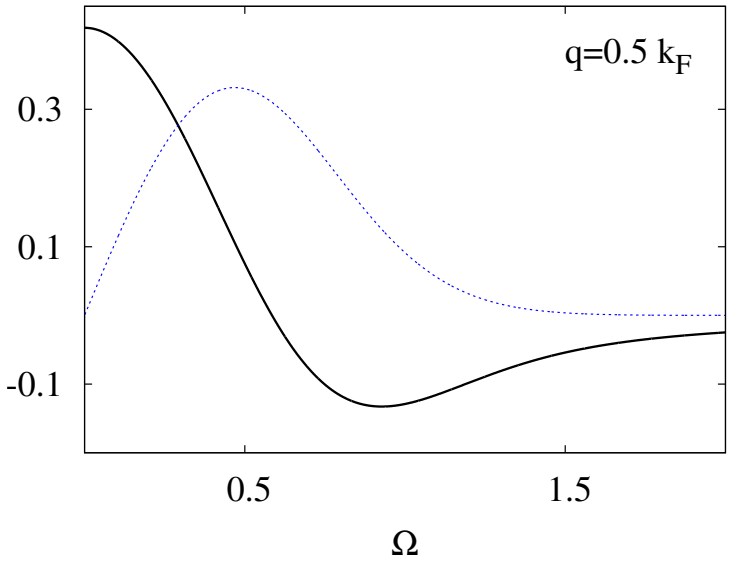

Figure 3.4: The real part (black line) and immaginary part (blue line) of $-\frac{\chi_0(q,\omega,T)}{N(0)}$ against the dimensionless variable $\Omega = \frac{\hbar\omega}{2E_F}$ for n-GaAs at electron density $n_e = 2.8 \times 10^{16}\ cm^{-3}$ and $T = 77K$ ($T_F = 58.2K$).

where v_q are the bare Coulomb potential Fourier components, in our case $v_q = \frac{e^2}{\varepsilon q^2}$. Within the RPA the density-density response function is obtained by a geometric series whose terms come from a limited subset of Feynman diagrams in many-body perturbation theory, see [51, 56]. RPA neglects exchange and short-range correlation effects in the motions of the electrons [51]. It is a high density approximation being good for $r_s \leq 1$ [57]. In the case of n-GaAs we plot r_s against the electron density in Figure 3.2 for the range of densities of interest and temperature $T = 300K$. We can see that RPA starts to breakdown going towards low concentrations, $n_e \approx 10^{16}\ cm^{-3}$. Within the range of its validity, RPA provides a good description of the effective screened Coulomb interaction. It may be improved by introducing the so-called many-body local field factors which include exchange and correlation effects [51]. These concepts are beyond the scope of this thesis. For the sake of completeness we need also to recall that being n-GaAs a multicomponent system there is a contribution to the dielectric function in RPA from the lattice charges [51, 53]. We shall not include the lattice screening in our calculations.

We conclude this section recalling how the Thomas-Fermi (T-F) screening comes from the dielectric function $\varepsilon(q,\omega)$ in the case of static perturbing potential, as it is the case of an impurity, and in the long wavelengths, i.e., $q \ll k_F$. In this case, the dielectric function becomes [51]

$$\varepsilon(q,0) = 1 + \frac{\beta_{TF}^2}{q^2}\,. \tag{3.37}$$

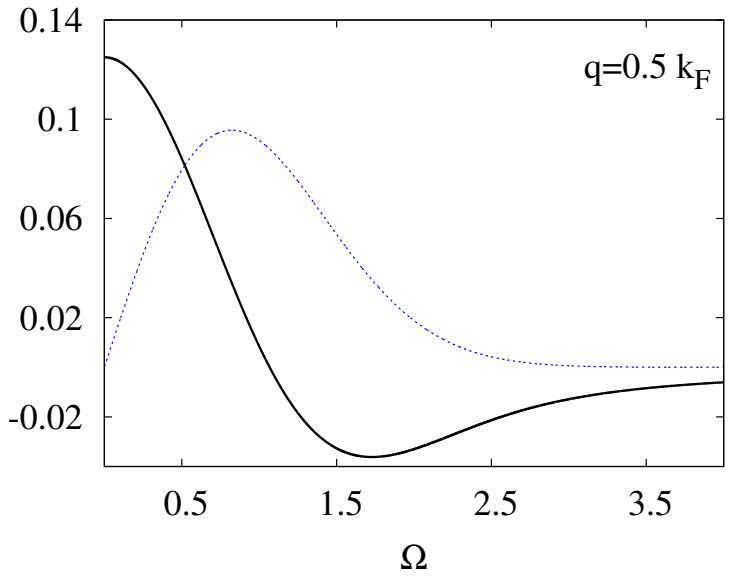

Figure 3.5: The real part (black line) and immaginary part (blue line) of $-\frac{\chi_0(q,\omega,T)}{N(0)}$ against the dimensionless variable $\Omega = \frac{\hbar\omega}{2E_F}$ for n-GaAs at electron density $n_e = 2.8 \times 10^{16}\ cm^{-3}$ and $T = 300K$ ($T_F = 58.2K$).

β_{TF} is called the Thomas-Fermi inverse screening length. Its calculation will crucial for this study. From (3.35) the Fourier transform provides

$$V_{sc}(r) = \frac{e^2}{4\pi\varepsilon}\frac{e^{-\beta_{TF}r}}{r}. \tag{3.38}$$

Equation (3.38) has the form a Yukawa screened potential, that means that the impurity is screened out within distances of $\lambda_{TF} = \beta_{TF}^{-1}$. It is worthwhile to recall here that T-F screening, and also the Yukawa potential, provides a good approximation of the screening and the effective potential only for the long wavelengths. In fact it is well known, that due to the singularity of the dielectric function at $k = 2k_F$, the latter being a signature of the Fermi surface, the potential V_{sc} goes like [45]

$$V_{sc} \sim \frac{1}{r^3}\cos(2k_F r) \tag{3.39}$$

which exhibits oscillatory behaviour (Friedel oscillations) at large distances and clearly it cannot be longer considered a merely Yukawa potential.

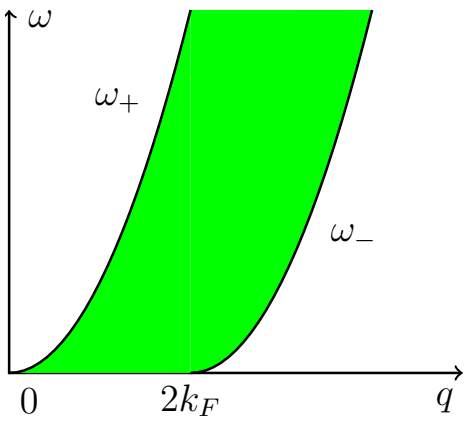

Figure 3.6: The electron-hole continuum in the plane (q, ω). The curves ω_- and ω_+ which determine the boundaries are defined in Appendix B.

3.5 A Finite Temperature Thomas-Fermi Approximation for Semiconductors

In the case of the n-type semiconductors neglecting the exchange and correlation effects Dingle has calculated the screening effects of the conduction electrons on a positive single-charge donor [58] . We shall not give here all his derivation but only his assumptions and the final result obtained. He assumed that in the presence of an external bare Coulomb potential V_{ext}, due to the impurity, the chemical potential μ is modified by $\mu + eV_{ext}(r)$. Then he calculated the electronic density $n_e(r)$ near the donor and expanded it in order to find the screened potential V_{sc} at large distances where he assumed it would be weaker. Finally solving the Poisson's equation for the screened potential

$$\nabla^2 V_{ext}(r) = -\frac{\rho}{\varepsilon}, \tag{3.40}$$

where ρ is the charge density, assumed to have a spherical symmetry around the donor, he got a Yukawa-type potential with T-F screening length given by

$$\beta_{TF}^2 = \frac{n_e e^2}{\varepsilon k_B T} \frac{\mathcal{F}_{-1/2}(\eta_F)}{\mathcal{F}_{1/2}(\eta_F)}. \tag{3.41}$$

Here $\mathcal{F}_j$ which denotes the Fermi-Dirac (F-D) integral of order j, see next section and the quantiy η_F is defined in Appendix C. We shall refer to Dingle's result as a finite temperature Linearized Thomas-Fermi Approximation (LTFA) [52, 53]. LTFA is equivalent to Thomas-Fermi theory, indeed the final result is the same, a screened Yukawa potential. Moreover the Thomas-Fermi theory is usually derived assuming $T = 0K$ meanwhile the equation (3.41) holds for any

temperature.

The Debye-Hückel inverse screening length [5] in the electrolyte theory is given by [27]

$$\beta_{DH} = \sqrt{\frac{n_e e^2}{\varepsilon k_B T}} \tag{3.42}$$

then we can write the equation (3.41) as

$$\beta_{TF}^2 = \beta_{DH}^2 \frac{\mathcal{F}_{-1/2}(\eta_F)}{\mathcal{F}_{1/2}(\eta_F)} \tag{3.43}$$

We shall assume that LTFA is a good approximation for screening insofar the momentum transfer q in electron-impurity (e-i) scattering is small, $q \to 0$ [52] and clearly small compared to k_F [45]. In Figure 3.7 we plot the histogram of electron-impurity scattering angles obtained from an Ensemble Monte Carlo simulation of $N = 5,000$ electrons at $T = 300K$ which shows that the majority of e-i collisional events cause small scattering angles and therefore small momentum transfers.

3.6 Calculation of Fermi-Dirac Integrals

Here and in the following sections we shall show how we calculated the inverse screening length from (3.41). Equation (3.41) looks like a harmless mathematical object, but its results are very difficult to work out.

In equation (3.41) the fundamental ingredient is Fermi-Dirac integral. The general mathematical definition of F-D integral of order j is

$$\mathcal{F}_j(x) = \frac{1}{\Gamma(j+1)} \int_0^\infty \frac{t^j}{e^{t-x}+1} dt \tag{3.44}$$

where $x \in \mathbb{R}$ and $\Gamma(n)$ is Euler's Gamma function. In our case we will need to calculate only F-D integrals with $j = \pm 1/2$, see (3.41), that is

$$\mathcal{F}_{1/2}(\eta_F) = \frac{1}{\Gamma(3/2)} \int_0^\infty \frac{\varepsilon^{1/2}}{e^{\varepsilon-\eta_F}+1} d\varepsilon\,, \tag{3.45}$$

and

[5] The Debye-Hückel inverse screening length comes directly from T-F theory when the values of the chemical potential become those of a classical ideal gas [54].

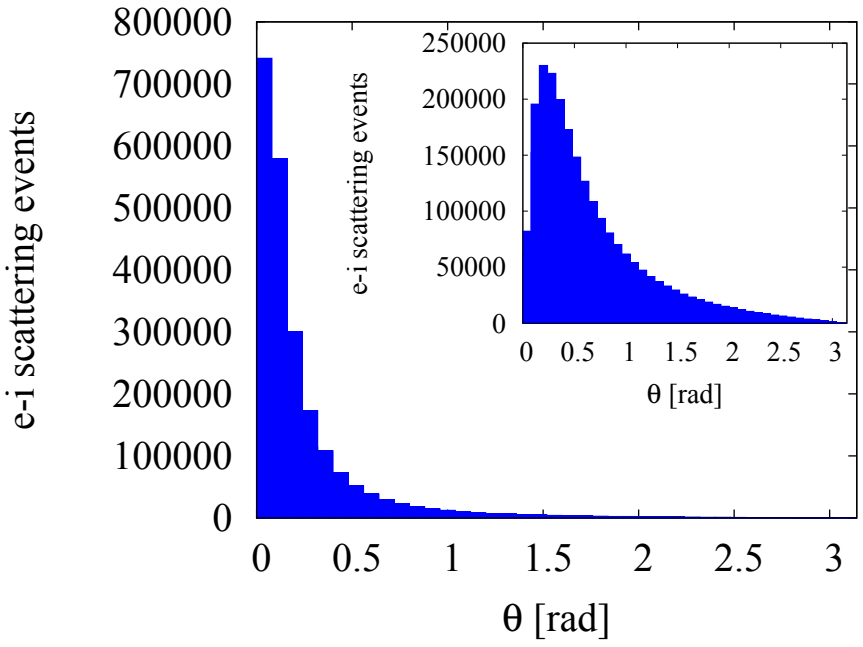

Figure 3.7: Histogram of the number of the electron-impurity scattering events against the polar angle θ from an EMC simulation of $5,000$ electrons at room temperature when electron-electron scattering is included. The electronic concentrations are $n_e = 10^{16}\ cm^{-3}$ (main panel), and $n_e = 2.5 \times 10^{17}\ cm^{-3}$ (inset). Note the different scales on the y-axis.

$$\mathcal{F}_{-1/2}(\eta_F) = \frac{1}{\Gamma(1/2)} \int_0^\infty \frac{\varepsilon^{-1/2}}{e^{\varepsilon-\eta_F}+1} d\varepsilon\,. \tag{3.46}$$

One important reference which gives very accurate and reliable numerical evalution tables of F-D integrals is Cloutman's paper [59]. This is used intensively in the field of astrophysics. Notice that the definition of F-D integral in [59] is slightly different as you can see below

$$F_j(\eta_F) = \int_0^\infty \frac{\varepsilon^j}{e^{\varepsilon-\eta_F}+1} d\varepsilon\,, \tag{3.47}$$

which differs from the definition (3.44) for lacking the prefactor $\Gamma(j+1)^{-1}$.

The F-D integrals are improper integrals and can be evaluated accurately by numerical integration, for example, the composite trapezoidal rule [60]. They can also be written as series on the domains of j and x [31]. In [31] there are different expansions of $F_j(x)$. The principal expansions are the following ones

$$\mathcal{F}_j(x) = \sum_{i=1}^{n} (-1)^{n-1} \frac{e^{nx}}{n^{j+1}}\,, \tag{3.48}$$

which is convergent for $x \leq 0$, and

$$\mathcal{F}_j(x) = \frac{x^{j+1}}{\Gamma(j+2)}\left\{1+\sum_{n=1}^{\infty}(-1)^{n-1}[(j+1)U(1,j+2,nx)-M(1,j+2,-nx)]\right\}, \tag{3.49}$$

convergent for $x > 0$. M and U represent Kummer's confluent hypergeometric functions, see next section 3.7. There is also a Taylor series expansion for $\mathcal{F}_j(x)$, convergent for $|x| < \pi$ where [31]

$$\mathcal{F}_j(x) = \sum_{n=0}^{\infty}\eta(j+1-n)\frac{x^n}{n!}. \tag{3.50}$$

Here $\eta(s) = (1-2^{1-s})\zeta(s)$ where $\zeta(s)$ denotes the Riemann zeta function. This was actually the first expression which we tried to implement. Unfortunately we found that (3.50) for different values of $\eta_F > 0$ was numerical unstable when $j = -1/2$. The problem was related to a CERN subroutine we use to calculate $\zeta(s)$. We could not retrive its documentation. There was also another drawback using the formula (3.50) as the integer overflow is easily reached due to the presence of the factorial (function) in the expression. This may also create problems in the accuracy of the calculation of F-D integrals, as we can keep only few terms in the series.

The asymptotic limits of F-D integrals provide some useful expressions for comparison with the previous expressions. They are given by [61]

$$\mathcal{F}_j(\eta_F) \sim e^{\eta_F}, \qquad \eta_F \ll 0, \tag{3.51}$$

and

$$\mathcal{F}_j(\eta_F) \sim \frac{\eta_F^{j+1}}{(j+1)\Gamma(j+1)}, \qquad \eta_F \gg 0. \tag{3.52}$$

In the next section we shall explain how we implemented the formula (3.47).

3.7 Kummer's Confluent Hypergeometric Functions

The Kummer's confluent hypergeometric function of first kind $M(a,b,z)$ or ${}_1F_1(a,b,z)$ [6] is an entire function of a, b and z, except for poles at $b = 0, -1, -2, \cdots$. It is given by a generalized hypergeometric series [62]

[6] Notice that the German word Kummer means grief, sorrow.

$$M(a,b,z) = \sum_{n=0}^{\infty} \frac{a^{(n)} z^n}{b^{(n)} n!}, \tag{3.53}$$

where

$$a^{(n)} = a(a+1)(a+2)\cdots(a+n-1), \tag{3.54}$$

is the rising factorial. The Tricomi confluent hypergeometric function $U(a,b,z)$ or $\Psi(a,b,z)$ is given by [62]

$$U(a,b,z) = \frac{\pi}{\sin \pi b}\left[\frac{M(a,b,z)}{\Gamma(1+a-b)\Gamma(b)} - z^{1-b}\frac{M(1+a-b,2-b,z)}{\Gamma(a)\Gamma(2-b)}\right]. \tag{3.55}$$

There are many algorithms in order to calculate the Kummer function of the first kind $M(a,b,x)$, see e.g. [63]. We chose the Method 1 described in [63]. $M(a,b,x)$ may be computed using the following steps. Let's define

$$M_I = \sum_{i=0}^{I} \frac{(a)_i}{(b)_i}\frac{x^i}{i!} \tag{3.56}$$

Let $T_0 = 1$ and, for $i > 0$,

$$T_{i+1} = T_i \frac{(a+i)}{(b+i)}\frac{x}{(i+1)} \tag{3.57}$$

Then $M_0 = 1$ and, for $i > 0$, use the recurrence relationship to compute

$$M_{i+1} = M_i + T_{i+1} \tag{3.58}$$

The process stops with sufficiently small $|T_{i+1}/M_{i+1}|$ or, if $|M_{i+1}| \approx 0$, or sufficiently small $|T_{i+1}|$. In some cases T_i increases in size before beginning to decrease. It is recommended using it if $|x| < 50$, and otherwise one needs to resort to the asymptotic approximations, see [63]. The function $M(a,b,x)$ is implemented as a Fortran 90 function according to the previous algorithm.

The implementation of the Tricomi function $U(a,b,z)$ comes straightforwardly from its expression in equation (3.55). Once j is fixed, i.e., $j = \pm 1/2$ one has to evaluate $\Gamma(n)$ function for the corrispondent values of a,b. This allows us to determine the numerical coefficients in (3.55). According to the previous observation two Fortran 90 functions must be implemented for $j = +1/2$ and $j = -1/2$ respectively. For the case $j = +1/2$ the relative coefficients of (3.55)

Table 3.1: Coefficients for $U(a,b,z)$ when $j=+1/2, a=1, b=5/2$.

$j=+1/2, a=1, b=5/2$		
$\Gamma(a)$	$\Gamma(1)$	1
$\Gamma(b)$	$\Gamma(5/2)$	$3\pi/4$
$\Gamma(1+a-b)$	$\Gamma(-1/2)$	$-2\sqrt{2}$
$\Gamma(2-b)$	$\Gamma(-1/2)$	$-2\sqrt{2}$

Table 3.2: Coefficients for $U(a,b,z)$ when $j=+1/2, a=1, b=5/2$.

$j=+1/2, a=1, b=3/2$		
$\Gamma(a)$	$\Gamma(1)$	1
$\Gamma(b)$	$\Gamma(3/2)$	$\sqrt{\pi}/2$
$\Gamma(1+a-b)$	$\Gamma(1/2)$	$\sqrt{\pi}$
$\Gamma(2-b)$	$\Gamma(1/2)$	$\sqrt{\pi}$

are shown in Table 3.1, and $U(a,b,z)$ becomes

$$U(a,b,z)=\pi\left[-\frac{2}{3}\frac{M(a,b,z)}{\pi}-z^{1-b}\frac{M(1+a-b,2-b,z)}{2\sqrt{\pi}}\right]. \tag{3.59}$$

For the case $j=-1/2$ the relative coefficients of (3.55) are shown in Table 3.2, and $U(a,b,z)$ becomes

$$U(a,b,z)=-\pi\left[\frac{2}{\pi}\frac{M(a,b,z)}{\pi}-z^{1-b}\frac{M(1+a-b,2-b,z)}{\sqrt{\pi}}\right]. \tag{3.60}$$

The evaluation of the coefficients can be found in Appendix B.

The number of terms retained in the series (3.47) is chosen in order to give the same accuracy of the numerical calculations of F-D integrals given in Cloutman's tables [59]. Also many values of $M(a,b,x)$ and $U(a,b,x)$ have been compared with those given by *Wolfram*© Mathematica software. We found a very good agreement.

3.8 Computing the Inverse Screening Length

Finally we can check whether the previous mathematical machinery gives the correct results. We expect that LTFA gives the Debye-Hückel theory screening in the limit of low electronic densities or more generally when the system becomes nondegenerate. A comparison of the inverse screening lengths β_{TF} cal-

culated by equation (3.41) and β_{DH} from equation (3.42) at $T = 300K$ is given in Table 3.3 for different electronic concentrations.

Table 3.3: Values of β_{TF} and β_{DH} calculated $T = 300$ K for n-GaAs.

$n_e\ (cm^{-3})$	$\beta_{TF}\ (m^{-1})$	$\beta_{DH}\ (m^{-1})$	$T_F\ (K)$
10^{14}	2329276.33	2329370.94	1.3
10^{15}	7363127.59	7366117.69	6.3
5×10^{15}	16437799.26	16471139.89	18.4
10^{16}	23199723.08	23293709.43	29.3
5×10^{16}	51062809.02	52086317.74	85.7
10^{17}	70856800.72	73661176.96	136.0
5×10^{17}	139732111.16	164711398.99	397.8
10^{18}	175899113.26	232937094.32	631.5

It is evident from the values of the Table 3.3 that $\beta_{TF} \to \beta_{DH}$ in the low density limit. In the present study we shall consider the carrier dynamics in the nondegenerate or intermediate regime. Nevertheless we can check if we get the correct answer for the degenerate regime. In this case we have to compare β_{TF} from Dingle's theory with Thomas-Fermi theory of screening [45, 54, 64] In the remainder of this chapter we shall give the derivation of T-F screening from Ashcroft and Mermin's book [45] and then we will compare our results to T-F theory. Let us place a positive charge at a given position in the electron gas. This charge is a source of an external electrostatic potential ϕ^{ext}. In order to find the charge density in the presence of the total potential ϕ [7]

$$\phi = \phi^{ext} + \phi^{ind}\,, \tag{3.61}$$

one must solve the one-electron Schrödinger equation [45]

$$-\frac{\hbar^2}{2m}\nabla^2\psi_i(\mathbf{r}) - e\phi(\mathbf{r})\,\psi_i(\mathbf{r}) = E_i\psi_i(\mathbf{r})\,, \tag{3.62}$$

and from one-electron wavefunction electronic density it is possible to construct the electronic density ρ_e

$$\rho_e(\mathbf{r}) = -e\sum_i |\psi_i(\mathbf{r})|^2\,. \tag{3.63}$$

The Thomas-Fermi theory assumes that the total potential $\phi(\mathbf{r})$ is a very slowly function of $(\mathbf{r})$. Therefore in the spirit of the semiclassical approximation the spatially varying energy $E(\mathbf{k})$ is given by this relation [45]

[7] The full physical potential ϕ is produced by both the positive charge and the cloud of the screening electrons.

$$E(\mathbf{k}) = \frac{\hbar^2 k^2}{2m} - e\phi(\mathbf{r}) . \tag{3.64}$$

We see from (3.64) that the free electron energy is modified by the total local potential. The electron density n_e is given by [45]

$$n_e = \int \frac{d\mathbf{k}}{4\pi^3} f_{FD}(E(\mathbf{k})) , \tag{3.65}$$

where f_{FD} denotes the Fermi-Dirac distribution, see the equation (C.1) in Appendix C. Inserting the new electronic energy dispersion relation (3.64) into (3.65) one finds

$$n_e(\mathbf{r}) = \int \frac{d\mathbf{k}}{4\pi^3} \frac{1}{\exp\left[\beta\left(\left(\hbar^2 k^2/2m\right) - e\phi(\mathbf{r}) - \mu\right)\right] + 1} . \tag{3.66}$$

The induced charged is $-en_e(\mathbf{r}) + en_e$ where en_e is the charge density of the uniform positive background. The density of the background is the density of the electron ensemble when ϕ^{ext} vanishes [8]

$$n_e(\mu) = \int \frac{d\mathbf{k}}{4\pi^3} \frac{1}{\exp\left[\beta\left(\left(\hbar^2 k^2/2m\right) - \mu\right)\right] + 1} . \tag{3.67}$$

The basic equation of nonlinear Thomas-Fermi theory is obtained from equations [9] (3.66) and (3.67) [45] [10]

$$\rho^{ind}(\mathbf{r}) = -\frac{e}{4\pi\varepsilon}\left[n_e(\mu + e\phi(\mathbf{r})) - n_e(\mu)\right] , \tag{3.68}$$

where ρ^{ind} is the charge density induced in the electron gas by the presence of the external charged particle. Assuming that in (3.68) ϕ is small enough for an expansion, one finds the following result in leading order [45]

$$\rho^{ind}(\mathbf{r}) = -\frac{e^2}{4\pi\varepsilon}\frac{\partial n_e}{\partial \mu}\phi(\mathbf{r}) . \tag{3.69}$$

Now according to the linear response theory in the Fourier space

$$\rho^{ind}(\mathbf{q}) = \chi_0(\mathbf{q})\,\phi(\mathbf{q}) , \tag{3.70}$$

[8] Notice that in this case the total potential ϕ also vanishes.

[9] The chemical potential μ in (3.66) and (3.67) can be assumed the same insofar that $\phi(\mathbf{r})$ is appreciable only in a finite region, see [45].

[10] Notice we are writing the formulae of Ashcroft and Mermin's book in S.I units.

and therefore comparing (3.69) with (3.70) one finds

$$\chi_0(\mathbf{q}) = -\frac{e^2}{4\pi\varepsilon}\frac{\partial n_e}{\partial \mu} \tag{3.71}$$

which shows that in the linearized Thomas-Fermi theory χ_0 is independent of $\mathbf{q}$. Recalling the definition of the dielectric function in RPA given in [45]

$$\varepsilon(\mathbf{q}) = 1 - \frac{4\pi}{q^2}\chi_0(\mathbf{q}), \tag{3.72}$$

and using the formula (3.71) finally ones finds

$$\varepsilon(\mathbf{q}) = 1 + \frac{e^2}{\varepsilon q^2}\frac{\partial n_e}{\partial \mu}. \tag{3.73}$$

Comparing (3.73) to the relation (3.37) the Thomas-Fermi inverse screening length [11] can be calculated by

$$\beta_{TF}^2 = 4\pi e^2 \frac{\partial n_e}{\partial \mu}. \tag{3.74}$$

One useful approximation for (3.74) can be derived for the electron gas when $T \ll T_F$. In this case $\partial n_e/\partial\mu$ is the total density of states per unit volume at Fermi energy $N(0)$, see formula (3.32), and then we can estimate (3.74) using this simple relation [45]

$$k_0 = 0.815 k_F r_s^{1/2}. \tag{3.75}$$

A simple check confirms that in the degenerate regime there is convergence. For electronic densities greater than $5 \times 10^{18}\ cm^{-3}$ the difference (relative error) between β_{TF} and k_0 is much smaller than 1%. In Figure 3.8 we plot the λ_{TF} according to equation (3.41) against the electronics densities at $T = 300K$ for n-type GaAs semiconductor.

[11] Notice that β_{TF} is called Thomas-Fermi wavevector and denoted by k_0 in Ashcroft and Mermin's book [45].

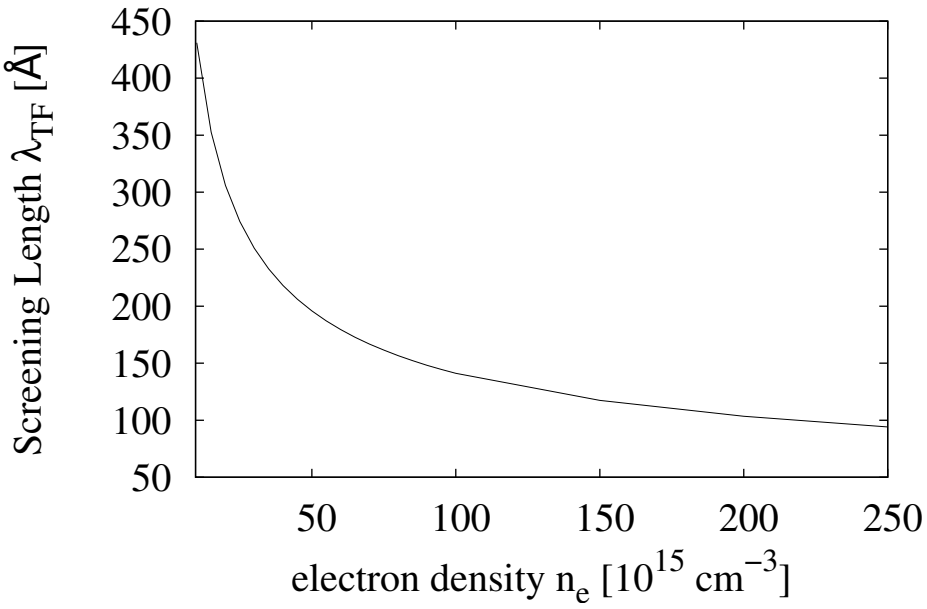

Figure 3.8: Finite temperature Thomas-Fermi Screening Length at $T = 300K$ against the electronic densities of interest at $T = 300K$.

Chapter 4

Spin-Orbit Interaction in Semiconductors

The concept of the spin, the intrinsic angular momentum, which has no classical equivalent originated from the fundamental experiment of O. Stern and W. Gerlach in 1922. They measured the effect of a magnetic field on a beam of silver atoms passing between the poles of a magnet. They observed two spots on the screen behind the magnet corresponding to two possible magnetic moments values. As in the case of a silver atom the only contribution to orbital angular moment is due to the 47th electron ($5s$), then it is possible to relate the oberved magnetic moments to the electron spin, indeed they are proportional [41]. Its existence well explains the observed spectral lines of atoms in the Zeeman effect for instance. The explanation of the Stern-Gerlach experiment, introducing the "wild "idea of the electron intrinsic angular momentum, was given in 1925 by P. Ehrenfest's young students G. Uhlenbeck and S. Goudsmit who were told by their professor "you are both young enough to be able to afford a stupidity ". In Quantum Mechanics (QM) the spin states are represented by a special mathematical object, called spinor or spinor wavefunction in a two-dimensional complex Hilbert space. This object is related to the simplest non-trivial irreducible unitary representation of the rotation group [41]. Curiously Pauli added the electron spin to the nonrelativistic Schrödinger's equation [1]before Dirac discovered his famous relativistic equation [2] where the electron spin was "built into the theory from the beginning "[38]. The Dirac's equation for an electron in atoms or solids gives rise to the spin-orbit interaction (SOI) which plays an important role in spintronics.

[1]W. Pauli: *Zur Quantenmechanik des magnetischen Elektrons*, Zeitschrift für Physik **43** (1927) 601623.

[2]P.A.M. Dirac: *The quantum theory of the electron*, Proceedings of the Royal Society of London **A117** (1928) 610624; **118** (1928) 351361.

4.1 Nonrelativistic Spin Formalism

The electron has spin angular momentum $s = 1/2$ in units of $\hbar$ which means that its components along any direction are $\hbar/2$ or $-\hbar/2$. The Stern-Gerlach experiment determines the quantized electron intrinsic magnetic momentum μ_s [43] which takes the values $\pm\mu_B$ where the Bohr magneton μ_B is defined as

$$\mu_B = \frac{e\hbar}{2m_e}. \tag{4.1}$$

The relation between spin $\mathbf{S}$ and its magnetic moment μ_s is

$$\mu_s = -\frac{e}{m_e}\mathbf{S}, \tag{4.2}$$

where the ratio e/m_e is twice of that one expected from the orbital magnetic moment. This is a result from relativistic Dirac's equation. Netherless QED gives very accurate corrections to the electron magnetic moment [42]. Considering the angular momentum $\mathbf{S}$ as a Hermitian operator in a two-dimensional Hilbert Space, then

$$\hat{\mathbf{S}} = \frac{\hbar}{2}\hat{\sigma}, \tag{4.3}$$

where $\hat{\sigma}$ is understood as a vector operator whose components are the Pauli matrices σ_x, σ_y, σ_z , explicitly written as

$$\sigma_x = \begin{pmatrix} 0 & 1 \\ 1 & 0 \end{pmatrix}, \qquad \sigma_y = \begin{pmatrix} 0 & -i \\ i & 0 \end{pmatrix}, \qquad \sigma_z = \begin{pmatrix} 1 & 0 \\ 0 & -1 \end{pmatrix}. \tag{4.4}$$

The Pauli matrices are Hermitian, unitary and

$$\mathrm{Tr}\,\sigma_i = 0, \tag{4.5}$$

where Tr denotes the trace of a matrix and the indexes $i = 1,2,3$ stand for x,y,z-components respectively. They satisfy the following anticommutator and commutator relationships

$$\{\sigma_i, \sigma_j\} = 2\delta_{ij}, \tag{4.6}$$

$$[\sigma_i, \sigma_j] = 2i\varepsilon_{ijk}\sigma_k, \tag{4.7}$$

where δ_{ij} is the usual Kronecker symbol and ε_{ijk} is the Levi-Civita symbol [3]. The previous two formulae can be combined in a single expression

$$\sigma_i \sigma_j = \delta_{ij} + i\varepsilon_{ijk}\sigma_k \,. \tag{4.8}$$

Using the previous matrix identies it is straightforward to show that the three components $\hat{S}_i$ of spin operator $\hat{\mathbf{S}}$ satisfy the following commutation relationship

$$\left[\hat{S}_i, \hat{S}_j\right] = i\hbar\varepsilon_{ijk}\hat{S}_k \,. \tag{4.9}$$

At once from (4.9) one recognizes that the operators $\hat{S}_i$ behave like the the ordinary (orbital) angular momentum operators $\hat{L}_x$, $\hat{L}_y$, $\hat{L}_z$ in QM. Indeed they form the same Lie Algebra of the group of rotations $SO(3)$ and as usual the operator $\hat{S}^2$

$$\hat{S}^2 = \hat{S}_x^2 + \hat{S}_y^2 + \hat{S}_z^2 \,, \tag{4.10}$$

is the Casimir operator of the algebra and commutates with all the $\hat{S}_i$ operators [41]. Clearly all the machinery of the angular momentum theory of QM, i.e., ladder operators, angular momentum addition theorem, etc can then be applied succesfully to the spin operators. Let us recall the physical meaning and the geometrical interpretation of the eigenstates of the spin operators $\hat{S}_i$. As the operator $\hat{S}_z$ is already diagonal, its eigenvalues are immediately given by

$$\hat{S}_z \begin{pmatrix} 1 \\ 0 \end{pmatrix} = \frac{\hbar}{2} \begin{pmatrix} 1 \\ 0 \end{pmatrix} . \tag{4.11}$$

$$\hat{S}_z \begin{pmatrix} 0 \\ 1 \end{pmatrix} = -\frac{\hbar}{2} \begin{pmatrix} 0 \\ 1 \end{pmatrix} . \tag{4.12}$$

The eigenstates (4.11) and (4.12) correspond to states with spin parallel (spin up: $\uparrow$) and spin antiparallel (spin down: $\downarrow$) states to the z-axis respectively. We shall denote them using Dirac's ket notation as well, $|\uparrow\rangle$ and $|\downarrow\rangle$ for spin up and spin down respectively and $|\chi\rangle$ for a general state. As a spin state is a vector in a 2- dimensional Hilbert space it can always be expressed as a linear combination of the eigenstates $|\uparrow\rangle$ and $|\downarrow\rangle$

$$|\chi\rangle = c_1 |\uparrow\rangle + c_2 |\downarrow\rangle \,, \tag{4.13}$$

where c_1, c_2 are in general complex numbers and the normalization of the probability gives

$$|c_1|^2 + |c_2|^2 = 1 \,. \tag{4.14}$$

[3] ε_{ijk} gives 1 for an even permutation of (123), -1 for an odd one and otherwise zero.

Using spherical polar coordinates the spin operator $\hat{\mathbf{S}}_n$ in any direction determined by the spherical polar angles (θ, ϕ) and denoted by the unit vector $\hat{\mathbf{n}}$ is

$$\hat{\mathbf{S}}_n = \hat{\mathbf{S}} \cdot \hat{\mathbf{n}}, \tag{4.15}$$

where $\hat{\mathbf{n}}$ is

$$\hat{\mathbf{n}} = \sin\theta\cos\phi\,\hat{\mathbf{x}} + \sin\theta\sin\phi\,\hat{\mathbf{y}} + \cos\theta\,\hat{\mathbf{z}}, \tag{4.16}$$

where $\hat{\mathbf{x}}$, $\hat{\mathbf{y}}$, $\hat{\mathbf{z}}$ are the unit vectors along the Cartesian axes. Then the eigenstates corresponding to spin up and spin down along the direction (θ, ϕ) are given by [41]

$$|\uparrow\rangle = \begin{pmatrix} \cos\left(\frac{\theta}{2}\right) e^{-i\phi} \\ \sin(\frac{\theta}{2}) \end{pmatrix}, \qquad |\downarrow\rangle = \begin{pmatrix} -\sin(\frac{\theta}{2}) e^{-i\phi} \\ \cos(\frac{\theta}{2}) \end{pmatrix}. \tag{4.17}$$

The two-components objects like the $|\chi\rangle$ in (4.13) are called spinors [4] as they do not transform like ordinary vectors under rotation. In the section 1.3 of Chapter 1 we said that we need a 4π rotation for a spinor wavefunction to get back to the same state. Here we shall show how it happens. In QM a general unitary rotation operator $\mathscr{D}(\hat{\mathbf{n}}, \varphi)$ of a finite angle φ rotation about the direction determined by the unit vector $\hat{\mathbf{n}} = (n_x, n_y, n_z)$ has the following 2×2 matrix representation for the spin $1/2$ particle [41]

$$\mathscr{D}(\hat{\mathbf{n}}, \varphi) = \exp\left(\frac{-i\mathbf{S} \cdot \hat{\mathbf{n}}\varphi}{\hbar}\right) = \exp\left(\frac{-i\sigma \cdot \hat{\mathbf{n}}\varphi}{2}\right). \tag{4.18}$$

It can be shown that [41]

$$\exp\left(\frac{-i\sigma \cdot \hat{\mathbf{n}}\varphi}{2}\right) = \mathbf{1}\cos\left(\frac{\varphi}{2}\right) - i\sigma \cdot \hat{\mathbf{n}}\sin\left(\frac{\varphi}{2}\right), \tag{4.19}$$

where $\mathbf{1}$ is the 2×2 identity matrix. We can also write the relation (4.19) explicitly [41]

$$\exp\left(\frac{-i\sigma \cdot \hat{\mathbf{n}}\varphi}{2}\right) = \begin{pmatrix} \cos\left(\frac{\varphi}{2}\right) + in_z \sin\left(\frac{\varphi}{2}\right) & (-in_x - n_y)\sin\left(\frac{\varphi}{2}\right) \\ (-in_x + n_y)\sin\left(\frac{\varphi}{2}\right) & \cos\left(\frac{\varphi}{2}\right) + in_z \sin\left(\frac{\varphi}{2}\right) \end{pmatrix}. \tag{4.20}$$

Then the rotation operator $\mathscr{D}(\hat{\mathbf{n}}, \varphi)$ acts on the spinor $|\chi\rangle$ in the following way [41]

$$|\chi\rangle \to \exp\left(\frac{-i\sigma \cdot \hat{\mathbf{n}}\varphi}{2}\right)|\chi\rangle, \tag{4.21}$$

and we see that a rotation of 2π does not bring the spinor back to the same

[4] "No one fully understand spinors. Their algebra is formally undestood but their geometrical significance is mysterious. In some sense they describe the 'square-root 'of geometry and, just as understanding the concept of the square root of -1 took centuries, the same might be true for spinors ". M.Atiyah

initial state, but gives a minus sign to it [5]. In fact it is evident from (4.20) that for $\varphi = 2\pi$ and any $\hat{\mathbf{n}}$ [6][41]

$$\exp\left(\frac{-i\sigma\cdot\hat{\mathbf{n}}\varphi}{2}\right)_{\varphi=2\pi} = -\mathbf{1}. \tag{4.22}$$

There is a useful and simple geometrical picture of any spin state of a spin-1/2 particle. If we draw a 3 -dimensional sphere and we identify its north and south poles with states $|\uparrow\rangle$, $|\downarrow\rangle$, we can think of any direction in space as a direction of a general spin state **S**, see Figure 4.1. This geometrical picture is called Riemann sphere [65, 66].

Moreover the direction of any spin state can be mapped to a point of a complex plane obtained via the stereographic projections from the south pole $|\downarrow\rangle$ to the equatorial plane of the Riemann sphere. This complex plane contains all the points given by the ratio of the quantum-mechanical amplitude c_2/c_1, allowing the infinity, of the spin state $|\chi\rangle$ in (4.13) [65]. The Riemann sphere can be related to a unit sphere called Bloch sphere [7] a very useful concept for representations of qubits and quantum operations on them, see [12].

[5] This happen because the special unitary group $SU(2)$ and the special orthogonal group $SO(3)$ of rotations, are locally isomorphic which means that only for infinitesimal rotations, they appear the same [65].

[6] Notice that we are assuming that the spinors $|\chi\rangle$ are eigenvectors of $\sigma\cdot\hat{\mathbf{n}}$.

[7] The representation of 1/2 spin by a point on the surface of the Bloch sphere, has the advantage to be independent of the overall normalization and phase of the spinor state. A useful generalization of the Bloch sphere is the Majorana sphere, see [65, 67].

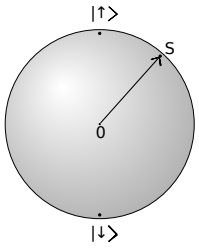

Figure 4.1: A general spin state **S** of spin-$\frac{1}{2}$ particle has an actual direction in space that is determined from the centre of the sphere to a point on the sphere surface.

4.2 Spin-Orbit Interaction

Dirac combining the principles of QM and of relativistic invariance obtained an equation for the wavefunction of a free electron ψ that can be written as [43]

$$i\hbar\frac{\partial\psi}{\partial t} = \left[c\alpha\cdot(-i\hbar\nabla) + \beta m_e c^2\right]\psi(x)\,, \tag{4.23}$$

where c the speed of light, x the four dimensional space-time coordinate of the particle, and the matrices $\alpha = (\alpha_1, \alpha_2, \alpha_3)$ and β are 4×4 Hermitian matrices satisfying

$$\{\alpha_i, \alpha_j\} = 2\delta_{ij} \quad \{\alpha_i, \beta\} = 0 \quad \beta^2 = 1, \quad i, j = 1, 2, 3\,. \tag{4.24}$$

We do not need here to give an explicit representation of these matrices. Instead it is worthwhile to notice that the equation (4.23) even if it is not written in the usual covariant form, is Lorentz invariant. Moreover the interpretation of ψ as a single particle wavefunction is no longer strictly correct. Now ψ is a four-component object called Dirac's spinor o bispinor that can be written as

$$|\psi\rangle = \begin{pmatrix}\chi\\ \varphi\end{pmatrix}, \tag{4.25}$$

where χ and φ are two spinors called the large and small components respectively as in the nonrelativistic limit χ is bigger than φ.

An electron inside an atom or a solid is in general in a potential field $\hat{V}$ that here we shall assume to be central and spin-independent. In this case the Dirac equation (4.23) for stationary solutions $|\psi\rangle$ of energy E becomes

$$\left(c\alpha\cdot\hat{\mathbf{P}} + \beta m_e c^2 + \hat{V}\right)|\psi\rangle = E\,|\psi\rangle\,, \tag{4.26}$$

where $\hat{\mathbf{P}}$ is the linear momentum operator of QM. This provides two coupled differential equations

$$\left(E - \hat{V} - m_e c^2\right)\chi - c\hat{\boldsymbol{\sigma}}\cdot\hat{\mathbf{P}}\varphi = 0\,, \tag{4.27}$$

$$\left(E - \hat{V} + m_e c^2\right)\varphi - c\hat{\boldsymbol{\sigma}}\cdot\hat{\mathbf{P}}\chi = 0\,, \tag{4.28}$$

and eliminating φ from these equations, one gets

$$\left(E - \hat{V} - m_e c^2\right)\chi = c\hat{\boldsymbol{\sigma}}\cdot\hat{\mathbf{P}}\left[\frac{1}{E - \hat{V} + m_e c^2}\right]c\hat{\boldsymbol{\sigma}}\cdot\hat{\mathbf{P}}\chi\,. \tag{4.29}$$

Given the nonrelativistic energy $\tilde{E}$, $\tilde{E} \ll m_e c^2$,

$$\tilde{E} = E - m_e c^2 , \tag{4.30}$$

then the term in parentheses in (4.29), assuming also that the potential is weak, i.e., $\left|\hat{V}\right| \ll mc^2$, can be written as

$$\frac{1}{E - \hat{V} + m_e c^2} \approx \frac{1}{2m_e c^2} - \frac{\tilde{E} - \hat{V}}{4m_e^2 c^2} . \tag{4.31}$$

Finally inserting it into (4.29) and after some algebraic manipulation one obtains the following eigenvalue equation

$$\left[\frac{\hat{P}^2}{2m_e} + \hat{V} - \frac{\hat{P}^4}{8m_e^3 c^2} - \frac{\hat{\mathbf{P}} \cdot \left[\hat{\mathbf{P}}, \hat{V}\right]}{4m_e^2 c^2} - \frac{i\hat{\boldsymbol{\sigma}} \cdot \hat{\mathbf{P}} \times \left[\hat{\mathbf{P}}, \hat{V}\right]}{4m_e^2 c^2} \right] \chi = \tilde{E}\chi . \tag{4.32}$$

The equation (4.32) is called the Pauli equation [38]. The first two terms give the Hamiltonian of the Schrödinger equation, the third is a relativistic correction to the kinetic energy, the fourth is simply an energy shift, and the last term is the spin-orbit coupling or spin-orbit interaction. The latter can be written in the following way

$$\hat{H}_{SOI} = \frac{\mu_B}{\hbar m_e e c^2} \frac{1}{r} \frac{\partial V(r)}{\partial r} \hat{\mathbf{S}} \cdot \hat{\mathbf{L}} , \tag{4.33}$$

which clearly clarifies the origin of its name. Notice that (4.33) is derived from Dirac's equation (4.23) keeping terms of order $1/c^2$. The equation (4.33) for a noncentral potential is often written as

$$\hat{H}_{SOI} = \frac{\hbar}{4m_e^2 c^2} \nabla_r V(r) \times \hat{\mathbf{P}} \cdot \hat{\boldsymbol{\sigma}} . \tag{4.34}$$

M.I. Dyakonov says that one does not need Dirac's equation nor QM to understand SOI because the electron has a magnetic moment [8]. In fact if an electron moves with velocity $\mathbf{v}$ in an external electric field $\mathbf{E}$ it will see a magnetic field [68]

$$\mathbf{B} = \frac{1}{c^2} \mathbf{E} \times \mathbf{v} , \tag{4.35}$$

that couples with the electron magnetic moment μ_s explaining the physical origin of SOI. It should be noted that starting from these premises, another ingredient is needed to derive SOI because the correct result is twice as big as in (4.33). This is why one needs a multiplication of SOI by the so called "Thomas' one half "factor. Its origin is the Thomas precession, again a relativistic effect. An elementary derivation of the Thomas precession can be found in [69, 70]. It is here sufficient to say that Thomas precession is a consequence of the fact that

the composition of two successive Lorentz boosts [8] that are not collinear, is no longer a pure boost but rather the product of a boost and a spatial rotation. In other terms the Lorentz boosts do not form a subgroup of the Lorentz group [71] In conclusion Dirac's equation leads naturally to the correct SOI and in the next section we will consider how SOI appears in semiconductors.

4.2.1 Spin-Orbit Coupling and the Dresselhaus Term

In presence of SOI the Hamiltonian $\hat{H}$ of an electron in a semiconductor becomes

$$\hat{H} = \frac{\hat{\mathbf{P}}^2}{2m_e} + \hat{V} - \frac{\hbar}{4m_e^2c^2}\hat{\boldsymbol{\sigma}} \cdot \hat{\mathbf{P}} \times \nabla_r V(r)\,, \tag{4.36}$$

where $\hat{V}$ is the periodic lattice potential energy. Within this single particle picture one wishes to solve the time independent Schrödinger equation for the Hamiltonian above in order to find the energy spectrum. There are two methods for tackling this problem, one is the group theory [25, 46] , the other is the Kane model [72]. Here we shall give only the basic physics behind the spin-orbit coupling, the subject being very technical and beyond the scope of this thesis.

The motions of the electrons in a semiconductor is characterized by the relation between the energy band $E_n(\mathbf{k})$ and the wavevector $\mathbf{k}$. The presence of SOI modifies the bandstructure of semiconductors, see for example the top most valence bands of GaAs. Thus the SOI affects the orbital motions of the electrons. It may affect also the spin dynamics through the combination of two symmetry operations in semiconductors, inversion and time-reversal (TR) symmetries.

The time-reversal (TR) plays an important role in semiconductors and in general for the physics of materials.

TR symmetry can be defined by the operator $\mathscr{T}$ [73]

$$\mathscr{T} : t \to -t\,, \tag{4.37}$$

i.e., a transformation which reverses the arrow of time. Wigner who introduced this concept in 1932, called it reversal of motion [41]. TR is a fundamental symmetry and here briefly we shall give the results for physical systems, both spinless and with spin $1/2$. If a system is TR invariant, then its Hamiltonian $\hat{H}$ commutates with $\mathscr{T}$

$$\left[\hat{H}, \mathscr{T}\right] = 0\,. \tag{4.38}$$

[8] A Lorentz boost is a Lorentz transformation which does not involve any rotation.

Notice that the Hamiltonian (4.36) is TR invariant even when spin-orbit coupling is absent. A general representation for the antiunitary operator $\mathscr{T}$ is [73]

$$\mathscr{T} = UK\,, \tag{4.39}$$

where K is the complex-conjugation operator and U is an unitary matrix [73]. In the spinless case $\mathscr{T} = K$, while in the spin half case it can be written as [46]

$$\mathscr{T} = K\sigma_y\,. \tag{4.40}$$

When spin is considered there is the twofold Kramers degeneracy [41, 73]. In fact let us denote with $|n\rangle$ the eigenstate of the operator $\hat{H}$ relative to the energy E_n, then the state $\mathscr{T}|n\rangle$ is also an eigenstate of $\hat{H}$ with the same energy E_n. Kramers theorem says that these two states are distinct for systems with half-integer spin, i.e., systems with an odd number of electrons [41]. Moreover if the lattice has inversion symmetry then [46]

$$E_{n\uparrow}(\mathbf{k}) = E_{n\downarrow}(\mathbf{k})\,, \tag{4.41}$$

see Figure 4.2. Instead when the lattice lacks of inversion symmetry as it is the case for a bulk GaAs the previous degeneracy (4.41) is removed, giving rise to a spin-dependent energy splitting in BZ [25, 46], see Figure 4.3.

In the case of the bulk GaAs, the SOI has been calculated in 1955 by G. Dresselhaus. He has found that in the neighbourhood of the Γ -point, $\mathbf{k} = 0$, and to the lowest order in the wavevector $\mathbf{k}$, the SOI Hamiltonian becomes H_D , the so-called Dresselhaus term, [5, 46, 74]

$$H_D = \hbar\Omega \cdot \sigma, \tag{4.42}$$

where the vector quantity $\Omega(\mathbf{p})$, Larmor frequency vector, is defined by

$$\Omega = \frac{\gamma_{so}}{\hbar^4}\{p_x(p_y^2 - p_z^2), p_y(p_z^2 - p_x^2), p_z(p_x^2 - p_y^2)\}\,, \tag{4.43}$$

In the equation (4.43) we assume a parabolic energy momentum dispersion relation, i.e., $\mathbf{p} = \hbar\mathbf{k}$ [9]. The coupling strength γ_{so} of this cubic Dresselhaus term has values in the range from 8.5 to 34.5 $eV\mathring{A}$, its exact value being not yet determined [74].

[9] The p_x, p_y, p_z denote the momentum components along the cubic crystal axes.

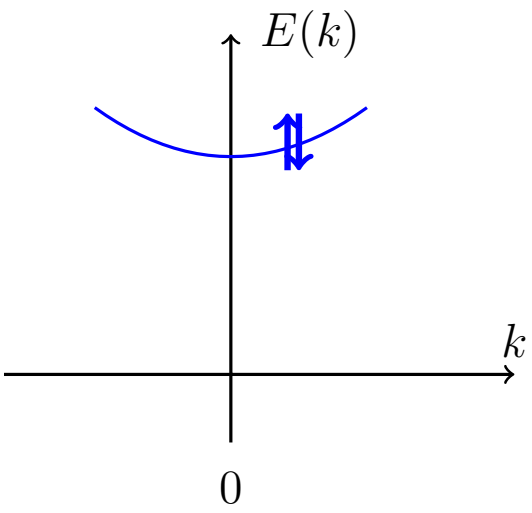

Figure 4.2: A sketch of a solid bandstructure where both spin-orbit interaction and inversion symmetry are present. The energy levels become doubly degenere.

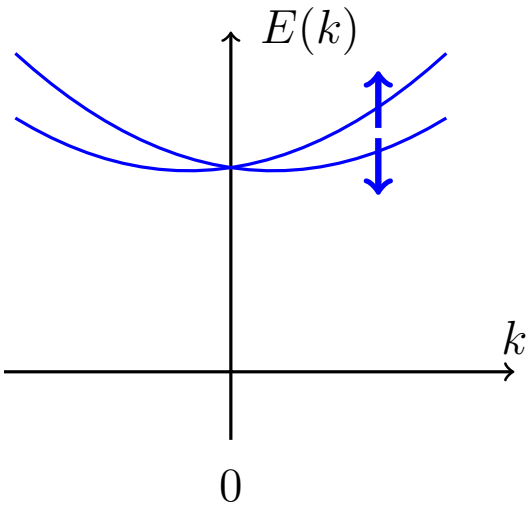

Figure 4.3: A sketch of a solid bandstructure where the spin-orbit interaction is present but there is lack of the inversion symmetry. The degeneracy is removed.

4.3 Density Matrix for an Ensemble of Spins

In QM some systems can be represented by a single state vector, i.e., a ray in Hilbert space and are called pure states. It is the case of systems prepared by performing a maximal measurement which determines the values of a complete set of commutating observables. The maximal measurement is not possible in systems which are prepared in such a way that some quantum numbers may be known only through a probability distribution. This is the case of a beam of particles which, for example, have 60% spin up and 40% spin down. In order to treat these physical systems, called mixed states, J. Von Neumann in 1927 introduced the density matrix formalism [37, 41].

Let us consider an ensemble of subsystems $\alpha = 1, 2, \cdots N$. Moreover let us assume that each subsystem is in a pure state $|\alpha\rangle$ that can be expanded into orthonormal eigenvectors $|n\rangle$ of some complete set of operators, then

$$|\alpha\rangle = \sum_n c_n^{(\alpha)} |n\rangle \,, \tag{4.44}$$

with

$$c_n^{(\alpha)} = \langle n \,|\, \alpha \rangle \quad \sum_n |c_n^{(\alpha)}|^2 = 1 \,. \tag{4.45}$$

The expectation value of an operator $\hat{A}$ in the pure state $|\alpha\rangle$ is then

$$\langle A \rangle_\alpha = \left\langle \alpha \left| \hat{A} \right| \alpha \right\rangle = \sum_n \sum_{n'} c_{n'}^{(\alpha)*} c_n^{(\alpha)} \left\langle n' \left| \hat{A} \right| n \right\rangle \,, \tag{4.46}$$

and its average value over the ensemble is

$$\langle A \rangle = \sum_{\alpha=1}^{N} P_\alpha \langle A \rangle_\alpha \,, \tag{4.47}$$

where P_α denotes the probability to obtain the subsystem α among the ensemble. Clearly being a probability the quantities P_α need to be such that

$$0 \leq P_\alpha \leq 1 \,, \quad \sum_{\alpha=1}^{N} P_\alpha = 1 \,. \tag{4.48}$$

Then the density operator $\hat{\rho}$ is defined as [37, 41]

$$\hat{\rho} = \sum_{\alpha=1}^{N} |\alpha\rangle P_\alpha \langle \alpha| \,, \tag{4.49}$$

and the density matrix

$$\rho_{nn'} = \langle n|\,\hat{\rho}\,|n'\rangle = \sum_{\alpha=1}^{N} \langle n\,|\,\alpha\rangle\, P_\alpha \,\langle \alpha\,|\,n'\rangle\,. \tag{4.50}$$

The advantage of the density matrix comes from the fact that its knowledge allows us to calculate the statistical average of any operator $\hat{A}$ via [41]

$$\langle A\rangle = \sum_{\alpha=1}^{N} \langle n\,|\,\hat{\rho}\hat{A}\,|\,n\rangle = Tr\left(\hat{\rho}\hat{A}\right)\,. \tag{4.51}$$

We recall that the density operator is positive semidefinite Hermitian, i.e.,

$$\hat{\rho} = \hat{\rho}^\dagger\,, \quad \rho_{nn} = \langle n|\,\hat{\rho}\,|n\rangle \geq 0\,, \tag{4.52}$$

where $\hat{\rho}^\dagger$ is the Hermitian conjugate of $\hat{\rho}$. Furthermore

$$Tr\left(\hat{\rho}^2\right) \leq Tr\hat{\rho} = 1\,. \tag{4.53}$$

The relation (4.53) holds for any density matrix representation as the trace is basis-independent. If the system is in a pure state $|\lambda\rangle$ then the density operator becomes a projection operator

$$\hat{\rho} = |\lambda\rangle\,\langle\lambda|\,. \tag{4.54}$$

The time-evolution of the density operator in the Schrödinger picture is given by the so-called Liouville-Von Neumann equation

$$i\hbar\frac{\partial\hat{\rho}}{\partial t} = [\hat{H},\hat{\rho}(t)]\,, \tag{4.55}$$

where $\hat{H}$ is the Hamiltonian operator relative to the physical system considered. In the case of a time-independent Hamiltonian, the differential equation (4.55) is readily solved, giving

$$\hat{\rho}(t) = e^{\frac{-i\hat{H}t}{\hbar}}\,\hat{\rho}(0)e^{\frac{i\hat{H}t}{\hbar}}\,. \tag{4.56}$$

We conclude this section, specializing in the previous formalism for a system of spin $\frac{1}{2}$ particles. Let us consider only the spin $\frac{1}{2}$ case, in a way that the 2×2 density matrix is evaluated over the eigenstates $|\chi\rangle$ of the spin operator along any direction $\hat{\mathbf{S}}_n$, i.e., $\langle\chi\,|\,\hat{\rho}\,|\,\chi'\rangle$. Then for a well known property of the Pauli

matrix, [41], the density matrix can be written as

$$\rho = a_0 I + a_x \sigma_x + a_y \sigma_y + a_z \sigma_z \,, \tag{4.57}$$

where I is the unit 2×2 matrix and $a_0 = \frac{1}{2}$ and a_x, a_y, a_z are three complex numbers. Defining the three-component vector $\mathbf{a} = (a_x, a_y, a_z)$, then (4.57) becomes

$$\rho = a_0 I + \mathbf{a} \cdot \sigma \,. \tag{4.58}$$

It follows from the above definitions and the properties of the Pauli matrices that

$$\rho = \frac{1}{2} \left(I + \sigma \cdot \tilde{\mathbf{P}} \right) , \tag{4.59}$$

where the spin polarization vector $\tilde{\mathbf{P}}$ is defined by

$$\tilde{\mathbf{P}} = \langle \sigma \rangle \,. \tag{4.60}$$

The physical meaning of the spin polarization vector can be understood if we diagonalize the matrix ρ in (4.59), finding [37]

$$\rho = \begin{bmatrix} \frac{1}{2}(1+\tilde{P}) & 0 \\ 0 & \frac{1}{2}(1-\tilde{P}) \end{bmatrix} , \tag{4.61}$$

where $\tilde{P}$ is the magnitude of the spin polarization vector. Clearly from (4.61) the eigenvalues $\frac{1}{2}(1+\tilde{P})$ and $\frac{1}{2}(1-\tilde{P})$ of ρ are the probabilities to find the pure states $|\uparrow\rangle$ and $\langle\downarrow|$ respectively in the ensemble. In this case as $\tilde{\mathbf{P}} = (0, 0, \tilde{P})$ and because a general spin state can be written as

$$|\chi\rangle = a_+ |\uparrow\rangle + a_- |\downarrow\rangle \,, \tag{4.62}$$

one finds

$$\tilde{P} = |a_+|^2 - |a_-|^2 \tag{4.63}$$

and therefore if $\tilde{P} = 0$ the two probabilities are equal to $\frac{1}{2}$ and the system is completely unpolarized. If $\tilde{P} = 1$ or $\tilde{P} = -1$ then the system is completely polarized and for the pure states $|\uparrow\rangle$ and $|\downarrow\rangle$ the density matrix becomes

$$\rho_{+\frac{1}{2}} = \begin{bmatrix} 1 & 0 \\ 0 & 0 \end{bmatrix} , \qquad \text{for} \quad \tilde{P} = 1 \,, \tag{4.64}$$

and

$$\rho_{-\frac{1}{2}} = \begin{bmatrix} 0 & 0 \\ 0 & 1 \end{bmatrix} , \qquad \text{for} \quad \tilde{P} = -1 \,, \tag{4.65}$$

Notice that for completely polarized pure states $\mathrm{Tr}\left(\rho^2\right) = 1$. If $0 < |\tilde{\mathbf{P}}| < 1$ then the system is said partially polarized. So it is common to call $|\tilde{\mathbf{P}}|$ the degree of polarization of the system [37].

4.4 Spin Relaxation Mechanisms in n-type GaAs

Let us assume that it is possible to inject an ensemble of spins, fully polarized, namely in the $z-$ direction, into a bulk nonmagnetic semiconductor. We observe that there are always some physical processes which lead to spin relaxation. Physicists describe the decoherence mechanisms using terms and concepts borrowed from Nuclear Magnetic Resonance (NMR). For a spin ensemble of mobile electrons there are two quantities T_1 , T_2 called spin relaxation time (also called longitudinal or spin-lattice time) and spin dephasing time (also transverse or decoherence time or spin-spin relaxation time) defined via the Bloch-Torrey equations [5, 12]. In NMR experiments a sample of spin $1/2$ nuclei is placed between the poles of a strong static magnetic field of strength B_0, let us say along the z- direction, and is inserted inside a coil driven by a pulsed radio frequency oscillator [12]. The overall magnetic $\mathbf{B}$ field acting on the nuclear spin is then

$$\mathbf{B} = B_0\hat{\mathbf{z}} + \mathbf{B}_1(t)\,, \tag{4.66}$$

where the magnetic oscillating field $\mathbf{B}_1$ is perpendicular to the unit vector $\hat{\mathbf{z}}$. The phenomenological Bloch-Torrey equations for the total magnetization $\mathbf{M}$, relative to an ensemble of mobile electron spins [5] are given by

$$\frac{\partial M_x}{\partial t} = \gamma(\mathbf{M}\times\mathbf{B})_x - \frac{M_x}{T_2} + D\nabla^2 M_x\,, \tag{4.67}$$

$$\frac{\partial M_y}{\partial t} = \gamma(\mathbf{M}\times\mathbf{B})_y - \frac{M_y}{T_2} + D\nabla^2 M_y\,, \tag{4.68}$$

$$\frac{\partial M_z}{\partial t} = \gamma(\mathbf{M}\times\mathbf{B})_z - \frac{M_z - M_z^0}{T_1} + D\nabla^2 M_z\,, \tag{4.69}$$

where $\gamma = g\mu_b/\hbar$ is the electron gyromagnetic ratio, g is the effective electron g-factor, D is the diffusion coefficient that for cubic semiconductors can be assumed a scalar quantity, $M_z^0 = \chi B_0$ is the thermal equilibrium magnetization, and χ is the system static magnetic susceptibility. The Bloch-Torrey equations well describe the experimental results of optical orientation and electron spin resonance. The terms containing T_1, T_2 in the above equations were introduced by F. Bloch in 1946 as he realized that a nuclear spin system was subject to

two different types of damping. The time constant T_1 is the time necessary for the longitudinal magnetization to reach equilibrium. In the case of longitudinal relaxation, there is change in energy accompanynig the variation of M_z typically due to the interaction of the electron spins with the crystalline lattice phonons, hence the name spin-lattice relaxation. In the absence of a magnetic field, T_1 describes the relaxation of a nonequilibrium spin population, i.e., the diagonal elements in the spin density matrix, towards equilibrium. The time constant T_2 is the time during which the ensemble of transverse electron spin components, initially in phase, lose their phase precessing about the longitudinal field, due to spatial and temporal fluctuations of the precessing frequencies [5]. The latter is in general a decay of coherent spin oscillations, or off-diagonal spin density matrix elements. As the energy-conserving changes in the transverse components of **M**, can occur only trough the interactions within the spin system itself, the name spin-spin relaxation is also used [12].

For mobile electrons a contribution to T_2 comes from the so-called inhomogeneous broadening, due to the g-factor spatial inhomogeneities that make the electrons to experience different spin precession rate and giving rise to dephasing. However in many situations this contribution is cancelled out by the so-called motional narrowing which is an inhibition of phase change by random fluctuations [5, 19], see the section 5.4 for a quantitative discussion.

In the present study we shall denote the spin dephasing time by one time-constant τ_s and call it spin relaxation time (SRT). The way in which τ_s is calculated in our case is shown in Appendix E .

In the case of GaAs there are four important spin relaxation mechanisms: the Bir-Aronov-Pikus (BAP) mechanism , the hyperfine interaction, the Elliott-Yafet (EY) mechanism and Dyakonov-Perel (DP) mechanism. In following a brief review of these decoherence processes is given.

A spin polarized electron population can trigger a dynamic nuclear polarization of lattice nuclei that have nonzero spin, like in GaAs. This process is very slow compared to characteristic electron time scale, i.e., a few picoseconds. Its effect is to create a random effective magnetic nuclear field that can have a magnitude of a few Tesla. This field influences only the spin dynamics, not the orbital motion, causing spin relaxation. This process is called Hyperfine Interaction [8]. It increases with the atomic number of the atoms. In bulk GaAs the experiments show that it is the main source of spin relaxation at low temperatures and for electronic concentrations below the metal-insulator transition, i.e. , about $5 \times 10^{16}\ cm^{-3}$ [15, 16].

Bir-Aronov-Pikus is the dominant spin relaxation mechanism in p-doped

semiconductors. In this case the electrons with spin up exchange their spin with holes with spin down. The spin relaxation rate is proportional to the number of holes [8, 19]. In n-type III-V semiconductors clearly this mechanism is ineffective due to the lack of holes.

Elliot-Yafet mechanism arises from the fact that SOI mixes the spin states of the electron wavefunction in the conduction band. In this case the single Bloch wavefunctions of an electron in the CB of index n can be written as [5]

$$\psi_{\mathbf{k}n\uparrow}(\mathbf{r}) = \left[a_{\mathbf{k}n}(\mathbf{r})\left|\uparrow\right\rangle + b_{\mathbf{k}n}(\mathbf{r})\left|\downarrow\right\rangle\right] e^{i\mathbf{k}\cdot\mathbf{r}}, \tag{4.70}$$

$$\psi_{\mathbf{k}n\downarrow}(\mathbf{r}) = \left[a^{*}_{-\mathbf{k}n}(\mathbf{r})\left|\uparrow\right\rangle + b^{*}_{-\mathbf{k}n}(\mathbf{r})\left|\downarrow\right\rangle\right] e^{i\mathbf{k}\cdot\mathbf{r}}, \tag{4.71}$$

where $a_{\mathbf{k}n}$, $b_{\mathbf{k}n}$ are complex lattice-periodic coefficients. Clearly they are not eigenstates of $\hat{\sigma}_z$ even if we still label them using $|\uparrow\rangle$, $|\downarrow\rangle$. This notation is used as in most of cases $|a_{\mathbf{k}n}| \approx 1$ meawhile $|b_{\mathbf{k}n}| \ll 1$ [5]. Because the electronic states in conduction band are no longer spin eigenstates, any perturbing potential even if spin-independent can cause electron spin-flip. Thus it follows that electron spin-flips may happen in electron scattering off the ionized impurities and phonons [75]. It was believed that EY becomes important in narrow band-gap III-V n-type semiconductors, for instance, n-InSb ($E_g = 0.2355\ meV$), at low temperature. Recently it was found using the kinetic spin Bloch equation (KSBE) that instead DP is still the dominant spin relaxation mechanism even at low temperature in the range of densities where the two mechanisms compete [76].

Finally the main source of spin relaxation in n-GaAs in the regime under our investigation is the Diakonov-Perel mechanism. The spin energy splitting due to the bulk inversion asymmetry of GaAs, is equivalent to an effective magnetic field whose Larmor frequency $\Omega(\mathbf{k})$ defined in (4.43), is electron momentum dependent. In this case during their motion the electrons undergo a spin precession given by the Dresselhaus term H_D in (4.42). Roughly we can say that spin relaxation due to DP happens as a result of the action of fluctuating effective magnetic fields. These fields cause spin precession at frequency ω and have a characteristic correlation time τ_c over which the fields can be approximately considered constant [8].

4.5 Ensemble Monte Carlo for Spin Dynamics

The Ensemble Monte Carlo method has been used extensively in modeling charge transport in semiconductor materials and devices. It can be used to

simulate specific devices and to include various scattering mechanisms, material properties and different boundary conditions, which makes it a highly flexible technique [26, 27].

This Monte Carlo method is a semiclassical approach in which the basic transport simulation in any semiconductor device begins with the random generation of free flight time for each particle which ends with a scattering event changing the energy and momentum of the particle. The process is then repeated for the next set of free flights. The free flight time is given by $\tau = -ln(r)/\Gamma$ where r is any random number between 0 and 1 and Γ is the total scattering rate (including self-scattering [10]) calculated at the beginning of the simulation. In between the scattering events the charge carriers are considered to propagate along a classical trajectory and are influenced by external forces due to applied electric and magnetic fields. The equations of motion for the free flight make use of the electric field obtained by solving the Poisson equation consistent with the device boundary conditions, see [27]. At the end of each free flight the type of scattering responsible for terminating it is chosen by using a random number between 0 and Γ, and then the new energy and momentum of the particle are calculated, see Appendix D. In order to update the momentum in an efficient way we implement a different algorithm described in Appendix D.

The scattering mechanisms considered in our simulation are scattering between electrons and phonons and scattering of electrons with ionized impurities. Phonon scattering involves both acoustic and optical modes as well as absorption and emission of phonons. The corresponding scattering rates are calculated using Fermi's Golden rule. Data sampling is done at regular time intervals Δt to allow for estimation of dynamic carrier parameters like position, velocity, energy as well as to update potentials and fields. The choice of this time interval Δt depends on the stability criteria [27].

The next step is to integrate the spin dynamics in the Monte Carlo simulation. At the beginning of the simulation when positions and velocities are assigned to carriers, a single electron spin density matrix ρ_i is defined for each particle as

$$\rho_i(t) = \begin{bmatrix} \rho_i \uparrow\uparrow (t) & \rho_i \uparrow\downarrow (t) \\ \rho_i \downarrow\uparrow (t) & \rho_i \downarrow\downarrow (t) \end{bmatrix}. \tag{4.72}$$

During the free flight sequence the spin of each particle evolves coherently which can be represented as

[10] Self-scattering is a fictitious scattering where actually nothing happens to the carrier. It is a scheme devised to greatly facilitate the calculation of the carrier time of flight [27].

$$\rho_i(t+\tau) = e^{-i(H_D)\tau/\hbar}\rho_i(t)e^{i(H_D)\tau/\hbar}. \tag{4.73}$$

Here, H_D is the spin dependent Hamiltonian (4.42) to incorporate the spin-orbit mechanism responsible for the relaxation of spin polarization. In the present calculations we have included only Dyakonov-Perel mechanism for spin relaxation as in n-type GaAs is the dominant one [15, 28, 76], at least in the range of temperatures and densities we consider. In DP mechanism, between the scattering events, electron spins precess with an effective, momentum dependent, Larmor frequency Ω. The direction of the momentum $\mathbf{p}$ changes due to electron scattering events, which results in spin reorientation. In our simulation the Hamiltonian H_D is given by the formula (4.42). Thus, the evolution operator in equation (4.73) is given by

$$e^{-i(H_D)\tau/\hbar} = \begin{bmatrix} cos(A\tau) - i\frac{C}{D}sin(A\tau) & -i\frac{B}{D}sin(A\tau) \\ -i\frac{B^*}{D}sin(A\tau) & cos(A\tau) + i\frac{C}{D}sin(A\tau) \end{bmatrix}. \tag{4.74}$$

In the above equation,

$$A = \frac{\gamma_{so}}{\hbar^3}\{[p_x(p_y^2 - p_z^2)]^2 + [p_y(p_z^2 - p_x^2)]^2 + [p_z(p_x^2 - p_y^2)]^2\}^{1/2},$$

$$B = [p_x(p_y^2 - p_z^2)] - i[p_y(p_z^2 - p_x^2)],$$

$$C = [p_z(p_x^2 - p_y^2)], \text{ and}$$

$$D = \{[p_x(p_y^2 - p_z^2)]^2 + [p_y(p_z^2 - p_x^2)]^2 + [p_z(p_x^2 - p_y^2)]^2\}^{1/2}.$$

The normalized spin polarization density can be written as

$$P_\alpha = \Sigma_i Tr(\sigma_\alpha \rho_i)/\Sigma_i Tr(\rho_i). \tag{4.75}$$

After each scattering event the particle momentum is updated and hence its Larmor frequency Ω. The spreading of these frequencies as the simulation proceeds ultimately causes the spin polarization to decay. In our simulation we consider the lowest conduction band in the effective mass approximation.

4.6 Results

This section is based on work done by S. Kapoor, myself, F. Rossi and I. D'Amico. We wish to analyze the effects of temperature and applied bias on electrically

injected spin polarization for the previous physical model where we discard the electron-electron interaction. We have simulated a simple spin-transport device consisting of a 3-dimensional n-type GaAs sample sandwiched between a ferromagnet (FM) and a non-magnetic material (NMS) as shown in Figure (4.4). It is a layered structure with electrical spin injection from the ferromagnet into the semiconductor layer. The presence of the FM and NM layers is simulated by implementing a fully polarized $\left(\rho_i(0) = \begin{bmatrix} 1 & 0 \\ 0 & 0 \end{bmatrix}\right)$ and an unpolarized $\left(\rho_i(0) = \begin{bmatrix} 0.5 & 0 \\ 0 & 0.5 \end{bmatrix}\right)$ spin reinjection from the left and right-end side respectively, into the GaAs layer. A bias is applied to the GaAs layer. Charge neutrality condition is implemented i.e. when an electron exits the GaAs layer, a new particle is reinjected at the other end of the device with a thermal velocity. The electric- field profile along the x direction is computed self-consistently at each time step via a coupled Poisson-Monte Carlo solution. Spin dynamics is calculated via the evolution of the spin polarization vector according to the equations (4.73-4.75).

Values of the spin-orbit coupling parameter γ_{so}, reported in the literature show a wide variation. Our studies on the temperature dependence of spin relaxation time in n-type *bulk* GaAs yields similar results to the ones obtained recently by Jiang et al. [76] using a kinetic spin Bloch equations approach when the same values of γ_{so} are used. Similar to [76], we also find a good agreement with experimental results in [15] for temperatures greater than 20 K with $\gamma_{so} = 8.2\ eV\mathring{A}^3$. Following [76] have used $\gamma_{so} = 23.9\ eV\mathring{A}^3$ for the range of temperatures and densities considered in the simulation results presented here.

In this section we analyze the effect of varying temperature and applied bias on the spin relaxation time in an n-type GaAs sample. The GaAs layer is uniformly doped with a carrier density of $1 \times 10^{17}\ cm^{-3}$ and its length is taken as

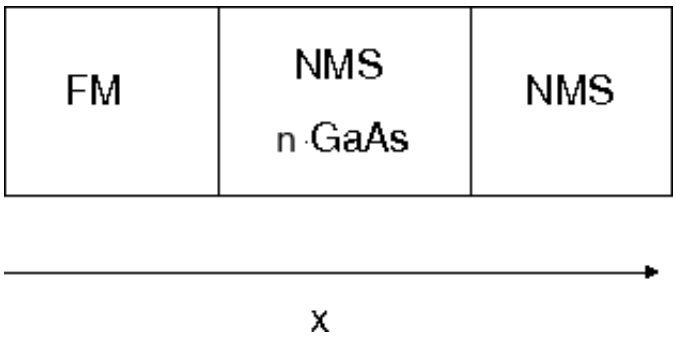

Figure 4.4: Sketch of the studied system

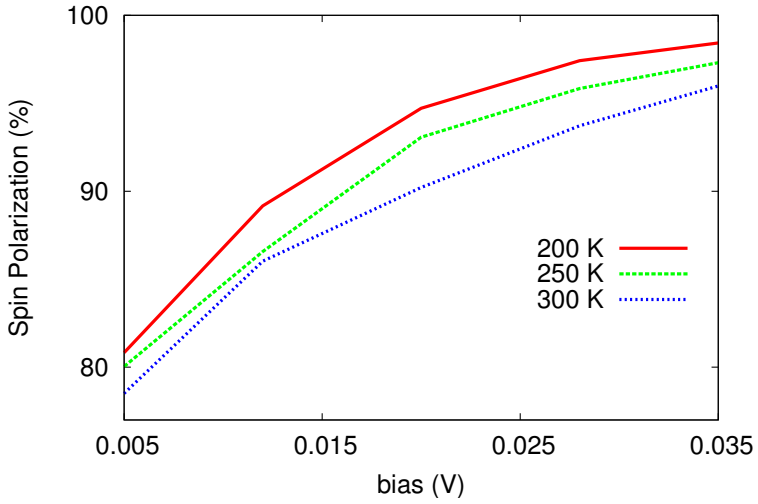

Figure 4.5: Variation of spin polarization with bias at the start of the simulated n-type GaAs layer at different temperatures after 20ps.

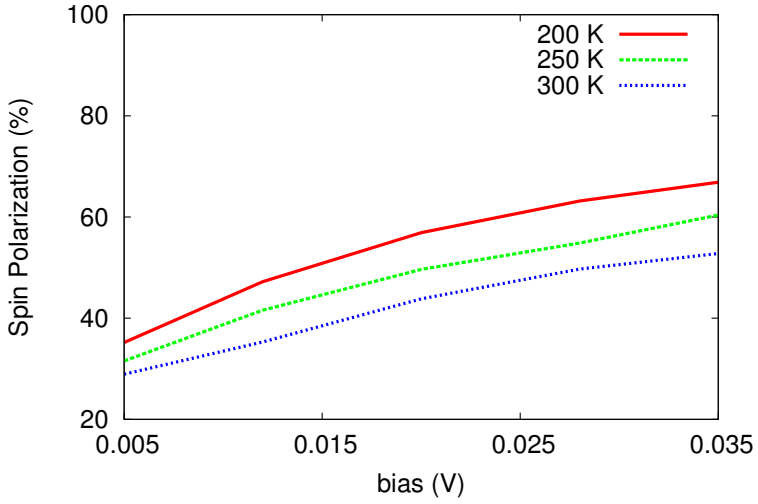

Figure 4.6: Variation of spin polarization with bias at the end of the simulated n-type GaAs layer at different temperatures after 20ps.

0.1 μm. The total number of simulated particles is 200000 and the sampling time step is $\Delta t = 0.1 fs$. Each simulation is run for 200000 time steps, i.e. for 20 ps. Figures 4.5 and 4.6 show the temperature and bias dependence of spin relaxation for the n-doped GaAs layer. The spin polarization decreases with the increasing temperature. For a particular temperature an increase in applied field enhances the spin polarization in the system. Figure 4.5 is plotted for the spin polarization (as defined by the equation (4.75)) at the left end of the GaAs layer whereas Figure 4.6 shows the residual spin polarization at the right end of the GaAs layer after a simulation time of 20 ps. Our results agree with the experimental [15, 77] and theoretical [76, 78] results which also predict that spin relaxation time decreases with increase in the temperature of the

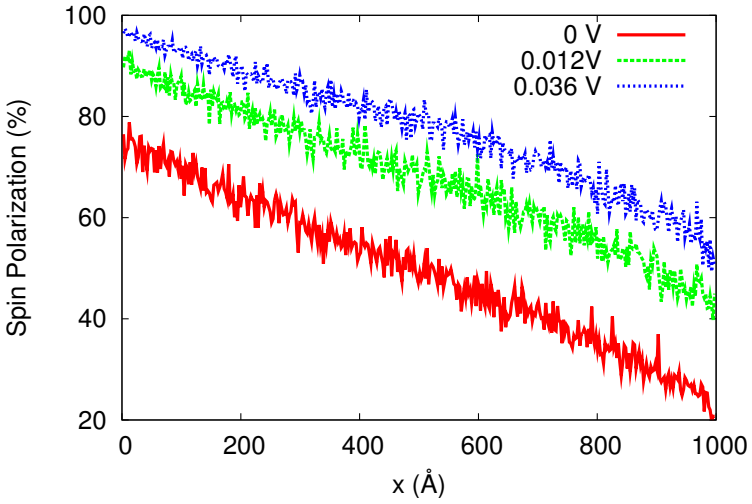

Figure 4.7: Spin polarization over the device length after 20 ps at 300 K and for varying applied bias.

system. In the high temperature regime, the effect of temperature on DP mechanism of spin relaxation is mainly determined by inhomogeneous broadening which is proportional to T^3 [76]. The spin dephasing is considerably affected by the applied fields. For no applied bias, at the start of the device the carriers show high spin-coherence which can be estimated in terms of approximately 80% spin polarization sustained in the device. We note that even though the injection condition from the FM interface is 100% polarization, the spin polarization close to the FM interface is decreased to less than 80% for no applied fields due to particle diffusion. This value decreases to about 20% at the end of the device. This can be seen in Figure 4.7 in which we have plotted the spin polarization over the whole length of the device after 20 ps, for a temperature of 300 K and for varying applied bias. At high applied fields the spin polarization is enhanced and at the end of the simulation more spin-coherence is retained in the system (approx. 50% at the right end of the GaAs sample for a bias of 0.036 V). This seems in agreement with the high-field effect predicted in [79]. We also have calculated the average spin polarization in the system at the end of the simulation time and this is shown in Figure 4.8. It is seen that for zero applied bias the system has an average of 50% spin polarization and this increases to nearly 80% for high bias (0.036 V) at 300 K. A similar trend is seen for lower temperatures but the system retains more spin-coherence in these cases, up to $\sim$ 85% at 200 K.

In conclusion our results show that increasing temperature reduces the spin relaxation times whereas high applied bias corresponds to a longer spin memory in the system.

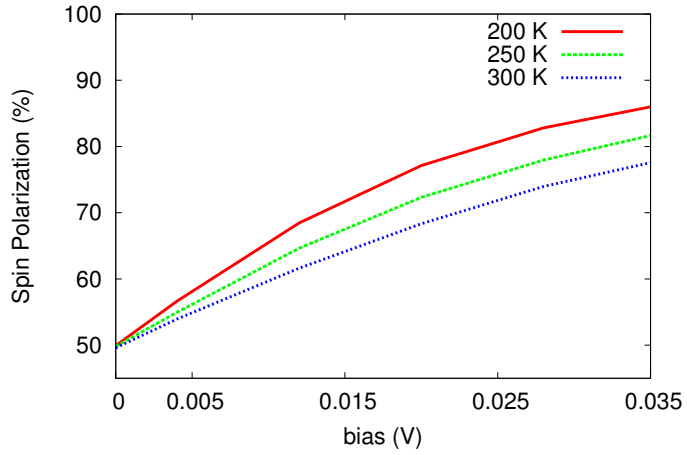

Figure 4.8: Spin polarization averaged over the device vs bias after 20 ps and for three different temperatures.

Chapter 5

The Effect of Electron-Electron Scattering on Spin Relaxation Time

The electron-electron (e-e) collisions are considered of minor importance for charge transport in semiconductors and in metals. As the total momentum of the electron gas is not changed by e-e collisions, the e-e scattering has a negligible effect on the mobility [80]. This is the reason why generally e-e scattering is not included in EMC calculations for charge transport, being also a difficult task, especially in the past when large computational resources were not available. In the metallic regime the Fermi gas with many-body Coulomb interaction is well describe by the framework of the Landau theory of the Fermi Liquid [45]. In this case the e-e scattering is very weak due to the Pauli exclusion principle and partly to the screening of the Coulomb interaction. This explains the success of the free electron model of metals (Drude Model) [10, 45]. However the e-e scattering affects the mobility in an indirect way as it modifies the energy distribution function and in particular is responsible for the thermalization of the non equilibrium carrier distribution. In fact from our EMC simulations we observed that without e-e scattering our system cannot reach the equilibrium even after a long time. The only dissipative scattering mechanism in our model is the POP scattering but its action evidently is not enough for the thermalization of the simulated electron ensemble. Despite the fact that the e-e scattering may be discarded for charge transport, some recent theoretical studies have shown that e-e interaction plays an important role in spin relaxation in III-V semiconductors [33, 76]. In particular Glazov and Ivechenko [33] have shown that e-e interaction slows down the spin relaxation due to the DP mechanism. In this chapter we shall present and discuss our results about the SRT due to DP mechanism in a n-type bulk GaAs.

5.1 The Electron-Electron Scattering in the Nondegenerate Regime

Within the RPA, Bohm and Pines [81] have shown that it is possible to describe the Coulomb interaction between the electrons as a result of two contributions. One is from the collective long-range behaviour (the electron-plasmon interaction) and the other comes from the individual electron-electron scattering. In the present work we consider only the latter as plasmon energies are very small compared to the other quasiparticles involved in collisions. For instance in GaAs plasmon energies becomes of the order 35 meV, i.e. likewise polar optical phonons, for electronic concentrations $n_e \sim 5 \times 10^{17}\ cm^{-3}$. Here we shall consider the following range of electron densities ($n_e = 10^{16}$ to $2.5 \times 10^{17}\ cm^{-3}$) at relatively high temperatures ($280 \leq T \leq 400K$) in order to compare our results with the experimental ones obtained by Oertel et al. [28]. However for the sake of completeness we should recall that for electronic concentrations greater than $n_e \sim 5 \times 10^{17}\ cm^{-3}$ the electron-plasmon scattering can no longer be ignored [1]. Moreover because GaAs is a polar semiconductor the situation becomes more complicated. In fact in the degenerate regime the longitudinal optical phonons becomes coupled via long-range polarization fields to the electronic system giving rise to plasmon-phonon coupled modes that are damped by the particle-hole excitations, the so-called Landau damping [82, 83]. From the phyiscal assumptions given in [81] the short range component of the e-e interaction can be approximated by the following screened (Yukawa-type) Coulomb potential for distances shorter than the screening length

$$v_{12}(|\mathbf{r}_1 - \mathbf{r}_2|) = \frac{e^2}{4\pi\varepsilon|\mathbf{r}_1 - \mathbf{r}_2|} e^{-\beta_{TF}|\mathbf{r}_1 - \mathbf{r}_2|} \tag{5.1}$$

$\mathbf{r}_1, \mathbf{r}_2$ are the (spatial) coordinates of the colliding electrons. Only binary electron-electron collisions are considered here as they are the most likely and effective scattering events. Indeed multiple scattering events can also happen, mainly in high carrier concentrations. The quantum states of the mobile electrons should be localized wavepackets but as it was already discussed in Chapter 2, they can be equivalently represented by plane wave states which we assume to hold in the following. Then the electron-electron (intravalley) scattering rate in the nondegenerate regime in EMC can be calculated by [2] [27]

[1] The plasmon energy is given by $\hbar\omega_p$ where the plasma frequency is $\omega_p = \sqrt{\frac{n_e e^2}{\varepsilon_0 m^*}}$ [10].

[2] For convenience the formula (5.2) can be transformed to an integral using the continuum limit $\sum_{\mathbf{k}} \to \frac{V}{(2\pi)^3} \int d\mathbf{k}$.

$$w_{ee}(\mathbf{k_0}) = \frac{m^* e^4}{\hbar^3 V \varepsilon^2} \sum_{\mathbf{k}} f_{\mathbf{k}} \frac{|\mathbf{k}-\mathbf{k_0}|}{\beta_{TF}^2 \left[|\mathbf{k}-\mathbf{k_0}|^2 + \beta_{TF}^2\right]^2}, \tag{5.2}$$

where V is the volume of crystal, $f_{\mathbf{k}}$ is the carrier distribution function, in general unknown except at equilibrium, $\mathbf{k_0}$ is the wavevector of the colliding electron and the sum runs over all the other states in the electon ensemble. Once the electron partner of wavevector $\mathbf{k}$ involved in the collision is chosen, the new updated states $\mathbf{k_0'}$, $\mathbf{k'}$ of the colliding electrons can be determined from the conservation of total energy and momentum and from the normalized scattering angular distribution [27]

$$P(\theta)d\theta = C \frac{\sin\theta d\theta}{\left[g^2 \sin^2(\theta/2) + \beta_{TF}^2\right]^2}, \tag{5.3}$$

where C is the following normalization constant

$$C = \frac{\beta_{TF}^2 \left(g^2 + \beta_{TF}^2\right)}{2}, \tag{5.4}$$

g denotes the magnitude of the vector $\mathbf{g} = \mathbf{k} - \mathbf{k_0}$, θ is the angle between $\mathbf{g}$ and its updated $\mathbf{g'} = \mathbf{k'} - \mathbf{k_0'}$ after the collision. A parabolic energy-momentum dispersion is assumed throughout.

The formula (5.2) needs to be given a careful consideration. From its derivation in [84] one realizes that the form of w_{ee} is due to our complete ignorance of the electron partner involved in the collision. This causes the necessity to include the distribution function of the electronic ensemble. Moreover the sum over all momenta of the carriers in conduction band is still a consequence of the ignorance about the scattering partner and makes (5.2) cumbersome and computationally demanding as the number of the carriers simulated in our case is at least $25,000$ particles. In Ensemble Monte Carlo simulations eventually one must choose randomly the scattering partner in the ensemble in order to update the dynamical variables of the scattered electron and its partner. So from this perspective we can argue about the actual necessity of (5.2) in EMC simulations. Once the scattering partner is given in some way, then considering the following facts it is possible to use a different formula for including the electron-electron scattering rate. Firstly we notice that (5.2) is derived by FGR as for all the scattering mechanisms in EMC. This is a constraint of the Ensemble Monte Carlo algorithm. Then if we consider the scattering between two electrons or between an electron and a single ionized impurity by looking at the matrix element in FGR, which gives the strength of the interaction, we realized there is no difference between an attractive and repulsive poten-

tial. This is a consequence of the BA. In other words Born approximation is not sensitive to the sign of the scattering potential. Therefore we may consider to use the electron-impurity scattering rate insofar some additional physical assumptions hold. In our model the internal structure of a single ionized impurity will be ignored. Also the antisymmetry of the colliding electrons will be ignored. Then that the Brooks-Herring for electron-impurity scattering rate (see formula (D.8) in Appendix D) can be used for the electron-electron case. Keeping in mind that now the masses involved in the collision are the same, in the following analysis we shall have $E = E_{lab}/2$ and $m^* = m^*_{lab}/2$, i.e., the energy and the effective mass of the colliding electron associated to the relative motion and E_{lab} is the electron energy in the laboratory frame, see equation (2.17) . In (D.8) we must identify the impurity doping concentration n_i with the electronic concentration n_e. The final scattering rate w_{ee} in BA for e-e scattering in EMC is then

$$w_{ee}(E) = \frac{2^{\frac{5}{2}}\pi n_e e^4}{(4\pi\varepsilon)^2\sqrt{m^*}E_\beta^2}\frac{\sqrt{E}}{1+4E/E_{\beta_{TF}}}\,. \tag{5.5}$$

$E_{\beta_{TF}}$ is defined by the relation (D.9), see Appendix D.

In the following we shall denote equivalently $w_{ee}(k)$ or $w_{ee}(E)$ or $w_{ee}(v)$ when referring to scattering rates expressed in terms of wavevector, energy or velocity variables, respectively. In Figure 5.1 it is shown the behaviour of the electron-electron scattering rates for two different electronic concentrations at $T = 300$ K. The maxima of the scattering rates happen at enery values $E_{\beta_{TF}}/4$.

It is evident that the scattering rates becomes very peaked towards low densities. This is a direct consequence of assuming that a Yukawa screend potential can describe the interelectronic potential even at low densities. The electron-electron scattering time τ_{ee} is of the order of few ps at room temperature and for the densities considered here.

It is important for the later discussion to recall here, in analogy with electron-impurity scattering, the angular scattering probability distribution for electron-electron scattering $P(\theta, E)$

$$P(\theta,E)d\theta = \frac{\left(1+\frac{E}{E_{\beta_{TF}}}\right)\sin\theta d\theta}{2\left[1+\frac{E}{E_{\beta_{TF}}}\sin^2\frac{\theta}{2}\right]^2}\,, \tag{5.6}$$

being θ the scattering angle in CoM [3].

[3] $P(\theta, E)$ can be derived from (5.6) or also from the scattering angular probability distribution for electron-impurity, see [27].

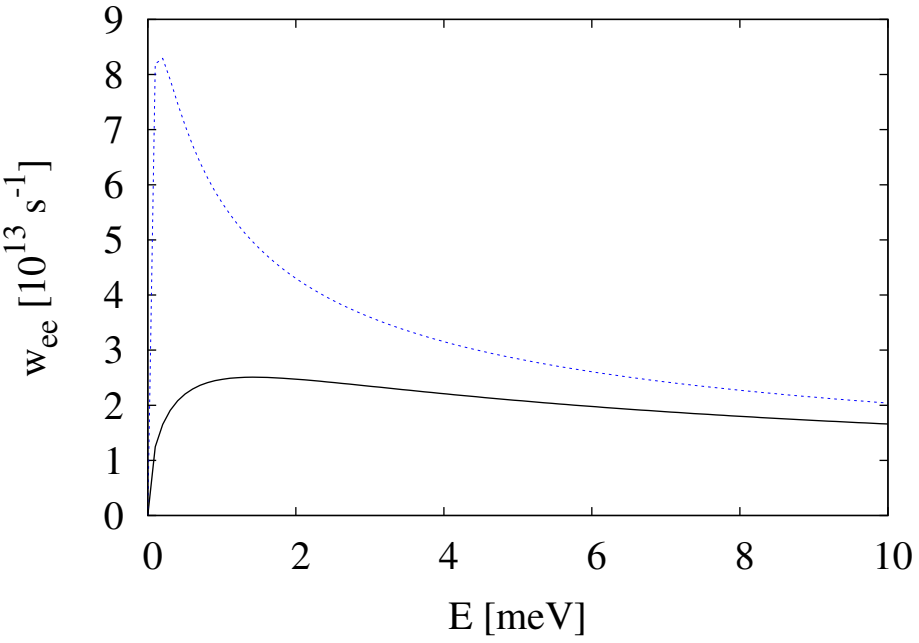

Figure 5.1: Comparison of the electron-electron intravalley scattering rates for different electronic concentrations, $n_e = 10^{16}\ cm^{-3}$ (dashed line) and $n_e = 10^{17}\ cm^{-3}$ (solid line) at room temperature in GaAs.

Let us now define the following parameter

$$\eta_E = \frac{4E}{E_{\beta_{TF}}}, \tag{5.7}$$

then $P(\theta, E)$ becomes

$$P(\theta, \eta_E)d\theta = \frac{2\,(4+\eta_E)\sin\theta d\theta}{\left[4+\eta_E \sin^2\frac{\theta}{2}\right]^2}. \tag{5.8}$$

The scattering angular distribution (5.8) is shown in the Figure 5.2 for different values of η_E. In comparison to (5.8) we notice that the scattering angular distribution of a pure Coulombic potential is energy independent, see Rutherford formula [37]

$$P(\theta)d\theta = \frac{d\theta}{\sin^4\frac{1}{2}\theta}, \tag{5.9}$$

and it diverges for small scattering angles. This is also the reason why the total cross-section of a pure Coulombic potential is infinite.

We show that for our model of the interelectronic potential, i.e., a screened Yukawa potential $V(r) = -(Ze^2/4\pi\varepsilon r)e^{-r/a}$ whose screening length a is given by a finite temperature LTFA, the Born approximation is never satisfied at low energies. The BA requires that close to the scattering centre at $\mathbf{r} = 0$ there is a distortion of the colliding particle wavefunction that we can assume roughly

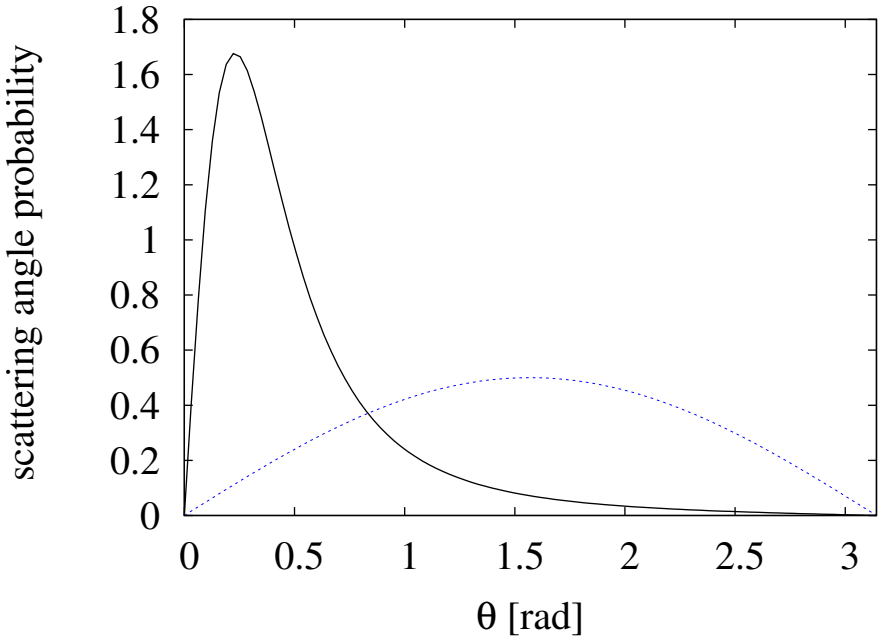

Figure 5.2: The scattering angle probability distribution $P(\theta, \eta_E)$ for different values of η_E, $\eta_E = 100$ (solid line) and $\eta_E = 0.01$ (dashed line). It is evident that increasing the parameter η_E, i.e., the energy of the colliding electron, the distribution becomes peaked at small angles. In other words the collisions in forward direction become favoured.

a plane wave. For a spherically symmetric potential $V(r)$ this condition can be written as [38, 43]

$$\frac{\mu_r}{\hbar^2 k}\left|\int_0^\infty \left(e^{2ikr}-1\right)V(r)\,dr\right| \ll 1\,, \tag{5.10}$$

and substituting the screened Coulomb potential (2.77) into (5.10) we obtain [38]

$$\frac{2\mu_r Z e^2 a}{\hbar^2 k}\left|\int_0^\infty \frac{\sin x}{x} e^{ix-x/ka}dx\right| \ll 1\,, \tag{5.11}$$

where $x = kr$ is a new variable of integration. In the low energy limit, $ka \ll 1$, the inequality (5.11) becomes [38]

$$\frac{2\mu_r Z e^2 a}{4\pi\varepsilon\hbar^2} \ll 1\,. \tag{5.12}$$

The low energy condition [4] (5.12) assuming that the interaction range $a \simeq \lambda_{TF}$

[4]The low energy limit within BA requires that $ka \ll 1$. We can express it in term of the colliding carrier energy E . Then it becomes $E \ll E_{\beta_{TF}}$ which may be barely satisfied by the most likely colliding electrons, recalling that the maxima of the scattering rates are at energy values $E = E_\beta/4$.

and recalling that in our case, $Z = 1$, $\mu_r = m^*/2$ becomes

$$R = \frac{m^* e^2 \lambda_{TF}}{4\pi\varepsilon\hbar^2} = \frac{\lambda_{TF}}{a_0^*} \ll 1\,, \tag{5.13}$$

where we used the definition of the effective Bohr radius (3.21). The inequality (5.13) is never satisfied for λ_{TF} calculated at $T = 300$ K in the range of the electronic densities of interest, see Figure 5.3 [5]

This confirms that the BA is not a good approximation for low energy collisions. One may think that including the second term of the Born series that the situation can improve. Unfortunately it has been shown that for a Yukawa potential the second Born approximation fails miserably[37]. The comparisons for the differential cross-section have been done with the exact results calculated using the partial wave method. The calculated differential cross-section in BA for a Yukawa gives values that in general can be slightly smaller or greater relative to the exact value. We do indeed conclude that clearly we cannot trust them too much.

How much the scattering is overstimated is a complicated issue which relies on the true knowledge of the interelectronic potential. Kukkonen and Smith [85] using the method of phase shifts assuming a scattering potential like (5.1) in metals have found that the electron-electron cross section is overstimated by a factor 2. As in the present work the antisymmetry of the colliding carriers is not taken into account, we should expect that in our case the electon-electron scattering probability overstimates by more than twice the actual probability in high density limit when the semiconductor becomes metallic.

5.2 Third-Body Rejection

The standard theory of scattering relies on the assumption that only binary collisions are likely to happen, this is why one requires that in the scattering experiments the target is thin enough. In nuclear and atomic physics, non-relativistic three-body scattering, in contrast to the three-body problem in classical mechanics, can be solved iteratively as done by Faddeev equations [37]. Instead of treating three-body collisions, it may be easier to exclude the third body. In the field of semiconductor physics this task has been accomplished by Ridley [86]. Requiring that only two particles are involved in a scattering event, Ridley has introduced a probability that weights a two-body scattering

[5] The right-hand term in the inequality (5.13) is nothing but than a rescaling of screening length.

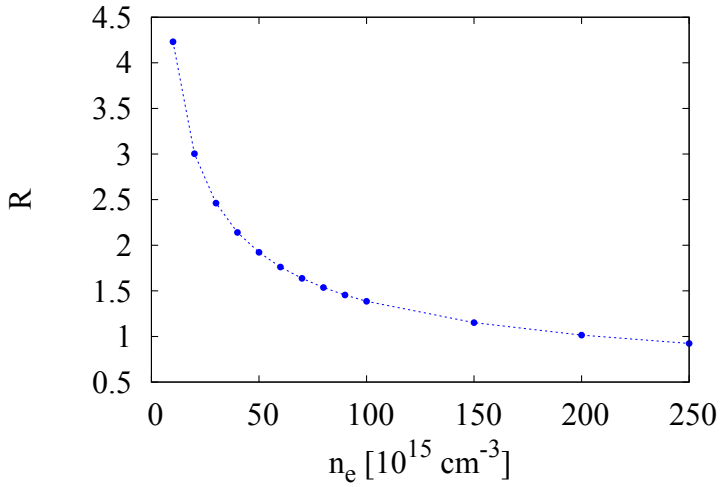

Figure 5.3: The ratio R in (5.13) is plotted against the electronic densities of interest at $T = 300$ K.

event in a way that there is no third-body within the impact parameter b of the colliding particles. Ridley did it in order to reconcile the calculations of the mobility in semiconductors which use two different scattering formulae for electron-impurity scattering, the Conwell-Weisskopf and Brooks-Herring for pure Coulombic potential and for a Yukawa screened potential, respectively. As we do not include the (fermionic) antisymmetry of the colliding electrons, we can extend a similar analysis to the electron-electron scattering in the non-degenerate regime. Then the probability $P^{(tbr)}$ is defined as [86]

$$P^{(tbr)} = e^{-\pi n_e a b^2}, \tag{5.14}$$

and the following quantity a, roughly the average distance between the scattering centres, is defined by [32]

$$a = \frac{4}{\pi} \frac{1}{\sqrt[3]{n_e}}. \tag{5.15}$$

Notice that the impact parameter b is essentially a classical concept, see Figure 5.4, as we need to know the actual trajectory of scattered particles to determine the differential cross-section. Clearly the classical concept of trajectory clashes with the Heisenberg's uncertainty principle. In classical physics in some cases it is possible to give the functional dependence of b upon the scattering angle θ.

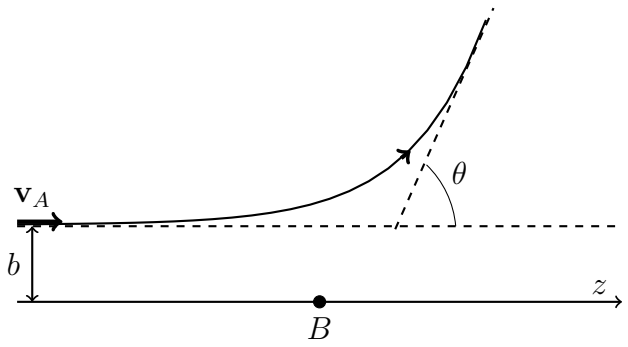

Figure 5.4: The scattering of a classical particle. The position of the colliding particle A with velocity $\mathbf{v}_A$ can be defined by the cylindrical coordinates (b, ϕ, z). B is the scattering centre and θ is the scattering angle. The impact parameter b is the distance of the asymptotic particle path from the line of head-on collision.

The general differential relation between b and θ is [37]

$$b\,db = b\left|\frac{b}{d(\cos\theta)}\right|\left|(\cos\theta)\right|, \tag{5.16}$$

and recalling the definition of the differential solid angle, the differential cross-section can be written as

$$\sigma(\theta) = \frac{b}{\sin\theta}\left|\frac{db}{d\theta}\right|. \tag{5.17}$$

The determination of $b(\theta)$ is not an easy task. In classical mechanics for central force problems it is determined from the orbit equation. For a pure Coulombic potential the following simple result is given [87]

$$b(\theta) = \frac{Z_1 Z_2 e^2}{2(4\pi\varepsilon)E}\cot\frac{\theta}{2}. \tag{5.18}$$

In the case of a Yukawa potential the relation is [6][86]

$$b^2(\theta) = \frac{C^2}{\left(1+\beta_{TF}^2\right)}\frac{\left(1-\sin^2\frac{\theta}{2}\right)}{\left(\sin^2\frac{\theta}{2}+\beta_{TF}^2\right)} \tag{5.19}$$

where C is defined as

$$C^2 = \frac{4e^2}{(4\pi\varepsilon)^2(4E)^2}. \tag{5.20}$$

For Ensemble Monte Carlo simulations we need a scattering rate $w_{ee}^{(tbr)}$ for the third-body rejection (tbr) . Van de Roer and Widdershoven derived the following formula [88]

[6]Notice that it may be useful to use this integral relation $\pi b^2 = \int_\theta^\pi \sigma(E,\theta')\sin\theta' d\theta'$, see [88].

$$w_{ee}^{(tbr)}(v) = \frac{v}{a}\left[1 - e^{\left(-\frac{a w_{ee}(v)}{v}\right)}\right]. \tag{5.21}$$

Van de Roer and Widdershoven stated that the scattering rate given by (5.21) should reduce the number of scattering events with large impact parameters, i.e., with small scattering angles [88]. Clearly in our model there may not be large arbitrary impact parameters. In fact the collisions of electrons happen in distances of order λ_{TF} according to model we consider here. There is also a bound for the impact parameter, i.e., $b < \lambda_{TF}$.

Now we shall give the reason for which we think third-body method is suitable in our model. In the scattering theory, see Chapter 2, the differential cross-section assumes that the collisions involve only two particles. Our electron-electron scattering rate is also derived assuming two-body collisions. When the electronic densities increase and consequently the average distance between the electrons in the conduction band decreases the ideal condition of two-body scattering on which the concept of cross-section is built probably is no longer satisfied. In strict analogy to electron-impurity scattering there are reasons for believing that scattering processes which involves more than two electrons simultaneously become important [32, 89]. In the case of the three-body collisions [7], there exist already some methods to treat them. For example, one can calculate the cross-section for a multi-potential scattering due to an electronic pair [90] or otherwise can resort to Faddeev equations [37]. As far as we know these quite difficult techniques are not yet implemented in Ensemble Monte Carlo. From this point of view it seems easier to use the method devised by Ridley. Basically the third-body method introduces an additional probability factor, "third-body exclusion factor "which assures that the collision are truly two-body processes. We can visualize how the third-body method works. In an ideal collision only two particles A and B are involved and σ_{AB} gives the probability of the collision, see Figure 5.5. Let us add a third-body C to the system, see Figure 5.6. If we now look at the subsystem $A+B$ we realize that the scattering of particle A with B has smaller probability because there is also a probability that A will scatter with C. Thus the cross-section σ_{AB} should decrease and its new value is given by a new cross-section $\sigma_{AB}^{(tbr)}$ obtained by the previous one multiplied by the exponential factor in (5.14).

[7] Notice that the fermion antisymmetry is not considered in our model. This means that we are treating the electrons like distinguishable classical particles.

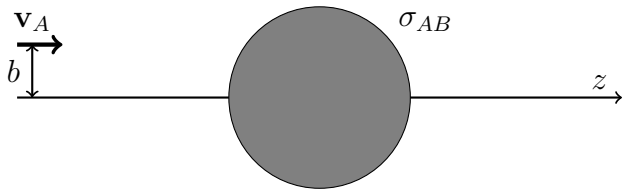

Figure 5.5: The collision of two particles A and B. The area of σ_{AB} is approximately proportional to the scattering probability of the system $A+B$.

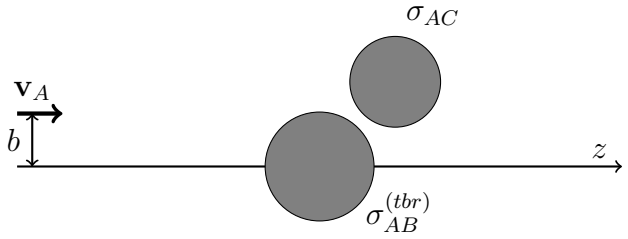

Figure 5.6: When a third body C is present, σ_{AB} is smaller and its value $\sigma_{AB}^{(tbr)}$ is now obtained by the third-body method.

5.3 Ensemble Monte Carlo Simulations

This work has been done together with Matthew Hodgson. My main contributions among the others were the implementation of scattering and screening theory and the final analysis of the results.

Let us summarize briefly the physical model which we consider for our simulations. We study carrier and spin dynamics in n-type bulk GaAs considering a single parabolic energy band, the central valley which determines an effective isotropic electron mass. This approximation is justified as we do not consider highly energetic electrons excited by laser pulse or by strong electric field, so that intervalley collisions are negligible. We include only normal-type scattering events as Umklapp processes are negligible in direct gap doped semiconductors. The scattering mechanisms considered are electron-acoustic phonon scattering, electron-polar optical phonon scattering, electron-single charged ionized impurity scattering in Brooks-Herring approach and finally electron-electron scattering. The polar optical phonon scattering which includes absorption and emission with a threshold energy of 35 meV is the only dissipative process. Phonons are considered at equilibrium at the lattice temperature T. The scattering rates of electrons from an initial state $|i\rangle$ and a final state $|f\rangle$ are calculated to first order according to the Fermi Golden Rule. The screened Coulomb potential for electron-electron and electron-impurity interactions are determined in the static limit and for a small momentum transfer

by LTFA as explained in Chapter 3. The scattering rates for each collisional mechanism are described in section 5.1 and Appendix D.

The carrier and spin transport are simulated through Ensemble Monte Carlo method. The initial electron positions and momenta are chosen in the following way. The electron positions are generated randomly inside the bulk semiconductor by the generation of uniform pseudorandom numbers. Their momenta are generated according to a Maxwell-Boltzmann distribution at $T = 130K$. After an initial transient period the system reaches thermal equilibrium at a given temperature T. The thermalization is mainly due to the strong POP collisions and the energy conserving e-e scattering. The first mechanism is the only source of the thermal contact with the enviroment in our simulated system.

In this work we improve over previous EMC schemes [27] for e-e scattering and allow electrons to scatter only with electrons which are within one screening length of each other. In our scheme both particles scatter and their momenta are both updated. This approach prevents the unphysical accumulation of energy or momentum prevalent in other methods, and the scattering of electrons at opposite ends of the device.

To implement this we effectively discretized the space into a grid of cubes of one screening length. We kept track of the number of potential scattering events, which include each particle scattering off any in the same grid or in any of the neighboring grids. Each time an electron- electron event is required we chose randomly from each of these potential pairings, checked that they were within one screening length of each other, and if they are we carry out the scattering, if they are not within one screening length of each other we choose a different electron as second particle in the scattering.

In order to ascertain that the thermalization is reached, we have to check whether the carriers' energy distribution is a Boltzmann one. In our simulations for lattice temperature $T = 300K$ we notice that the system reaches the equilibrium after the first 20 picoseconds. At this point we set the electronic spins fully polarized along one direction, namely, the z-axis, and then we start to collect the data from the simulations.

We are interested in the calculations of spin relaxation times τ_s during the spin dynamics. The spin dephasing in a bulk n-GaAs is mainly due to Dyakonov-Perel mechanism, see Chapter 4, in the range of the moderate doping concentrations ($n = 10^{16}$ to $2.5 \cdot 10^{17}\ cm^{-3}$) and the high temperatures ($280 \leq T \leq 400\ K$) considered here due to the availability of the experimental data obtained by Oestreich's group [28].

In the present work the spin dynamics is implemented in a different way with respect to our previous work discussed in section 4.5. We present this different method based on Crank-Nicholson algorithm and the way we estimate the spin relaxation times in Appendix E.

Thus in the following sections we shall compare our results from EMC simulations with the experimental ones obtained by Oertel et al. [28].

5.4 Results and Comparison with Experiments

Apart from assuming an exponential decay of the total spin polarization in the z-direction, we note that our simulations have *no fitting parameters*. In particular the spin orbit coupling value used is *not* fitted, but we use the value suggested by Oertel et al. [28] for their experimental data: $\gamma_{so} = 21.9\text{eV}\,\mathring{A}^3$.

In Figure 5.9 we plot results from simulations with (τ_s^{ee}) and without ($\tau_s^{no\ ee}$) electron-electron scattering to examine the effect that the inclusion of electron-electron scattering has on τ_s at room temperature. When we plot τ_s against the range of densities $n_e = 1 \times 10^{16} cm^{-3}$ to $n_e = 2.5 \times 10^{17}\ cm^{-3}$, we see that the inclusion of electron-electron scattering causes a net increases of τ_s at all densities. Glazov and Ivchenko [33] predicted a similar result in the case of a two-dimensional non-degenerate electron gas in GaAs, explaining it with additional motional narrowing caused by the e-e scattering. Our result suggests that this effect is present also in the three-dimensional case.

Here we need to say a few words about the physics behind the motional narrowing, a term borrowed from nuclear spin resonance research in liquids [19]. Let us consider a spin wich precesses about the z axis with Larmor frequency Ω. Let us assume that the frequency changes randomly between Ω and $-\Omega$ with correlation time τ_c. This means that after time τ_c, the spin has the same probability to continue its precession in the same direction or in the opposite one. During τ_c the phase accumulated is $\delta\varphi = \Omega\tau_c$ [19]. If now we consider the spin precession like a random walk with step $\delta\varphi$, after N steps the spread of the phase is given by the standard deviation [19]

$$\varphi = \delta\varphi\sqrt{N}. \tag{5.22}$$

We define the spin dephasing time τ_s the time at which the standard deviation $\varphi \approx 1$ [19]. Since $N = t/\tau_c$, one obtains

$$1 = \delta\varphi^2 \frac{\tau_s}{\tau_c}, \tag{5.23}$$

and then the spin relaxation rate is given by

$$\frac{1}{\tau_s} = \Omega^2 \tau_c \,. \tag{5.24}$$

The equation (5.24) explains how the DP mechanism works. In fact the Dyakonov-Perel spin dephasing can be understood as a random precesssion of the electron spin due to the fluctuations of the orientations and the precession frequencies [19].

For instance if we look at Figure 5.9 we can interpret the greater spin relaxation times when we include the e-e scattering due to the fact that the number of the collisions in the system is now increased and therefore the correlation time τ_c is smaller, see the relation (5.24).

If now we look at the curve τ_s^{ee} only in Figure 5.9, we can still intepret its monotonic behaviour within the counterintuitive motional narrowing phenomenon. In fact in the nondegenerate regime the electron-electron scattering rate is proportional to the electron density n_e [76] [8] therefore the increasing of the e-e collisions in the high concentration region slows down the spin relaxation time rate.

Finally we notice that the percentage increase of τ_s with respect to its non-interacting approximation decreases with increasing density, from about $\sim 90\%$ to about $\sim 70\%$, remaining though always very substantial even for $n_e = 2.5 \times 10^{17}\ cm^{-3}$. Its absolute increment $\tau_s^{ee} - \tau_s^{no\ ee}$ instead increases with the electronic density.

We observe that, when including e-e interaction, our results for densities $10^{16} cm^{-3} \leq n_e \overset{\sim}{<} 10^{17} cm^{-3}$ are in *very good agreement with the experimental data* reproduced in Figure 5.7 which we also included in Figure 5.9.

However, at higher densities, our results for τ_s^{ee} start to overestimate the experimental data for τ_s, reaching $\sim 20\%$ overestimate when $n_e = 2.5 \times 10^{17} cm^{-3}$.

5.4.1 Effect of Including the Third-Body Rejection Correction

We speculate that the overestimate of τ_s for $n_e \overset{\sim}{>} 10^{17} cm^{-3}$ is due to the BA overestimating the e-e scattering rate, as discussed in section 5.1 ; in the following we will then check if including corrections due to third-body-rejection to the e-e interaction improves our results.

In Figure 5.10 we compare calculations of the spin relaxation time when we

[8] Notice that the e-e scattering rate (5.5) we use in our calculations has a more complicated behaviour with the electron density, as $E_{\beta_{TF}}$ depends also on n_e.

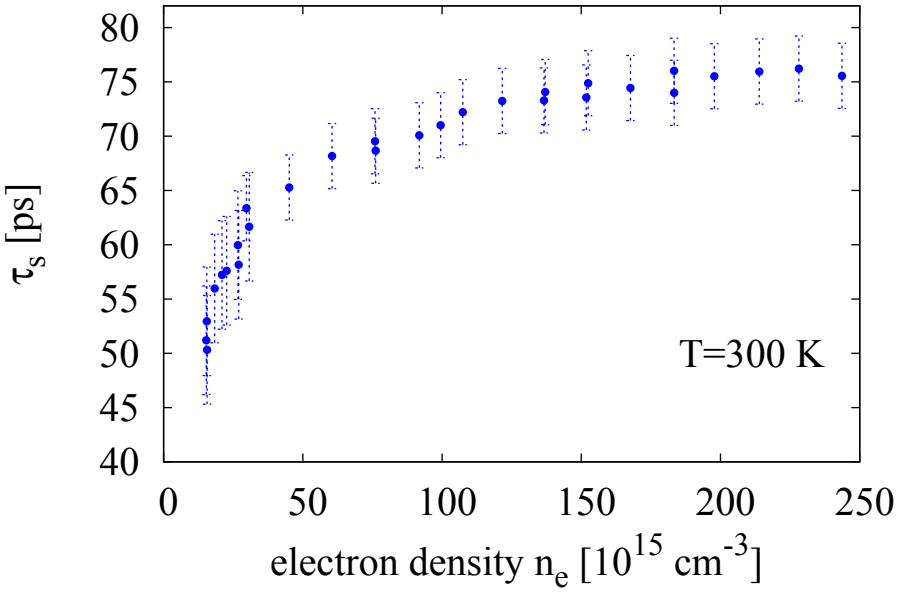

Figure 5.7: Experimental spin relaxation times τ_s versus electron density n_e measured at $T = 300$ K. Data are extracted from Oertel's original curve in Figure E.2 in Appendix E.

include e-e interactions with ($\tau_s^{ee,tbr}$) and without (τ_s^{ee}) corrections due to third-body rejection. As expected, the reduction of the e-e scattering rate due to the inclusion of third-body rejection results in a reduction of the spin relaxation time at all densities, which, for the range of densities studied, becomes more significant with increasing density.

In Figure 5.10, we observe that, at relatively high densities, $\tau_s^{ee,tbr}$ significantly improves over τ_s^{ee}, giving *results within the experimental error bars* for $1.5 \times 10^{17} \leq n_e \leq 2.5 \times 10^{17}$.

However for decreasing densities we see that $\tau_s^{ee,tbr}$ departs from the experimental results, underestimating τ_s, and significantly so for the density range where τ_s^{ee} has a good agreement withdifferent the experimental data.

5.4.2 Temperature Dependence

We wish now to focus on the effect of temperature on the spin relaxation time.

To make contact with the experimental results reproduced in Figures 5.11 and 5.12 , we consider the temperature range 280 $K \leq T \leq 400$ K and two (fixed) densities, $n = 2.7 \times 10^{16} cm^{-3}$ and $n = 3.8 \times 10^{16} cm^{-3}$. In both cases we will consider interacting carriers, but with and without third-body-rejection corrections.

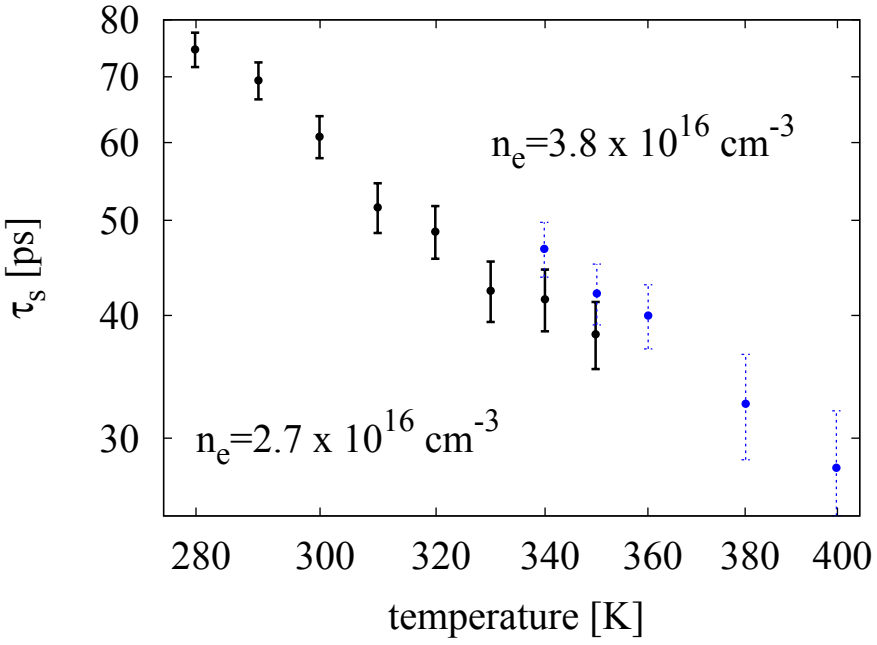

Figure 5.8: Experimental spin relaxation times τ_s versus temperature T measured at two different densities (doubly logarithmic scale). Data are extracted from Oertel's original curve in Figure E.3 in Appendix E.

In Figure 5.11 we present our results for $n = 2.7 \times 10^{16} cm^{-3}$, and in Figure 5.12 when the carrier density is $n = 3.8 \times 10^{16} cm^{-3}$. We find good agreement over the entire temperature range between τ_s^{ee} and the experimental data; however when corrections due to the third-body rejection are included, our results for the lowest temperatures for each density underestimate the experimental results, remaining compatible with them at the highest temperatures.

This is in agreement with the results shown in Figure 5.10 where, for $T = 300$ K and the two values of n_e the considered here, third-body rejection becomes less important, and $\tau_s^{ee,tbr}$ converges towards τ_s^{ee}.

The agreement between τ_s^{ee} and the experimental results – good at all temperatures – improves for increasing temperature. This could be explained with the fact that increasing the temperature, the colliding (thermal) electrons are on average more energetic and therefore the accuracy of the Born Approximation should be improving.

5.4.3 Dependence on the Value of the Spin-Orbit Coupling

In our model there may be only one potentially free parameter, the spin-orbit coupling due to its experimental uncertainty [74]. In fact the values of the spin orbit coupling for GaAs found in the literature vary greatly [74]; one of the

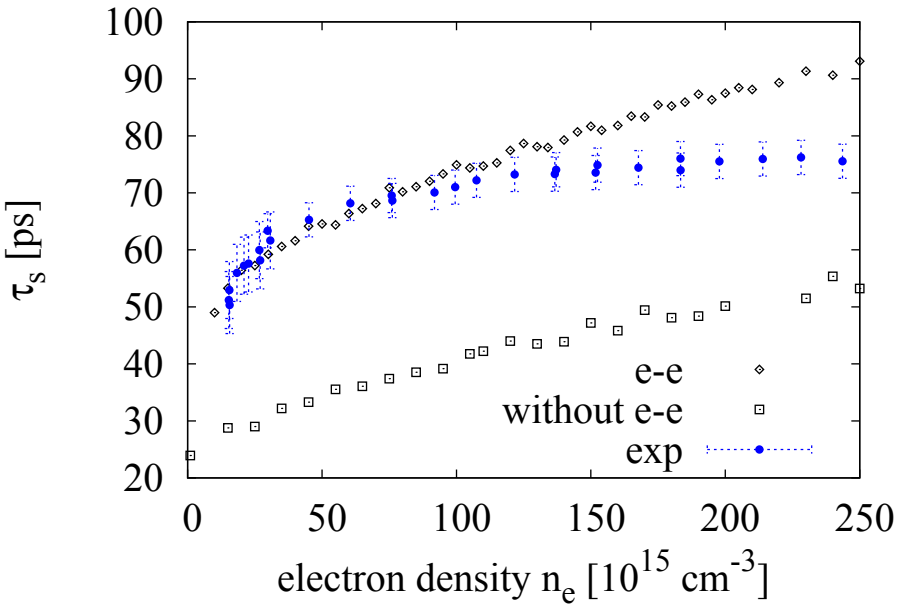

Figure 5.9: Results for τ_s vs electronic density calculated with and without electron-electron interaction. Here: $N = 25,000$, $T = 300$ K and $\gamma_{so} = 21.9\ eV\AA^3$.

main points in our work is that we *do not* treat γ_{so} as an adjustable parameter, but simply use the value provided by experimentalists [28]. In order to let the reader appreciate how valuable this is, and in this respect how surprising is the very good agreement between our data and the experimental ones, in this section we wish to show how sensible our simulations are with respect to the value of γ_{so}. In Figure 5.13 we plot τ_s^{ee} for three different values of γ_{so}, all within the range suggested in the literature. It can be seen that by varying γ_{so}, results for the spin relaxation time would vary within *one order of magnitude*, and this *for the whole density range* here considered. We think that this is a convincing proof that the very good agreement between our results and the experiments is not accidental, but derives from the improvements we have devised in treating the e-e interaction within the EMC method. These improvements allow us to account properly for the electron-electron interaction within the simulations.

5.4.4 The Effectiveness of Third-Body Rejection in Higher Electronic Concentrations

We implemented third-body rejection in the following way. In ensemble Monte Carlo the carriers during the free flight between two consequent scattering events have a certain average speed v. The average interparticle distance a in formula (5.21) can be thought of as the distance between two scattering centres.

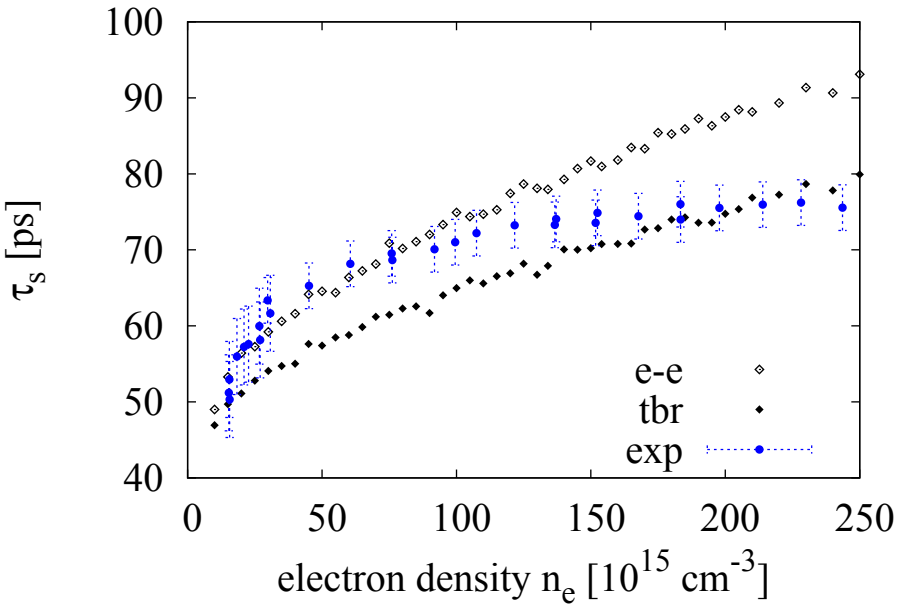

Figure 5.10: Spin relaxation time versus electron density. All data include e-e scattering, with (lower curve, $\tau_s^{ee,tbr}$), and without (upper curve, τ_s^{ee}) third-body rejection corrections. Parameters: $N = 25,000$, $T = 300$ K, and $\gamma_{so} = 21.9$ $eV\AA^3$.

From this perspective the e-e scattering time, i.e., the average collision time, is roughly a/v. Thus in our EMC implementation, the formula for third-body rejection (5.21) becomes

$$w_{ee}^{(tbr)} \simeq w_{ee}\left[1 - e^{\left(-\frac{aw_{ee}}{v}\right)}\right]. \tag{5.25}$$

Now the probability $w_{ee}^{(tbr)}$ on the left hand side is equivalent to a probability, w_{ee}, multiplied by a weighting factor, the term in the parentheses on the left hand side. We expect the $w_{ee}^{(tbr)}$ as given by the relation (6.2) where an exponential factor multiplies the Yukawa differential cross-section, decreases the e-e scattering probability. This seems also evident from our results for SRT, see Figure 5.10. In order to ascertain how effective the reduction is, we evaluated the term in the parentheses of (5.25) for different energies of the colliding electrons. We plotted it versus the electronic density n_e in Fig. 5.14.

In Figure 5.14 it is evident that tbr method reduces the e-e scattering rate strongly in the higher electronic concentration region. This explains its effectiveness in the calculations of the spin relaxation times in that region. Incidentally tbr method seems to confirm that BA overestimate the e-e scattering at least in that region because $\tau_s^{ee,tbr}$ is in good agreement with the experimental data meanwhile τ_s^{ee} is overestimated as we discussed in the section 5.4.

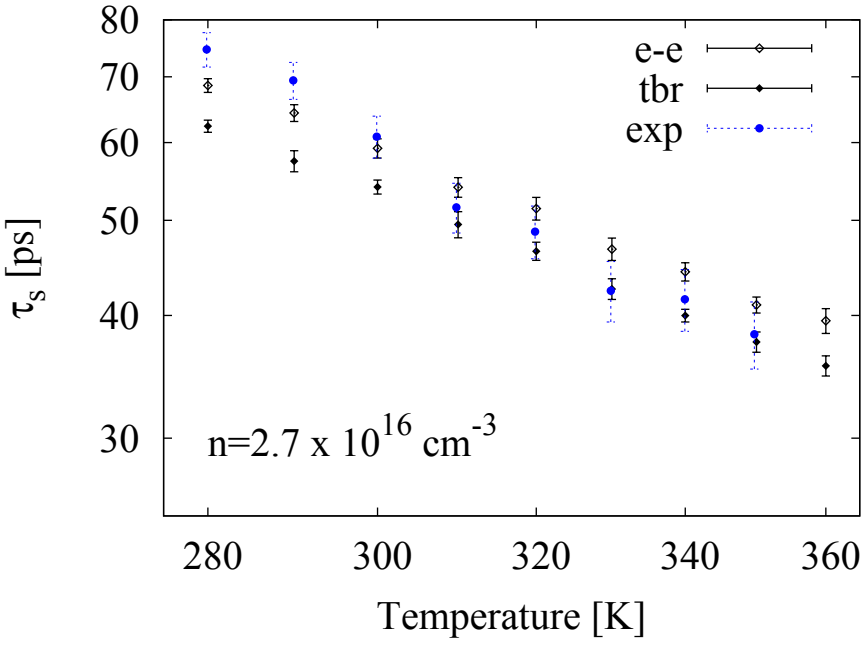

Figure 5.11: Spin relaxation time versus temperature (log-log scale). All data include e-e scattering, with (lower curve, $\tau_s^{ee,tbr}$), and without (upper curve, τ_s^{ee}) third-body rejection corrections. Parameters: $N = 25{,}000$, $n_e = 2.7 \times 10^{16}$ cm^{-3}, and $\gamma_{so} = 21.9$ $eV\AA^3$.

Besides, in Figure 5.14 we can see that at low electronic densities there is convergence of the plots only for collisional electron energies lower than the thermal energy E_{th} (~ 19.39 meV) associated to the relative motion. If now we look at the convergence of the $\tau_s^{ee,tbr}$ and τ_s^{ee} values at low electronic densities in Figure 5.10, we may speculate that in that region only "slow "electrons, i.e., electrons with energy smaller than the thermal energy are likely to be involved in e-e collisions. This also seems to be consistent with the feature of the e-e scattering rate (5.5) we have implemented in the code. In fact the e-e scattering rate becomes peaked at lower energies than the thermal energy in low electronic concentrations, see Figure 5.1.

5.4.5 Statistical Analysis of Spin Relaxation Times against Electron Density via Coulombic Differential Cross-Sections

We wish to understand better the results relative to the e-e curve in Figure 5.9. To do so we focus only on the e-e scattering mechanism, assuming that the other scattering mechanisms give a correct collisional probability. By comparing our calculations with the experimental data we see that the e-e scattering overestimates τ_s at higher concentrations. This may be due to the fact that the

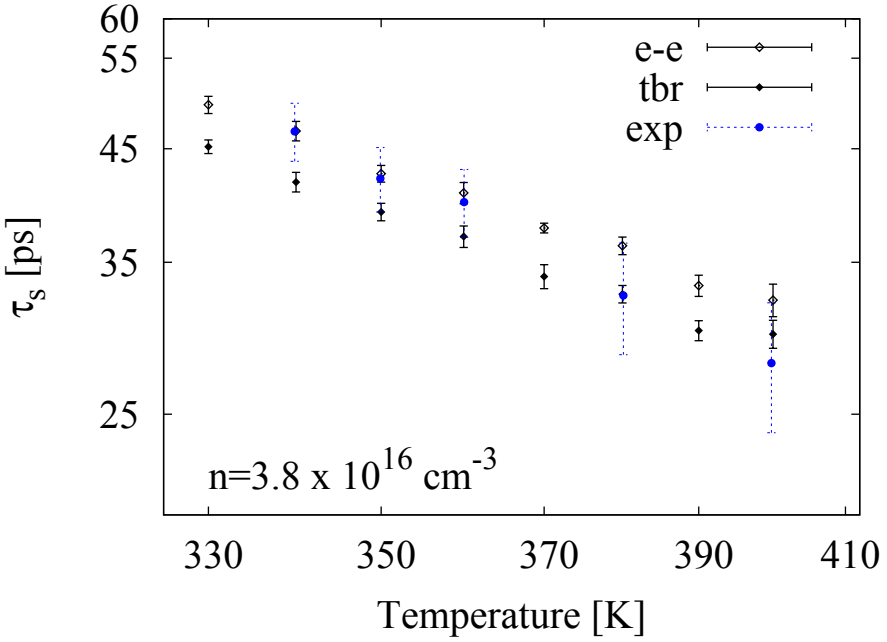

Figure 5.12: Spin relaxation time versus temperature (log-log scale). All data include e-e scattering, with (lower curve, $\tau_s^{ee,tbr}$), and without (upper curve, τ_s^{ee}) third-body rejection corrections. Parameters: $N = 25{,}000$, $n_e = 3.8 \times 10^{16}$ cm^{-3}, and $\gamma_{so} = 21.9$ $eV\AA^3$.

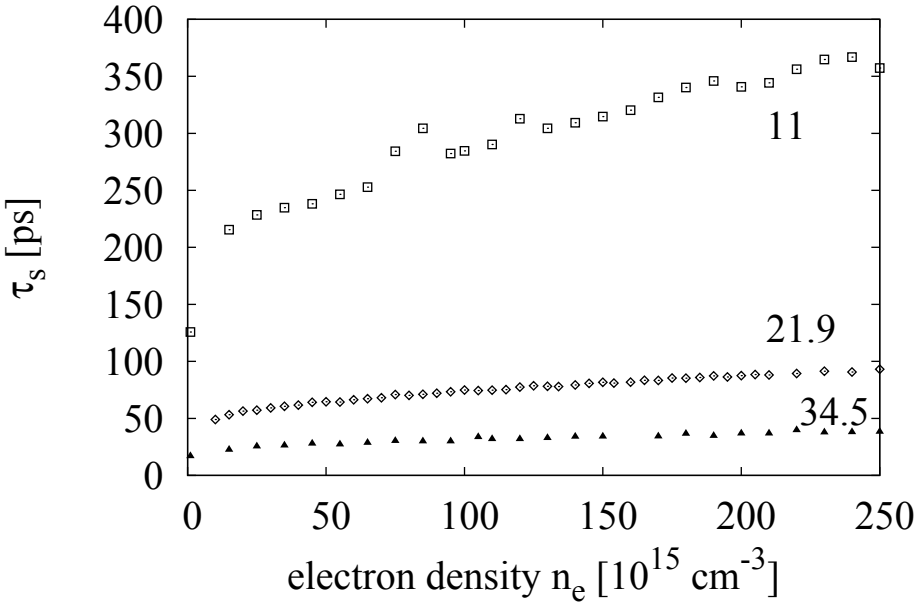

Figure 5.13: Spin relaxation time τ_s^{ee} versus density and for three different values of the spin-orbit coupling, $\gamma_{so} = 11,\ 21.9,\ 34.5$ $eV\AA^3$. Other parameters: $N = 25{,}000$ and $T = 300K$.

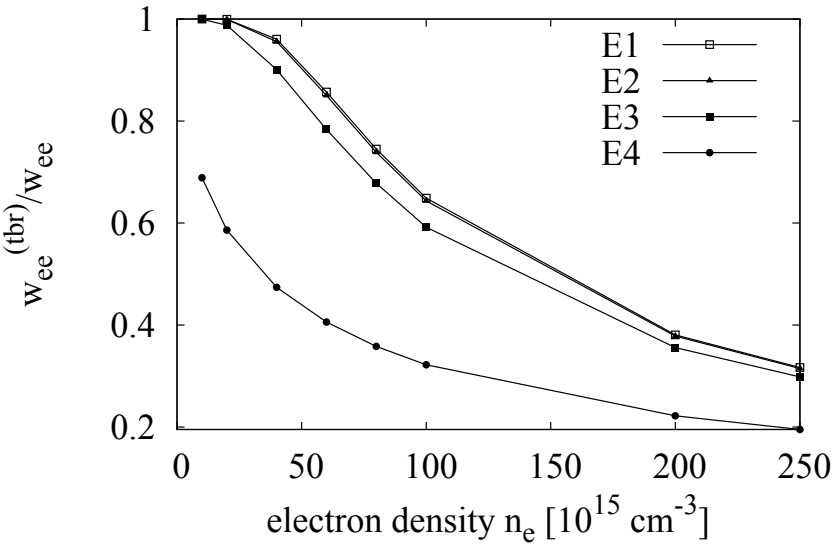

Figure 5.14: The ratio $w_{ee}^{(tbr)}/w_{ee}$ estimated from the term in parentheses of (5.25) versus n_e at $T = 300$ K. Here $E1 = 10^{-3} \times E_{th}$, $E2 = 10^{-2} \times E_{th}$, $E3 = 10^{-1} \times E_{th}$ and $E4 = E_{th} \sim 19.39\ meV$.

e-e scattering itself is overestimated because the BA is not such a good approximation for low energy carriers. Surprisingly, though, we find very good agreement with experimental data for densities lower than $10^{17}\ cm^{-3}$, while, as BA worsen at lower densities, we would expect that the SRT curve we obtained from our calculations lies above the experimental curve for the entire range of densities.

To explain this good agreement in the low density limit, we make some general considerations about Coulomb scattering, RPA and screening. Going towards low densities the RPA starts to break down, which means that in our model we are no longer allowed to split the e-e interaction in two parts. This can be also understood by looking at r_s as a criterion for the validity of RPA is [57]

$$r_s \lesssim 1. \tag{5.26}$$

Form Figure 3.2 we see that in our system RPA criterion starts to break down for $n_e \lesssim 1.5 \times 10^{17}\ cm^{-3}$, interestingly a range comparable to the one in which we find agreement between our results for τ_s^{ee} and the experimental data. This shows that, at low densities, the potential energy starts to dominate over the kinetic energy. In other words the long-range component of the Coulomb interaction becomes relevant, and a Yukawa-type potential may be no longer sufficient to realistically describe the inter-electronic potential.

The breakdown of RPA in low electronic densities may affect also the screen-

ing length whose calculation strongly relies on this approximation in our model and consequently making the scattering probability less reliable.

The RPA breaking down means that e-e scattering should in the real system be more effective. However we still use a Yukawa potential in our calculations, so, as the density decreases, we should be underestimating the e-e scattering and so we should obtain a τ_s^{ee} *smaller* than the real τ_s. However the lower range of density we consider corresponds to the regime where RPA *starts* to break down (which is compatible with the system r_s values) so that the e-e scattering which results from our simulations is accidentally correct. We can think of 3 regimes: in the first, with $n_e \gtrsim 1.5 \times 10^{17}\ cm^{-3}$, RPA is appropriate as $r_s \lesssim 1$, BA works well enough as $R \sim 1$, and as a result our simulations overestimate the e-e scattering, i.e. $\tau_s^{ee} > \tau_s$.

In the opposite limit ($r_s \gg 1$) RPA is completely inadequate: here the dominant part of the e-e scattering comes from the long range component of the Coulomb interaction, and, if a Yukawa potential would still be used, the simulations would *under-estimate* the e-e scattering and, as a result $\tau_s^{ee} < \tau_s$. From the trend of r_s (see Figure 3.2) this should happen for densities $n_e < 10^{16}\ cm^{-3}$, which we do not simulate and are not realistic because the system becomes an insulator.

The third regime is intermediate, and corresponds to r_s of the order of 1, with $r_s > 1$. In this regime RPA has not completely broken down, but the long-range part of the Coulomb interaction starts to become relevant. Using a Yukawa potential then underestimates the e-e interaction *but* at the same time the use of BA (which overestimating the e-e interaction) compensates for this, and we get as a result that $\tau_s^{ee} \sim \tau_s$. By looking at the values of r_s versus density (Figure 3.2) $r_s \gtrsim 1$ for the density range $1 \times 10^{16}\ cm^{-3} \lesssim n_e \lesssim 1.5 \times 10^{17}\ cm^{-3}$. We indeed find that $\tau_s^{ee} \sim \tau_s$ for the density range $1 \times 10^{16}\ cm^{-3} \lesssim n_e \lesssim 1.2 \times 10^{17}\ cm^{-3}$ (see Figure 5.9).

Another way of looking at the previous considerations is that, for low electronic densities, the system differential cross-section, as described by our simulations, is in some way mimicking a bare Coulomb potential one. Because the later is the exact differential cross-section of the system [39], if our simulations are mimicking it the related scattering probability would not be overestimated and the quantitative agreement with the experimental result explained.

We will now demonstrate that indeed in our simulations and for the low density range, $\sigma^{bare} \approx \sigma^{Y}$, with σ^{bare} the bare Coulomb differential cross-section and σ^{Y} Yukawa differential cross-section in BA. To do so we will then consider the ratio $\sigma^{ratio} = \sigma^{Y}/\sigma^{bare}$ and determine the conditions such that $\sigma^{ratio} \approx 1$.

The Yukawa differential cross-section in BA is given by [43]

$$\sigma^{y}(\theta) = \frac{e^4}{(4\pi\varepsilon)^4}\frac{1}{\left(E_{\beta_{TF}} + 4E\sin^2(\theta/2)\right)^2}, \tag{5.27}$$

where θ is the scattering angle associated to the relative motion. The bare Coulomb differential cross-section is obtained from (5.27) in the limit of $\beta_{TF} \to 0$, i.e. no screening. Then σ^{ratio} is

$$\sigma^{ratio}(\theta,\xi) = \frac{\xi^2\sin^4(\theta/2)}{(1+\xi\sin^2(\theta/2))^2} \tag{5.28}$$

$$= \frac{s^2(\xi;\theta)}{[1+s(\xi;\theta)]^2}, \tag{5.29}$$

where we have defined the dimensionless quantities $\xi = 4E/E_{\beta_{TF}} = 2E_{lab}/E_{\beta_{TF}}$ and $s = \xi\sin^2(\theta/2)$. From (5.28) we note that $\sigma^{ratio} \leq 1$ *always*. For a given set of energies E of the collisional electrons and a *threshold* value σ^* of σ^{ratio} close to unity, there may exist the set of scattering angles $I_{\theta^*} = \{\theta \in [\theta^*,\pi] : \sigma^* \leq \sigma^{ratio} \leq 1\}$. From the angular probability distribution $P(\theta,E)$, see the equation (5.6), we can determine the probability F_{θ^*} that, for a given E, $\sigma^* \leq \sigma^{ratio} \leq 1$

$$F_{\theta^*}(E) = \int_{\theta^*}^{\pi} P(\theta,E)\,d\theta\,. \tag{5.30}$$

This integral can be solved analytically and we get

$$F_{\theta^*}(\xi) = \frac{\cos^2\left(\frac{\theta^*}{2}\right)}{1+\frac{\xi}{4}\sin^2\left(\frac{\theta^*}{2}\right)} \tag{5.31}$$

$$= \frac{4}{4+s(\xi;\theta^*)}\frac{\xi - s(\xi;\theta^*)}{\xi}. \tag{5.32}$$

Because the system is at equilibrium we can use the Boltzmann distribution $f_B(E)$ to weight the function F_{θ^*} over the whole energy spectrum, giving the probability that an e-e collisional event gives $\sigma^* \leq \sigma^{ratio} \leq 1$. By using that for fixed σ^*, $s(\xi;\theta^*)$ becomes a constant, s^*, which can be determined from the

equation (5.29), this probability is given by the integral I [9]

$$I(E^*_{lab}) = 2\sqrt{\frac{1}{\pi}}\frac{1}{(k_BT)^{3/2}}\int_{E^*_{lab}}^{\infty}\sqrt{E_{lab}}e^{-E_{lab}/k_BT}F_{\theta^*}(E_{lab})dE_{lab} \quad (5.33)$$

$$= \frac{8\alpha^{3/2}}{\sqrt{\pi}}\frac{4}{(4+s^*)}\int_{\frac{2E^*_{lab}}{E_{\beta_{TF}}}}^{\infty}\frac{\xi - s^*}{\sqrt{\xi}}e^{-\alpha\xi}d\xi\,, \quad (5.34)$$

where $\alpha = E_{\beta_{TF}}/(2k_BT)$ and the lower integral limit E^*_{lab} must be determined. This is the the smallest energy for which it is still possible to obtain $\sigma^{ratio}(\theta,\xi)$ as large as σ^*. In the limit $E_{lab} \to E^*_{lab}$, we have that $\theta^* \to \pi$. Imposing the condition $\sigma^{ratio}(\theta^*,\xi) \geq \sigma^*$ we obtain $s(\xi;\theta^*) \geq \frac{\sigma^*+\sqrt{\sigma^*}}{1-\sigma^*}$ from which, in the limit $\theta^* \to \pi$, we get

$$\frac{2E^*_{lab}}{E_{\beta_{TF}}} = \frac{\sigma^* + \sqrt{\sigma^*}}{1-\sigma^*}\,. \quad (5.35)$$

The integral I is function of the electronic density through α, so it is possible to compare the probabilities for different electronic densities at $T = 300K$. We calculate I for $\sigma^* = 0.7$ and $\sigma^* = 0.9$, see Figure 5.15. The results indicate that the e-e collisions with differential cross-section close to the bare one are more favored at lower densities, which proves our point. The curves in Figure 5.15 show that, for density as high as $n_e = 2.5 \times 10^{17}\ cm^{-3}$, only 8% of the total number of carriers would scatter with a differential cross section such that $0.7 \leq \sigma^{ratio} \leq 1$.

[9] Here we are assuming that it is possible to multiply the two probability distribution, i.e., we are assuming they are independent.

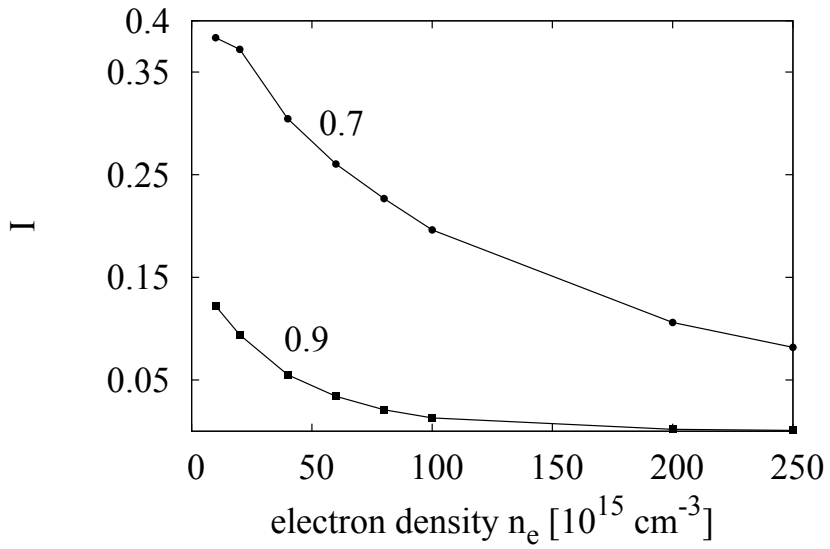

Figure 5.15: The statistical integral I versus electron density at $T = 300$ K for two different values of σ^*, i.e., 0.7 and 0.9.

Chapter 6

Conclusions

Despite the simple physical jellium model we used for our calculations we found in general a good agreement of our results with the experimental data. This is also remarkable if we consider there is no free adjustable parameter in our system, including the spin-orbit coupling parameter γ_{so}. We tried also to understand the effect of the electron-electron interaction on the spin relaxation times with the help of the differential cross-section concept. It is evident from our results that the electron-electron interaction plays an important role in spin transport slowing down the spin relaxation times. Moreover it seems possible that we can gain some information on the interelectronic potential from the spin dynamics observing the spin relaxation times.

We wish to understand better the validity of RPA in our model as unfortunately there is no feasible way to improve the Born Approximation for a Yukawa potential. This is crucial as we determine the interelectronic potential from it. In the distant future we may consider to include the exchange and correlation effects through the the many-body local field factors [51] to see what is really happening in the low electronic concentration regime where RPA starts to breakdown. This should be accomplished in a way that is consistent with the ensemble Monte Carlo method. As far as we know, this has not been done. We can argue whether it is possible to improve our results retaining this model. In the high concentration regime where the third-body method becomes effective probably it may be quite easy to exploit the Friedel Sum Rule to get new results.

In the last section we shall also say a few words about the third-body rejection method as we wish to understand how it really works.

6.1 Further Works

6.2 The Friedel Sum Rule

We have already discussed about the validity of the first BA approximation in our model. Including the second BA approximation for the Yukawa potential scattering rate is a very difficult and not rewarding task, because the formula involved is very complicated [37] and completely unreliable. The reason of this unexpected result is explained in [37]. One then needs to resort to the third BA which is extremely complicated, in order to obtain the correct scattering probability. In conclusion, improving the BA directly may not be such a good idea. But surprisingly going beyond of the first BA by the method of partial waves may be very rewarding for improving the screening length.

The method of partial waves allows us to find a complete solution of the scattering problem for central scattering potentials where the angular momentum is conserved [43]. This method calculates the scattering amplitude through some quantities called phase shifts [37, 43].

Firstly let us make some physical considerations. We noticed that the τ_s^{ee} curve starts to deviate from the experimental data at $n_e = 10^{17}\ cm^{-3}$. Indeed this problem was fixed by the third-body rejection which diminishes the scattering probability where multiple scattering events may become likely. But if we now look at our results in that region from the perspective of the screening we should expect that the Yukawa potential to become more reliable and consequently its scattering rate, for two simple reasons. One is the validity of the RPA which we investigated in the previous chapter. The second one is physical. Increasing the electronic densities the number of the itinerant electrons available in the conduction band for screening also increases, making the screening more effective and likely to be complete. The screening is complete when the total induced electronic charge completely neutralize the perturbing impurity charge. The latter condition can be enforced by the Friedel sum rule (FSR) [91].

The FSR states that the electric charge of the impurity must be neutralized by the free moving electrons within a short distance and the Fermi wavevector k_F at large distances from the impurity should be the same as for an ideal electron gas [91]. The first requirement that the impurity should appear neutral at large distances constrains the phase shifts η_l for a given angular momentum l [37, 38] and in turn also constrains the scattering potential considered [89].

For a semiconductor with one parabolic band, FSR is given by [89]

$$\pi^{-1}\sum_{l}(l+1)\int_{-\infty}^{\infty} f_{FD}(E)\,\frac{d\eta_l}{dE}dE = -Z, \tag{6.1}$$

where for single-charge impurity $Z = 1$. In general it is easy to calculate the phase shifts η_l for a Yukawa potential in the Born approximations whose exponential factor, let us call it β, is assumed unknown. Therefore we can use the equation (6.1) to determine the new inverse screening lengths, $\beta^{(1)}$ in the first BA, $\beta^{(2)}$ in second the BA and etc, all consistent with the FSR. Then it will be interesting to compare the new results with the β_{TF} calculated in LTFA. We should expect that in the first BA they give the same value according to [52]. In the second BA the small differences between the inverse screening lengths can give rise to an important effect on spin relaxation times because the differential cross-section may be very sensitive to small variations of the inverse screening length. More importantly this can make third-body rejection not necessary as we expect FSR should work propertly in the same electronic density region.

6.3 An Inverse Problem for Third-Body Rejection

We wish to understand better and maybe generalize the third-body rejection method. The third-body rejection method provides a new differential cross-section σ^{tbr} given by the following relation [32]

$$\sigma^{tbr}(\theta) = \sigma^{y}(\theta)\exp(-\pi n_e a b^2), \tag{6.2}$$

where $\sigma^{y}(\theta)$ is the Yukawa differential cross-section in BA. It is evident from equation (6.2) that tbr method reduces the scattering probability. Let us see the problem from a different perspective. In (6.2) we can assume that the scattering potential from which we calculate $\sigma^{tbr}(\theta)$ is unknown. We shall call it $V^{tbr}(r)$ assuming it also central. Then from the right hand side of (6.2) it is possible to determine a quantity equivalent to a scattering amplitude. Inverting the general relation between the scattering amplitude and the scattering potential in BA, see definition(2.65), it is then in principle possible to work out $V^{tbr}(r)$. We can interpret this new scattering potential as the result of applying the tbr method. What should we expect from applying it? Let us see the Figures 6.1 and 6.2 where for simplicity we consider the case of scattering by a potential well.

The Figures 6.1 and 6.2 are very suggestive. Surely we shall expect a weaker potential after applying the third-body rejection, but for its new range, we

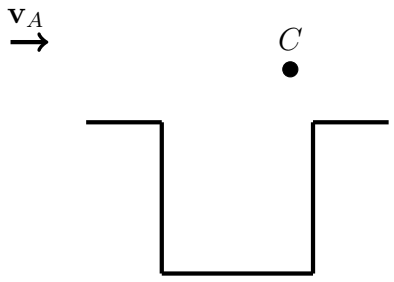

Figure 6.1: Before the applying tbr. The third-body *C* is in the range of the scattering potential well.

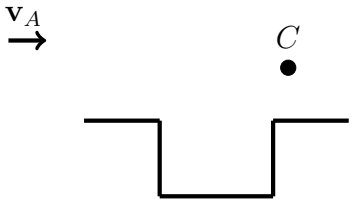

Figure 6.2: After applying tbr. The potential well is clearly weakened. If the range becomes shorter, as we wish, then the scattering potential does not see the third-body *C* anymore.

must solve the inverse problem. A new weaker potential $V^{tbr}(r)$ which also "expels "a third-body outside of its range remains a desirable feature for improving the scattering where multiple collision are likely to happen.

Appendix A

A.1 Bulk GaAs Parameters

GaAs is III-V cubic polar semiconductor with zincblende crystal structure. Its basis consists of two different atoms, gallium and arsenic. This fact implies that the GaAs structure lacks the inversion symmetry. Its BZ is a truncated octahedron. In BZ there are some important points, denoted by Γ, X, L, etc and lines as well according to the point group symmetry of the lattice [46]. Γ identifies the zone center ($\mathbf{k} = 0$), X denotes the zone end along a $< 100 >$ direction, and L denotes the zone end along a $< 111 >$ direction.

The second rank tensor $\mathscr{E}_{ij}$ in the acoustic deformation potential $\hat{V}_{e-ap}$, see the equation (2.114), in the center of the Brillouin Zone of a cubic semiconductor, is diagonal, i.e.,

$$\mathscr{E}_{ij} = \begin{bmatrix} \mathscr{E}_1 & 0 & 0 \\ 0 & \mathscr{E}_1 & 0 \\ 0 & 0 & \mathscr{E}_1 \end{bmatrix}. \tag{A.1}$$

The numerical values for the relevant parameters of a bulk GaAs semiconductor in Table A.1 are taken from [76, 92].

A.2 Density of States

Assuming a parabolic energy dispersion and including a factor two for the spin degeneracy, the density of energy states (DOS) per unit volume and per unit energy $\rho_f(E)$, is [43]

$$\rho_f(E) = \frac{1}{2\pi^2} \left(\frac{2m^*}{\hbar^2} \right)^{3/2} E^{1/2}. \tag{A.2}$$

GaAs Parameters	Recommended Values
$\mathscr{E}_1\ (eV)$	7.0
ε_b	12.90
ε_∞	10.92
$\rho_m\ (Kg/m^3)$	5.36×10^3
$v_s\ (cm/s)$	5.24×10^5
$a\ (\mathring{A})$	5.6533
$\omega_{LO}\ (Thz)$	53.7139
ω_{LO}/ω_{T0}	1.07
E_g(eV)	1.519
$E_g^X\ (eV)$	1.981
$E_g^L\ (eV)$	1.815
$\Delta_{so}\ (eV)$	0.341
$\alpha\ (eV)^{-1}$	0.61
m^*/m_e	0.067
$m_e\ (Kg)$	9.1×10^{-31}

Table A.1: v_s is the longitudinal sound velocity, a is the lattice constant. ω_{LO} value holds for the long wavelength limit. m^* is the electron effective mass at the bottom of Γ valley. The energy gaps are measured at $T = 300\ K$.

Appendix B

B.1 Fourier Transform

In the present work we adopted the following convention for the Fourier transform $\tilde{f}$ of a function $f(\mathbf{r},t)$

$$\tilde{f}(\mathbf{k},\omega) = \int\int d\omega\, d\mathbf{r}\, f(\mathbf{r},t)\, e^{-i\mathbf{k}\cdot\mathbf{r}} e^{i\omega t}\,, \tag{B.1}$$

and the relative inverse transform is then

$$f(\mathbf{r},t) = \frac{1}{(2\pi)^3}\int\int dt\, d\mathbf{k}\, \tilde{f}(\mathbf{k},\omega)\, e^{i\mathbf{k}\cdot\mathbf{r}} e^{-i\omega t}\,, \tag{B.2}$$

where the integration is understood extended to the entire spatial and temporal domains of $f(\mathbf{r},t)$. It is also customary to use the same notation for the functions and their Fourier transforms, as we can distinguish them writing their variables explicitly. We shall follow this convention in the main text of the thesis.

For convenience here we give the result for the Fourier transform of a general Yukawa potential $f(r) = (V_0/r)\, e^{-\lambda r}$ where V_0, λ are two positive constants. Then its Fourier transform is

$$\tilde{f}\,(q) = V_0 \frac{4\pi}{q^2+\lambda^2}\,. \tag{B.3}$$

In the case of a bare Coulomb potential, (B.1) is not applicable as the function which defines the potential is not square integrable function. Despite of this fact, one can use the result (B.3) for a Yukawa potential and then take the limit $\lambda \to 0$ which gives

$$v_q = \frac{e^2}{\varepsilon}\frac{1}{q^2}\,. \tag{B.4}$$

where v_q stands for $\tilde{f}(q)$. In (B.4) we also assume that

$$V_0 = \frac{e^2}{4\pi\varepsilon}\,. \tag{B.5}$$

B.2 Implementation of Finite Temperature Lindhard Function

Here we shall show how we implemented the finite temperature Lindhard function $\chi_0(q,\omega,T)$. For convenience let's recall the definition and some useful symmetry properties of this function.

$$\chi_0(q,\omega,T) = \Re e\chi_0(q,\omega,T) + i\Im m\chi_0(q,\omega,T)\,, \tag{B.6}$$

where q, ω, T are the wavevector, the frequency and the temperature respectively. $\Re e\chi_0$ and $\Im m\chi_0$ are the real and imaginary part of the Lindhard function respectively. We shall use this shorthand notation for them

$$\chi_0' = \Re e\chi_0(q,\omega,T)\,, \tag{B.7}$$

$$\chi_0'' = \Im m\chi_0(q,\omega,T)\,. \tag{B.8}$$

The functions χ_0' and χ_0'' are related to each other by K-K relations due to causality assumption. K-K relations provide the real part through the principal value integral below [51]

$$\chi_0'(q,\omega,T) = -\frac{1}{\pi} PV \int_{-\infty}^{+\infty} d\omega' \frac{\chi_0''(q,\omega,T)}{\omega-\omega'} \tag{B.9}$$

Notice that the integration is over the frequency. The useful symmetries with respect to the frequency are given by

$$\chi_0'(q,-\omega) = \chi_0'(q,\omega)\,, \tag{B.10}$$

and

$$\chi_0''(q,-\omega) = -\chi_0''(q,\omega)\,. \tag{B.11}$$

In other words χ_0' and χ_0'' are the even and odd functions of ω respectively.

B.2.1 Some Useful Dimensionless Units

Some tricky but useful dimensionless units are introduced in [51] to deal with the Lindhard function properly. The relations between the new and the old units are

$$Q = \frac{q}{k_F}, \quad \Omega = \frac{\hbar}{2E_F}\omega, \quad t = \frac{k_B T}{2E_F}, \quad \mu^* = \frac{\mu}{2E_F} \tag{B.12}$$

where Q, Ω, t, μ^* denote the wavevector, the frequency, the temperature and the chemical potential in the new units. In these units the imaginary part of the finite temperature Lindhard function becomes [1]

$$\frac{\chi_0''}{N(0)} = -\pi \left\{ \frac{Q}{\Omega} + \frac{t}{Q} \ln \frac{1 + e^{\frac{1}{t}A_-}}{1 + e^{\frac{1}{t}A_+}} \right\}, \tag{B.13}$$

where for convenience we have defined the following quantities $A_\pm$ and $v_\pm$ as

$$A_\pm = \frac{v_\pm^2}{2} - \mu^*, \tag{B.14}$$

$$v_\pm = \frac{\Omega}{Q} \pm \frac{Q}{2}. \tag{B.15}$$

B.2.2 The Calculation of the Integral

Integrals like (B.9) can be calculated by the subtraction of the singulariy provided the function that appears on the numerator of the integrand has continuous derivative in the singularity [93]. If a function $f(y)$ in the interval (a,b) possesses a continuous derivative at $y = x$ then

$$PV \int_a^b \frac{f(y)}{y-x} dy = \int_a^b \frac{f(y) - f(x)}{y-x} dy + f(x) \ln \left| \frac{b-x}{x-a} \right| \tag{B.16}$$

In our case it is straightforward to apply (B.16) identifying f with χ_0'' as the latter satisfies the conditions above. We calculate it by means of an adpative Simpson method implemented in a Fortran 90 subroutine. The integration interval (a,b) in the frequency domain is defined by the electron-hole continuum domain in the (ω, q) plane. The electron-hole continuum is the set of points on which χ_0'' differs from zero.

[1] Notice that the dimensions of the total density of states per unit volume are $[N(0)] = \frac{1}{EL^3} = [\chi_0]$

B.2.3 Temperature Dependence of the Electron-Hole Continuum Domain

For a three-dimensional electron gas the electron-hole continuum in the (ω, q) plane is defined by the following inequalities for the frequency ω at $T = 0$ K, see [51]

$$max(0, \omega_{-}(q)) \leq |\omega| \leq \omega_{+}(q)\,, \tag{B.17}$$

where

$$\omega_{\pm}(q) = \frac{\hbar q^2}{2m^*} \pm v_F q\,. \tag{B.18}$$

In the new units the relation (B.18) becomes

$$\Omega_{\pm}(Q) = \frac{Q^2}{2} \pm Q\,. \tag{B.19}$$

When $T > 0$ the function χ_0'' is always non zero, but decays exponentially to zero outside a given range. We have implemented this numerically by setting $\chi_0'' = 0$ for

$$\Omega_{+}(Q) = \frac{Q^2}{2} + Q + 10Q\sqrt{t}\,. \tag{B.20}$$

Therefore the temperature dependent frequency domain of integration (a, b) of integral $(B.9)$ when $T > 0$, due to the symmetry of χ_0'' is defined by the following curves in the (Q, Ω) plane

$$a(Q) = -\Omega_{+}(Q)\,, \tag{B.21}$$

$$b(Q) = +\Omega_{+}(Q)\,. \tag{B.22}$$

A sketch of the integration domain is shown in the Figure B.1. For each fixed value $\bar{Q}$ the integral is evaluated along a line which passes through it and is parallel to the frequency Ω axis and whose endpoints are given by the intersections with the curves $a(Q)$ and $b(Q)$.

In Figure B.2 we also plot the result of the integration for the wavevector $q = 2.5k_F$ at $T = 5$ K.

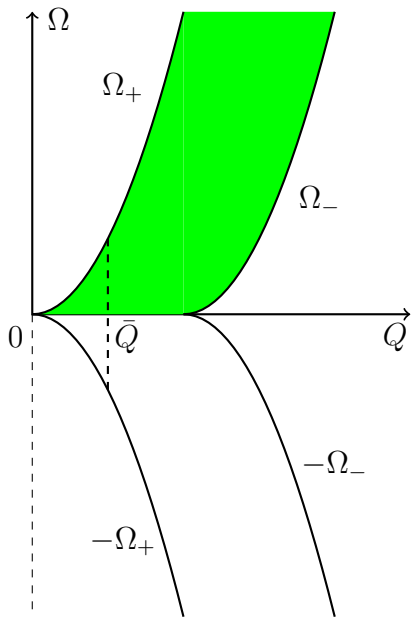

Figure B.1: The shaded region in the first quadrant of the plane (Q,Ω) is the electron-hole continuum. The curves a and b defined by equations (B.21) and (B.22) are labelled by $-\Omega_+$ and Ω_+ respectively.

B.3 Evaluation of The Coefficients of the Tricomi Function $U(a,b,z)$

For $\nu > 0$, the Gamma function Γ is defined by

$$\Gamma(\nu) = \int_0^\infty e^{-t} t^{\nu-1} dt\,. \tag{B.23}$$

If ν is a positive integer, then

$$\Gamma(\nu) = (\nu-1)!\,. \tag{B.24}$$

In our case the most useful results are $\Gamma(1) = 0! = 1$, $\Gamma(1/2) = \sqrt{\pi}$, $\Gamma(3/2) = \sqrt{\pi}/2$, $\Gamma(-3/2) = 4\sqrt{\pi}/3$, $\Gamma(5/2) = 3\sqrt{\pi}/4$ and using the following useful relation

$$\Gamma\big(1/2-\nu\big) = \frac{(-4)^n n!\sqrt{\pi}}{(2n)!}\,, \tag{B.25}$$

we can evaluate the remaining coefficients of $U(a,b,z)$.

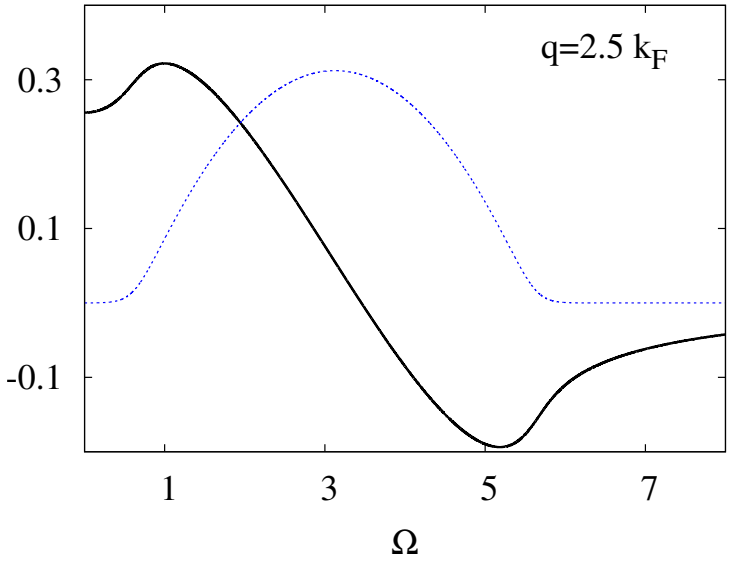

Figure B.2: The real part (black line) and immaginary part (blue line) of $-\frac{\chi_0(q,\omega,T)}{N(0)}$ against the dimensionless variable $\Omega = \frac{\hbar\omega}{2E_F}$ for n-GaAs at electron density $n_e = 2.8 \times 10^{16}\ cm^{-3}$, $T = 5$ K and $q = 2.5k_F$.

Appendix C

C.1 The Chemical Potential for Semiconductors with Parabolic Band

At equilibrium, for a non-interacting system of fermions, the Fermi-Dirac (F-D) statistics holds. The F-D distribution f_{FD} is

$$f_{FD}(E) = \frac{1}{e^{(E-\mu)/k_BT} + 1}, \tag{C.1}$$

which gives the probability to find a fermion such as an electron, in a single particle state of energy E. Notice that if $E = \mu$, then the probability is just $1/2$. The quantity μ is the chemical potential. In statistical mechanics the chemicalpotential is defined by [40]

$$\mu = \left(\frac{\partial F}{\partial N}\right)_{T,V}, \tag{C.2}$$

where N is the number of the electrons, V and F are the volume and the free energy of the system respectively. The free energy is defined as [40]

$$F = U - TS. \tag{C.3}$$

Here U is S the internal energy and S the entropy of the electronic system. In order to calculate the chemical potential of a semiconductor with parabolic band whose carrier concentration is given some approximate espressions are given in Nilsson's paper [94].

The reduced chemical potential η , assuming the energy zero at the edge of the conduction band, is defined by [94]

$$\eta = \frac{\mu}{k_BT}. \tag{C.4}$$

At equilibrium the electronic concentration n_e in a semiconductor with parabolic band, is [94]

$$n_e = N_0 \mathcal{F}_{1/2}\,, \tag{C.5}$$

where N_0 is the effective electron density of states, given by

$$N_0 = \frac{1}{4}\left(\frac{2mk_BT}{\pi\hbar^2}\right)^{3/2} \tag{C.6}$$

and $\mathcal{F}_{1/2}$ is the Fermi-Dirac Integral of order $1/2$, see section 3.6.

Defining the following quantity $u = n_e/N_0$, a simple expression is obtained in [94], which allow us to use it at least up to $\eta = 5$

$$\eta = \ln u + \frac{u}{(64+3.6u)^{1/4}}\,. \tag{C.7}$$

The error from (C.7) is less then 10^{-2} up to $\eta = 5.7$ compared to tabulated values [94]. If it is necessary to compute η accurately for even higher values, for example, in the case of high doped semiconductors (metallic regime) then the previous approximation can be extended to [94]

$$\eta = \ln u + \frac{u}{\left[64+0.05524u(64+u^{1/2})\right]^{1/4}}\,. \tag{C.8}$$

The error of (C.8) is less than 5×10^{-5} up to $\eta = 12.7$ compared to the tabulated values [94]. Both formulae (C.7) and (C.8) are implemented in our code. The calculations of some values η and μ, at room temperature for common concentrations are shown, for convenience, in the table C.1 below.

It is evident from the data in the table C.1 that the range of η is in the interval $(-6,2)$ for ordinary $n-$type GaAs semiconductors.

$n\ (cm^{-3})$	η	μ (meV)
10^{15}	-6.07	-157.05
5×10^{15}	-4.46	-115.35
10^{16}	-3.76	-97.33
5×10^{16}	-2.12	-54.88
10^{17}	-1.38	-35.92
5×10^{17}	0.53	13.92
10^{18}	1.62	41.88

Table C.1: Values of η and μ calculated at $T = 300$ K.

When μ is in the semiconductor energy gap, and is separated by more than several thermal energy k_BT from the edges of either the conduction band or valence band, namely $(E_{CB} - \mu > 3k_BT)$, the semiconductor is called non-degenerate (Boltzmann statistics, $\eta << 0$). When μ enters either conduction or valence bands, the semiconductor is called degenerate (Fermi-Dirac statistics, $\eta >> 0$).

A comparison between the previous criterion with the inequality $T \gg T_F$ shows that at room temperature $T = 300K$ a semiconductor can be considered non-degenerate for doping density of about $10^{15}\ cm^{-3}$. We found in fact that $E_{CB} - \mu = 115.35\ meV$ and $3k_BT = 77.5\ meV$ meanwhile $T_F = 18.4K$.

Appendix D

The following scattering rates, calculated through the FGR, of electrons off the lattice hold if the lattice can be considered in equilibrium at temperature T. As the phonons are bosonic particles, then they obey Bose-Einstein distribution

$$f_{BE}(E) = \frac{1}{\exp(E - \mu/k_B T) - 1}\,. \tag{D.1}$$

In the case of phonons (D.1) becomes [32]

$$N_0(\omega_{\mathbf{q}}) = \frac{1}{\exp(\hbar\omega_{\mathbf{q}}/k_B T) - 1}\,, \tag{D.2}$$

where $N_0(\omega)$ denotes the average number of phonons with energy $E = \hbar\omega_{\mathbf{q}}$. In the case of acoustic phonons which scatter with thermal electrons in nondegenerate regime, the equation (D.2) can be approximated in the following way [32]

$$N_0(\omega_{\mathbf{q}}) \approx \frac{k_B T}{\hbar\omega_{\mathbf{q}}} \qquad \frac{\hbar\omega_{\mathbf{q}}}{k_B T} \ll 1\,. \tag{D.3}$$

This is called equipartition approximation.

D.1 Electron-Longitudinal Acoustic Phonon Scattering Rate

FGR for electron-longitudinal acoustic phonons intravalley collisions, assuming a parabolic band and a deformation potential (see 2.7), gives the following scattering rate $w_{e,ac}$ [27]

$$w_{e,ac}(E) = \frac{\sqrt{2}\,(m^*)^{3/2} k_B T \mathscr{E}_1^2}{\pi\hbar^4 v_s^2 \rho_m}\sqrt{E}\,. \tag{D.4}$$

Here we assume the equipartition approximation to be valid. As the electron-acoustic phonon collision processes result elastic, there is no distinction of the

electronic final states due to either phonon absorption or phonon emission. Further the scattering is isotropic. For the meaning of the physical constants in (D.4), see the table A.1 in Appendix A. This scattering rate is implemented in our EMC code. For the sake of completeness we should mention another possible scattering mechanism in III-V and II-VI semiconductors which involves emission and absorption of acoustic phonons. It is called piezoelectric scattering and it may arise from strain-induced macroscopic electric fields due to the lacking of the inversion symmetry [32]. It becomes important at low temperatures and for pure compound semiconductors and therefore we do not consider it in the present work.

D.2 Electron-Longitudinal Polar Optical Scattering Rate

The GaAs is a polar crystal therefore lattice vibrations are accompanied by oscillating electrics fields. FGR from the Fröhlich Hamiltonian (see 2.7), gives in this case the following scattering rates [32, 95]

$$w_{abs}(E) = C\frac{N_0}{\sqrt{E}}\ln\left(\frac{\sqrt{E+\hbar\omega_{LO}}+\sqrt{E}}{\sqrt{E+\hbar\omega_{LO}}-\sqrt{E}}\right), \tag{D.5}$$

$$w_{em}(E) = C\frac{(N_0+1)}{\sqrt{E}}\ln\left(\frac{\sqrt{E}+\sqrt{E-\hbar\omega_{LO}}}{\sqrt{E}-\sqrt{E\hbar-\omega_{LO}}}\right), \tag{D.6}$$

for absorption and for emission processes respectively. Here the constant C is defined as

$$C = \frac{\sqrt{m^*}e^2\omega_{LO}}{16\sqrt{2}\pi^2\varepsilon_0\hbar}\left[\frac{1}{\varepsilon_\infty}-\frac{1}{\varepsilon_b}\right], \tag{D.7}$$

and N_0 is given by Bose-Einstein distribution (D.2). This scattering mechanism is anisotropic and favours small angle scattering events. It is inelastic and very important for GaAs at room temperature and for II-VI semiconductors. These formulae are implemented together with EMC algorithm in our code.

D.3 Electron-Impurity Scattering Rate

The scattering rate for electron-impurity w_{ei}, assuming a parabolic band and Yukawa screened potential, is given by [27]

$$w_{ei}(E) = \frac{2^{\frac{5}{2}}\pi n_i e^4 Z^2}{(4\pi\varepsilon)^2\sqrt{m^*}E_\beta^2}\frac{\sqrt{E}}{1+4E/E_{\beta_{TF}}}\,. \tag{D.8}$$

Here Ze is the charge of the ionized impurity whose internal structure is ignored, i.e., we assume they are point-like particles and E_β is defining by

$$E_\beta = \frac{\hbar^2\beta_{TF}^2}{2m^*}\,. \tag{D.9}$$

In our work we shall consider only single ionized impurities and therefore $Z = 1$. The equation (D.8) is referred to as Brooks-Herring approach in the literature, see Chattopadhyay 's paper [96] for an exhaustive treatment of electron-impurity scattering mechanism in semiconductors. We use this scattering rate for our EMC code.

D.4 Scattering Angular Distributions and its EMC Implementations

EMC algorithm includes the angular probability according to the type of interaction involved in the scattering event. This is necessary for updating the momentum of the scattered carrier after a collision. For isotropic scattering, like the case of electron-acoustic phonon scattering considered here, every scattering direction after a collision event is equivalent and independent of the interaction. Then the polar angles θ, ϕ are given by

$$\cos\theta = 1 - 2r_1\,, \tag{D.10}$$

$$\phi = 2\pi r_2\,, \tag{D.11}$$

where r_1, r_2 are random numbers uniformly distributed between 0 and 1 [27]. The relation (D.11) is assumed to hold for every scattering mechanism in present work. In other words there is no dependence on the azimuthal angle. The equations (D.10) and (D.11) are equivalent to an arbitrary rigid rotation of the carrier's momentum. From a geometric point of view, this rotation determines a sphere with a radius equal to the magnitude of the momentum. Then we can work out the updated momentum in a way equivalent to choosing a point on

this sphere. Thus we can exploit some efficient methods devised by Marsaglia for choosing a point on a sphere [97]. After a comparison of the different methods proposed in [97], we found that the most efficient for a numerical implementation is the following one. We generate two independent pseudo random numbers r_1, r_2 on $(-1,1)$ until

$$S = r_1^2 + r_2^2 < 1\,, \tag{D.12}$$

then the point on the sphere surface has the following cartesian coordinates

$$\left(2r_1\,(1-S)^{\frac{1}{2}}\,, 2r_2\,(1-S)^{\frac{1}{2}}\,, 1-2S\right)\,. \tag{D.13}$$

In the case of the electron-impurity scattering the angular probability distribution for the polar angle θ is [27]

$$\cos\theta = 1 - \frac{2\,(1-r)}{1+\delta r}\,, \tag{D.14}$$

where $\delta = 4E/E_{\beta_{TF}}$ and r is a pseudo random number in the interval $(0,1]$.

Finally in the case of electron-POP scattering the angular probability distribution is [95]

$$\cos\theta = \frac{(1+\xi) - (1+2\xi)^r}{\xi}\,, \tag{D.15}$$

where r is a pseudo random number in the interval $(0,1)$ and

$$\xi = \frac{2\sqrt{E \pm \hbar\omega_{LO}}}{\left(\sqrt{E} - \sqrt{E \pm \hbar\omega_{LO}}\right)^2}\,, \tag{D.16}$$

where the signs $+$ and $-$ in (D.16) refer to POP absorption and POP emission processes respectively.

Appendix E

E.1 Spin Evolution

In the following we neglect dipole-dipole interaction between the spins. In this way, during free-flight the spin of each electron undergoes individual coherent evolution according to the Schrödinger equation.

Initially each electron spin is assumed to be polarized in the z direction, after which the spin relaxes via the Dyakonov-Perel mechanism, whereby each spinor wavefunction is acted upon by the time evolution operator generated by the Dresselhaus Hamiltonian H_D (4.42).

The time-evolution operator U in spin space for a single particle spinor wavefunction Ψ over the timestep δt is

$$U(\delta t) = e^{-iH_D \delta t/\hbar}, \tag{E.1}$$

so that the spinor wavefunction $\Psi(t)$ at time δt is related to its value at initial time, $t = 0$ by

$$\Psi(\delta t) = U(\delta t)\Psi(0)\,. \tag{E.2}$$

In order to integrate numerically equation (E.2) we resort to the Crank-Nicolson (C-N) method [98]. This numerical method integrates by interpolating between two consecutive timesteps, hence

$$\Psi^{n+1} = \Psi^n - \frac{i\delta t}{2\hbar} H_D(\Psi^n + \Psi^{n+1})\,, \tag{E.3}$$

where $\Psi^n = \Psi(n\delta t)$ denotes the spinor wavefunction at the nth-timestep. Then the C-N method leads to the solution

$$\Psi^{n+1} = \left(1 + \frac{i\delta t}{2\hbar} H_D\right)^{-1} \left(1 - \frac{i\delta t}{2\hbar} H_D\right) \Psi^n, \tag{E.4}$$

which is correct up to $\mathscr{O}(\delta t^4)$.

The C-N method is particularly good for the problem of spin evolution as it gives a unitary evolution of the spinor wavefunction in time, hence it conserves its norm. In contrast to the commonly used Heun scheme, the C-N method has the advantage that we do not need to renormalise the spinor wavefunction after each timestep. The exact numerical scheme is

$$\Psi(t=\delta t) = C \begin{pmatrix} 1-\frac{h^2\delta t^2}{4} - ih_z & ih_x + h_y \\ ih_x - h_y & 1-\frac{h^2\delta t^2}{4} + ih_z \end{pmatrix} \Psi(t=0)\,, \tag{E.5}$$

where

$$C = 1 + h^2 \frac{\delta t^2}{4}\,, \tag{E.6}$$

and h_i are the i-components of the effective field, given by the Hamiltonian (4.42),

$$h_i = 2\Omega_i\,, \tag{E.7}$$

and finally $h^2 = \sum_{i=1}^{3} h_i^2$.

At any given time we can extract the expectation values of the S_x, S_y and S_z components of the individual electron spin operator S to get the probability that the spin is aligned along each direction. Finally this can be averaged over all spins to give the net spin in any direction. As in this work we are starting from an electronic ensemble fully polarized in the z direction, we will be interested in looking at the time evolution of the z-component of the total spin $S_{z,tot}$. At the n-th timestep this is given by

$$\begin{aligned} S_{z,tot}\,(n\delta t) &= \frac{1}{N} \sum_{i=1,N} \langle S_z \rangle_i & \text{(E.8)} \\ &= \frac{\hbar}{2N} \sum_{i=1,N} \langle \Psi_i\,(n\delta t)\,|\sigma_z|\Psi_i\,(n\delta t)\rangle, & \text{(E.9)} \end{aligned}$$

where N is the number of electrons in the simulation, and σ_z the z-Pauli matrix.

E.2 Estimating the Spin Relaxation Time

Using the above methodology we are capable of simulating the time evolution of the total electronic spin and of its components in the sample. The quantity of interest to us is the characteristic spin relaxation time of the material. This

can be extracted from the time evolution of $S_{z,tot}$.

We assume that, after a transient period, the spin relaxation behavior in the bulk semiconductor takes the form

$$S_{z,tot} = Ae^{Bt}. \tag{E.10}$$

It is then possible to fit the data from the simulation of the spin time evolution to such a curve, and produce values for the parameters A and B in the exponential fit. In particular, the parameter B has units of s^{-1} and is identified as the characteristic spin relaxation time of the sample, $B = 1/\tau_s$. The spin relaxation curve has characteristics different from an exponential during the first picoseconds: it in fact starts from a maximum at $t = 0$ where it then displays a quadratic behavior, see Figure E.1.

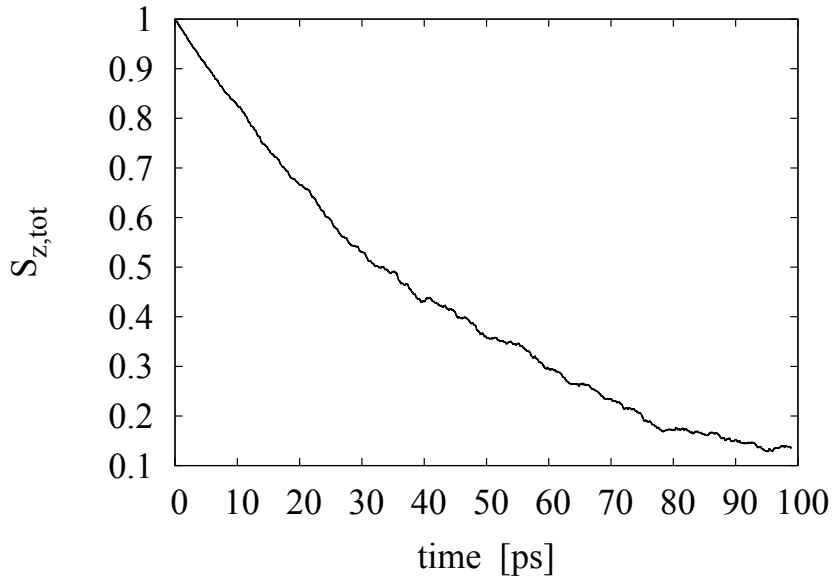

Figure E.1: $S_{z,tot}$ against time at $T = 300$ K and $n_e = 10^{16} cm^{-3}$.

We then fit the simulation data exponentially only after this initial transient period. From the analysis of the data in the parameter range we are interested in, we see that neglecting the first 10 ps after thermalization is sufficient for this scope.

E.3 Experimental Curves from Oestreich's group

In this section we show the original experimental curves obtained by Oertel et al. in [28] and from which we extracted the data for the discussion of our results in Chapter 5.

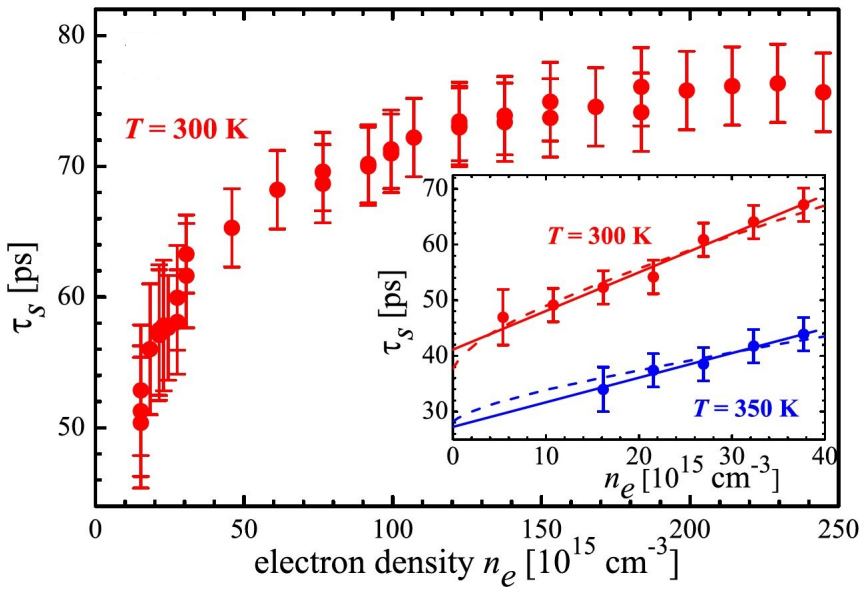

Figure E.2: (b). Spin relaxation times τ_s versus electron density n_e measured at $T = 300$ K by Oertel et al. Reprinted with permission from S. Oertel, J. Hübner and M. Oestreich, APPLIED PHYSICS LETTERS, **93**,132112 (2008). Copyright [2008], AIP Publishing LLC.

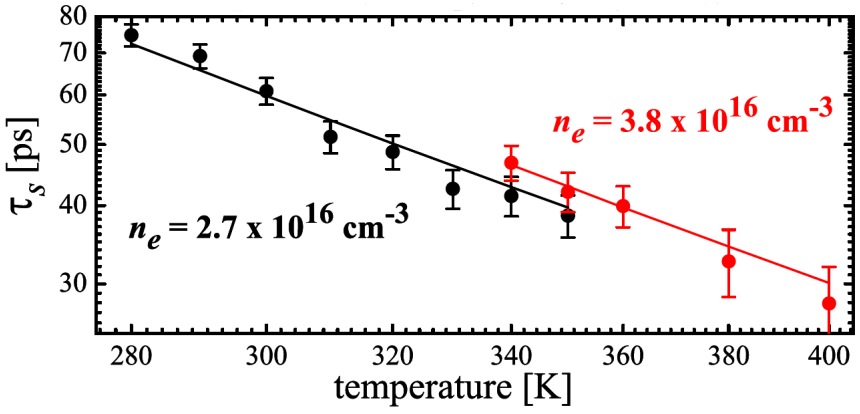

Figure E.3: (b). Spin relaxation times τ_s versus temperature T at two different densities (doubly logarithmic scale) measured by Oertel et al. Reprinted with permission from S. Oertel, J. Hübner and M. Oestreich, APPLIED PHYSICS LETTERS, **93**,132112 (2008). Copyright [2008], AIP Publishing LLC.

List of Acronyms

GMR	Giant Magneto Resistance	12
SHE	Spin Hall Effect	12
QC	Quantum Computation	13
SI	International System of Units	18
QED	Quantum Electrodynamics	19
LS	Laboratory System	20
CoM	Center of Mass System	21
FGR	Fermi Golden Rule	25
$L-S$	Lippmann-Schwinger equation	29
BA	First Born Approximation	32
$I.P$	Interaction Picture	36
DOS	Density of states	39
$S.Q$	Second Quantization	42
POP	Polar Optical Phonon	42
BZ	Brillouin Zone	43
QFT	Quantum Field Theory	44
DFT	Density Functional Theory	48
LRT	Linear Response Theory	44
RPA	Random Phase Approximation	44
$K-K$	Kramers-Krönig	46
CB	Conduction Band	47
EMC	Ensemble Monte Carlo	48
$T-F$	Thomas-Fermi	54
$LTFA$	Linearized Thomas-Fermi Approximation	56
$F-D$	Fermi-Dirac	56
$e-i$	Electron-Impurity	57
QM	Quantum Mechanics	66
SOI	Spin-Orbit Interaction	66
$SU(2)$	Special Unitary Group	70
$SO(3)$	Special Orthogonal Group	70
TR	Time Reversal Symmetry	73

NMR	Nuclear Magnetic Resonance	79
SRT	Spin Relaxation Time	80
BAB	Bir-Aronov-Pikus Mechanism	80
EY	Elliott-Yafet Mechanism	80
DP	Dyakonov-Perel Mechanism	80
KSBE	Kinetic Spin Bloch Equation	81
$e-e$	Electron-Electron	88
tbr	Third-Body Rejection	96
FSR	Friedel Sum Rule	114
$C-N$	Crank-Nicolson Algorithm	132

List of Symbols

Bibliography

[1] S. A. Wolf, D. D. Awschalom, R. A. Buhrman, J. M. Daughton, S. von Molnar, . M. L. Roukes, A. Y. Chtchelkanova, and D. M. Treger, "Spintronics: A spin-based electronics vision for the future," *Science*, vol. 294, 2001.

[2] C. Chappert, A. Fert, and F. N. V. Dau, "The emergence of spin electronics in data storage," *Nature*, vol. 6, 2007.

[3] Y. G. Kusrayev, "Spintronics," *Physics-Upsekhi*, vol. 53, no. 7, 2010.

[4] S. Bader and S. Parkin, "Spintronics," *Annu. Rev. Condens. Matter. Phys.*, 2010.

[5] I. Žutić, J. Fabian, and S. D. Sarma, "Spintronics: Fundamentals and applications," *Rev. Mod. Phys.*, vol. 76, no. 2, 2004.

[6] A. M. Bratkovsky, "Spintronic effects in metallic, semiconductor, metaloxide and metalsemiconductor heterostructures," *Rep. Prog. Phys.*, vol. 71, no. 026502, 2008.

[7] A. Fert, "The origin, development and future of spintronics," *Nobel Lecture, December 8, 2007*, 2007.

[8] M. I. Dyakonov, *Spin Physics in Semiconductors*. Springer, 2008.

[9] S. Datta and B. Das, "Electronic analog of the electro-optic modulator," *Appl. Phys. Lett.*, vol. 56, no. 7, 1989.

[10] C. Kittel, *Introduction to Solid State Physics*. J. Wiley, 1996.

[11] V. Galitski and I. B. Spielman, "Spin-orbit coupling in quantum gases," *Nature*, vol. 494, no. 49, 2013.

[12] M. Fox, *Quantum Optics. An Introduction*. Oxford University Press, 2011.

[13] D. P. DiVincenzo, "Quantum computation," *Science*, vol. 270, no. 5234, 1995.

[14] B. W. Lovett and A. Nazir, "Aspects of quantum coherence in nanosystems," *arXiv: 0903.2/46v1 [quant-ph]*, 2009.

[15] J. M. Kikkawa and D. D. Awschalom, "Resonant spin amplification in n-type GaAs," *Phys. Rev. Lett*, vol. 80, no. 4313, 1998.

[16] R. Dzhioev, K. V. Kavokin, V. L. Korenev, M. V. Lazarev, B. Y. Meltser, and M. N. Stepnova, "Low-temperature spin relaxation in n-type GaAs," *Phys. Rev. B*, vol. 80, no. 245204, 2002.

[17] D. Awschalom and N. Samarth, "Spintronics without magnetism," *Advances in Physics*, vol. 2, no. 50, 2009.

[18] L. Chirolli and G. Burkard, "Decoherence in solid state qubits," *Advances in Physics*, vol. 57, no. 3, 2008.

[19] J. Fabian, A. Mates-Abiague, C. Erstler, P. Stano, and I. Žutić, "Semiconductor spintronics," *Acta Physica Slovaca*, vol. 57, no. 565, 2007.

[20] G. Schmidt, "Concepts for spin injection into semiconductor - a review," *J. Phys. D: Appl. Phys.*, 2005.

[21] B. van Wees, "Spins go their own way," *Nature Physics*, vol. 3, 2007.

[22] H. Ohno, "Making nonmagnetic semiconductors ferromagnetic," *Science*, vol. 281, 1998.

[23] I. D'Amico and G. Vignale, "Theory of spin coulomb drag in spin-polarized transport," *Phys. Rev. B*, vol. 62, no. 4853, 2000.

[24] J. Fabian and I. Žutić, "The standard model of spin injection," *arXiv: 0903.2500v1 [cond-mat.other]*, 2009.

[25] G. Dresselhaus, "Spin-orbit coupling effects in zinc blende structures," *Phys. Rev. B*, vol. 100, no. 2, 1955.

[26] S. Saikin, Y. V. Pershin, and V. Privman, "Modeling in semiconductor spintronics," *Proc.-Circuits Devices Syst.*, vol. 142, no. 366, 2005.

[27] C. Jacoboni and P. Lugli, *The Monte Carlo Method for Semiconductor Device Simulation*. Springer-Verlag, 1989.

[28] S. Oertel, J. Hubner, and M. Oestreich, "High temperature electron spin relaxation in bulk GaAs," *Appl Phys. Lett.*, vol. 93, no. 132112, 2008.

[29] G. Vignale, *The Beautiful Invisible*. Oxford University Press, 2011.

[30] W. Greiner and B. Müller, *Quantum Mechanics. Symmetries*. Springer-Verlag, 1994.

[31] M. Goano, "Algorith 745: Computation of the complete and incomplete Fermi-Dirac integral," *ACM Transactions on Mathematical Software*, vol. 21, no. 3, 1995.

[32] B. K. Ridley, *Quantum Processes in Semiconductors*. Oxford Science Publications, 2000.

[33] M. M. Glazov and E. L. Ivchenko, "Effect of electron-electron interaction on spin relaxation of charge carriers in semiconductors," *Journal of Experimental and Theoretical Physics*, vol. 99, no. 6, 2004.

[34] R. Feynman, *QED-The Strange Theory of Light and Matter*. Penguin, 1990.

[35] M. Veltman, *Facts And Mysteries In Elementary Particle Physics*. World Scientific, 2003.

[36] J. A. Shapiro, *The Birth of String Theory*. Cambridge University Press, 2012.

[37] C. Joachain, *Quantum Collision Theory*. North-Holland, 1987.

[38] L. Schiff, *Quantum Mechanics*. McGraw-Hill, 1968.

[39] S. Weinberg, *Lectures On Quantum Mechanics*. Cambridge University Press, 2013.

[40] K. Huang, *Statistical Mechanics*. John Wiley & Sons, 1987.

[41] J. J. Sakurai, *Modern Quantum Mechanics*. Addison-Wesley, 1994.

[42] F. Mandl and G. Shaw, *Quantum Field Theory*. J. Wiley, 1984.

[43] F. Mandl, *Quantum Mechanics*. J. Wiley, 1992.

[44] J. H. Davies, *The Physics of Low-Dimensional Semiconductors*. Cambridge University Press, 1997.

[45] N. W. Ashcroft and N. D. Mermin, *Solid State Physics*. Saunders College, 1976.

[46] G. D. Dresselhaus, M. S. Dresselhaus, and A. Jorio, *Group Theory: Application to the Physics of Condensed Matter*. Springer-Verlag, 2008.

[47] G. D. Mahan, *Many-Particle Physics*. Kluwer Academic, 2000.

[48] E. Antončík and P. T. Landsberg, "Overlap integrals for bloch electrons," *Proc. Phys. Soc.*, vol. 82, no. 337, 1963.

[49] R. D. Mattuck, *A Guide to Feynman Diagrams in the Many-Body Problem*. Dover Publications, 1992.

[50] F. Wilczek, "Majorana returns," *Nature Physics*, vol. 5, 2009.

[51] G. Giuliani and G. Vignale, *Quantum Theory of The Electron Liquid*. Cambridge University Press, 2008.

[52] B. A. Sanborn, P. B. Allen, and G. D. Mahan, "Theory of screening and electron mobility: Application to n-type silicon," *Phys. Rev. B*, vol. 46, no. 23, 1992.

[53] B. A. Sanborn, "Electron-electron interactions, coupled plasmon-phonon modes, and mobility in n-type GaAs," *Phys. Rev. B*, vol. 51, no. 20, 1992.

[54] M. Polini and M. Tosi, *Many-body physics in condensed matter systems*. Edizioni Della Normale, 2006.

[55] P. Maldague, "Many-body corrections to the polarizability of the two-dimensional electron gas," *Surface Science*, vol. 76, no. 296-302, 1978.

[56] E. K. U. Gross, E. Runge, and O. Heinonen, *Many-Particle Theory*. Adam-Hilger, 1991.

[57] B. Bennacer and A. A. Cottey, "Acoustic plasmons in two- and three- component degenerate Fermi gas, with application to the gallium arsenide electron-hole plasma," *J. Phys.: Condens. Matter*, vol. 1, no. 1809-1829, 1989.

[58] R. B. Dingle, "Scattering of electrons and holes by charged donors and acceptors in semiconductors," *Phil.Mag.*, vol. 46, no. 379, 1955.

[59] L. D. Cloutman, "Numerical evaluation of the Fermi-Dirac integrals," *The Astrophysical Journal Supplement*, vol. 71, no. 677-699, 1989.

[60] K. Raseong and M. Lundstrom, "Notes on Fermi-Dirac integrals," *arXiv: 0811.0116 [cond-mat.mes-hall]*, 2008.

[61] X. Aymerich-Humet, F. Serra-Mestres, and J. Millán, "A generalized approximation of Fermi-Dirac integrals," *J. Appl. Phys.*, vol. 54, no. 5, 1983.

[62] M. Abramowitz and I. A. Stegun, "Handbook of mathematical functions with formulas, graphs, and mathematical tables," *Numerische Mathematik*, vol. 90, no. 179-196, 197.

[63] K. E. Muller, "Computing the confluent hypergeometric function m(a,b,x)," *Numerische Mathematik*, vol. 90, no. 179-196, 2001.

[64] J. Sólyom, *Fundamentals of the Physics of Solids*. Springer-Verlag, 2010.

[65] R. Penrose, *The Road to the Reality*. Vintage, 2007.

[66] S. Blundell, *Magnetism in Condensed Matter*. Oxford University Press, 2009.

[67] M. R. Dennis, "Canonical representation of spherical functions: Sylvester's theorem, maxwell's multipoles and majorana's sphere," *J. Phys. A: Math. Gen.*, vol. 37, no. 9487-9500, 2004.

[68] J. D. Jackson, *Classical Electrodynamics*. Addison-Wesley, 1967.

[69] E. F. Taylor and J. A. Wheeler, *Spacetime Physics*. Freeman, 1966.

[70] K. O'Donnell and M. Visser, "Elementary analysis of the special relativistic combination of velocities, wigner rotation and thomas precession," *European Journal of Physics*, vol. 32, 2011.

[71] C. Itzykson and J. Zuber, *Quantum Field Theory*. McGraw-Hill, 1985.

[72] R. Winkler, *Spin-Orbit Coupling effects in two-dimensional electron and hole systems*. Springer-Verlag, 2003.

[73] B. A. Bernevig, *Topological Insulators and Topological Superconductors*. Princeton University Press, 2013.

[74] J. Y. Fu, M. Q. Weng, and M. W. Wu, "Spin-orbit coupling in bulk GaAs," *Physica E*, vol. 40, no. 2890-2893, 2008.

[75] P. Boguslawski, "Electron-electron spin-flip scattering and spin relaxation in iii-v and ii-vi semiconductors," *Solid State Communicatons*, vol. 33, no. 389-391, 1980.

[76] J. H. Jiang and M. W. Wu, "Electron-spin relaxation in bulk iii-v semiconductors from a fully microscopic kinetic spin bloch equation approach," *Phys. Rev. B*, vol. 79, no. 125206, 2008.

[77] M. I. Miah, "Spin lifetimes of electrons injected into GaAs and GaN," *J. Phys. D: Appl.Phys.*, vol. 41, no. 185503, 2008.

[78] S. Krishnamurthy, M. van Schilfgaarde, and N. Newman, "Spin lifetimes of electrons injected into GaAs and GaN," *Appl Phys. Lett.*, vol. 83, no. 1761, 2003.

[79] Z. G. Yu and M. Flatt, "Electric-field dependent spin diffusion and spin injection into semiconductors," *Phys. Rev. B*, vol. 66, no. 235302, 2002.

[80] D. Chattopadhyay, "Effect of electron-electron scattering on mobility in GaAs," *J. Appl. Phys.*, vol. 53, no. 4, 1982.

[81] D. Pines and D. Bohm, "A collective description of electron interactions: Ii. collective *vs* individual particle aspects of the interactions," *Phys. Rev. B*, vol. 85, no. 2, 1952.

[82] M. E. Kim, A. Das, and S. D. Senturia, "Electron scattering interaction with coupled plasmon-polar-phonon modes in degenerate semiconductors," *Phys. Rev. B*, vol. 18, no. 12, 1978.

[83] P. Borowik, "Ensemble monte carlo study of the influence of plasmon-phonon coupled modes on hot electron transport in GaAs," *J. Appl. Phys.*, vol. 82, no. 9, 1997.

[84] M. I. N. Takenaka and Y. Inuishi, "Influence of inter-carrier scattering on hot electron distribution in GaAs," *J. Phys. Soc. Jpn.*, vol. 47, no. 861-868, 1979.

[85] C. A. Kukkonen and H. Smith, "Validity of the born approximation as applied to electron-electron scattering in metals: Implications for thermal conductivity," *Phys. Rev. B*, vol. 8, no. 10, 1973.

[86] B. K. Ridley, "Reconcilation of the conwell-weisskopf and brooks-herring formulae for charge-impurity scattering in semiconductors: Third-body interference," *J. Phys. C: Solid State Phys.*, vol. 10, no. 296-302, 1978.

[87] H. Goldstein, C. Poole, and J. Safko, *Classical Mechanics*. Addison Wesley, 2002.

[88] T. G. V. de Roer and F. P. Widdershoven, "Ionized impurity scattering in monte carlo calculations," *J. Appl. Phys.*, vol. 59, no. 3, 1985.

[89] F. Stern, "Friedel phase-shift sum rule for semiconductors," *Phys. Rev.*, vol. 158, no. 3, 1967.

[90] H. Kosina and G. Kaiblinger-Grujin, "Ionized-impurity scattering of majority electrons in silicon," *Solid-State Electronics*, vol. 42, no. 3, 1998.

[91] J. M. Ziman, *Principles of the Theory of Solids*. Cambridge University Press, 1964.

[92] I. Vurgaftman, J. R. Meyer, and L. R. Ram-Mohan, "Band parameters for iii-v compound semiconductors and their alloys," *J. Appl. Phys.*, vol. 89, no. 11, 2001.

[93] P. J. Davis and P. Rabinowitz, *Numerical Integration*. Blaisdell, Waltham, Mass., 1967.

[94] N. G. Nilsson, "Empirical approximations for the Fermi energy in a semiconductor with parabolic bands," *Appl. Phys. Lett.*, vol. 33, no. 7, 1978.

[95] S. Mordechai, *Applications of Monte Carlo Method in Science and Engineering*. InTech, 2011.

[96] D. Chattopadhyay and H. J. Queisser, "Electron scattering by ionized impurities in semiconductors," *Rev. Mod. Phys.*, vol. 53, no. 4, 1981.

[97] G. Marsaglia, "Choosing a point from the surface of a sphere," *The Annals of Mathematical Statistics*, vol. 43, no. 645-646, 1972.

[98] J. Crank and P. Nicolson, "A practical method for numerical evaluation of solutions of partial differential equations of the heat conduction type," *Proc. Camb. Phil. Soc.*, vol. 43, no. 1, 1947.